

UNCLASSIFIED

AD **409 622**

DEFENSE DOCUMENTATION CENTER

FOR

SCIENTIFIC AND TECHNICAL INFORMATION

CAMERON STATION, ALEXANDRIA, VIRGINIA



UNCLASSIFIED

NOTICE: When government or other drawings, specifications or other data are used for any purpose other than in connection with a definitely related government procurement operation, the U. S. Government thereby incurs no responsibility, nor any obligation whatsoever; and the fact that the Government may have formulated, furnished, or in any way supplied the said drawings, specifications, or other data is not to be regarded by implication or otherwise as in any manner licensing the holder or any other person or corporation, or conveying any rights or permission to manufacture, use or sell any patented invention that may in any way be related thereto.

63 4-2

CATALOGED BY JJC

AS AD No. 409622

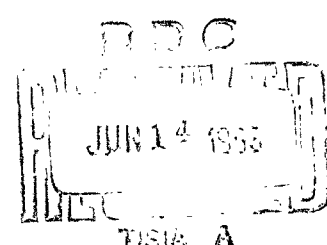
409 622

IRREVERSIBLE THERMODYNAMIC EFFECTS
IN INHOMOGENEOUS MEDIA AND THEIR
APPLICATIONS IN CERTAIN
GEOELECTRIC PROBLEMS

February 8, 1963

Project DSR 9017

Geophysics Laboratory
Massachusetts Institute of Technology
Cambridge 39, Massachusetts



Reproduction in whole or in part is
permitted for any purpose of the
United States Government.

IRREVERSIBLE THERMODYNAMIC EFFECTS
IN INHOMOGENEOUS MEDIA AND THEIR
APPLICATIONS IN CERTAIN
GEOELECTRIC PROBLEMS

MIT Project DSR 9017
Allied Research PO 20634
Report 9017-4

Report by : Bijan Nourbehecht

Project Supervisors: T. Cantwell
T.R. Madden

February 8, 1963

Geophysics Laboratory
Massachusetts Institute of Technology
Cambridge 39, Massachusetts

IRREVERSIBLE THERMODYNAMIC EFFECTS
IN INHOMOGENEOUS MEDIA AND THEIR
APPLICATIONS IN CERTAIN
GEOELECTRIC PROBLEMS

by

BIJAN NOURBEHECHT

Gp.E., Colorado School of Mines
(1959)

SUBMITTED IN PARTIAL FULFILLMENT OF THE
REQUIREMENTS OF THE DEGREE OF
DOCTOR OF PHILOSOPHY
at the
MASSACHUSETTS INSTITUTE OF TECHNOLOGY
February 1963

Signature of Author *Bijan Nourbehecht*
Department of Geology and Geophysics
November 20, 1962

Certified by *Herbert R. Mader*
Thomas Cantwell Thesis Supervisor

Accepted by *H.W. Fairbairn*
Chairman, Departmental Committee on Graduate
Students

ABSTRACT

Title: Irreversible Thermodynamic Effects in Inhomogeneous Media and Their Applications in Certain Geoelectric Problems.

Author: Bijan Nourbehecht

Submitted to the Department of Geology and Geophysics on November 19, 1962 in partial fulfillment of the requirements for the degree of Doctor of Philosophy at the Massachusetts Institute of Technology

A theoretical investigation of irreversible coupling effects in the earth is carried out to get a better understanding of the role of coupling in producing spontaneous polarization currents. It is found that electrokinetic and electrochemical couplings are the most important, and in certain cases, the thermoelectric coupling can also be important. The electric current is found to depend on the gradient of a potential f , called the "total electric potential," which satisfies the Laplace's equation. The boundary value of f depends on the driving pressure P (or chemical potential μ) and the electric potential ϕ .

The effect of geometry is investigated by solving the equation for using horizontally and vertically layered earths, buried slab, and half space with random coupling properties as models. It is found that when the equal pressure surfaces cut across the rock boundaries, an electric current is generated as the surface. The magnitude of this current depends on the geometry as well as the differences in coupling properties.

The ground potentials observed following an underground nuclear detonation are shown to be induced by electrokinetic coupling. The computed streaming potentials for one layer over a half space are found to agree fairly well with the field data. Quantitative interpretation of the results gave a depth estimate slightly higher than the actual depth.

Electrochemical diffusion is found to be capable of producing only small S. P. anomalies of a few tens of

millivolts, because the variations in the concentrations of the diffusing ions are small. However, the diffusion potentials are of sufficient magnitude to account for much of the background noise. In the presence of electronic conductors, the self-potentials are determined by the concentrations of reacting species (e.g. Fe^{++} and Fe^{+++}). When iron is the only important reacting species, the maximum potentials are of the order of one volt. The effect of geometry on the rms value of the background noise is evaluated by using a model composed of randomly distributed vertical dikes.

Thesis Supervisor: T. R. Madden

Title: Associate Professor of Geophysics

ACKNOWLEDGEMENTS

It gives me great pleasure to express my sincere gratitude to Prof. T. R. Madden for having originally suggested the topic and for having served as advisor throughout the investigation. Without his guidance and inspiration, this project would not have been completed.

I wish to acknowledge my gratitude to Prof. T. Cantwell for his stimulating encouragement and many constructive suggestions. His interest and criticisms are most appreciated.

I also wish to acknowledge the interest and assistance of Mr. J. Claerbout, Mr. J. Galbraith, Prof. H. Hughes, Prof. E. Mencher, Miss S. Nourbehecht, Prof. G. Scatchard, Prof. R. Siever, and Prof. S. M. Simpson.

Support for the work presented here came from the departmental faculty fund, the Petroleum Research Fund of the American Chemical Society, and the Vela-Uniform research project at M. I. T. done under a subcontract from the Allied Research Associates. Much of this research was carried out while I was a Gulf Research and Development Fellow. I am grateful to the Gulf Oil Company for this most welcome award.

I am grateful to Miss Dauna Trop for her assistance in the preparation of this thesis.

TABLE OF CONTENTS

	Page
Abstract	ii
Acknowledgements	iv
Lists of Tables and Figures.	vii
Table of Conversion Factors.	viii
List of Symbols.	ix
Chapter I - Introduction	1
Purpose	1
Underground Nuclear Blast	2
Spontaneous Polarization.	6
Historical Review	7
Outline of the Thesis	10
Chapter II - Review of Irreversible Thermodynamics	13
Section I - Onsager's Relations.	13
Section II - Forces and Flows in Onsager's Relations	17
Section III - Discussion of the Coefficients L_{ij}	19
Mobility.	19
Electrical Conductivity	21
Thermal Conductivity.	21
Section IV - Application of Irreversible Thermodynamics to Study Coupling Effects in the Earth.	24
Electrokinetic Coupling	25
Thermoelectric Coupling	31
Electrochemical Coupling.	35
Several Ionic Flows	36
Summary of Coupling Equations	37
Chapter III - Theoretical Solutions for Some Simple Geometries	39
Section I - Horizontally Layered Earth.	40
Homogeneous Half Space.	40
One Layer over a Half Space	42
Application to Buried Heat Source	44
Application to Buried Pressure Source	47
Two Layers over a Half Space.	48
Section II - Buried Slab	49
Section III - Vertically Layered Earth.	51
Vertical Contact Problem.	51
Application to Electrochemical Diffusion Problem	54

Vertical Dike	56
Section IV -Random Distribution of Inhomogeneities	58
Chapter IV - Application to the Detection of Underground	
Nuclear Blasts.	63
Purpose	63
Temperature and Pressure Changes.	63
Thermoelectric Effect of a Bomb	65
Electrokinetic Effect of a Bomb	67
Nevada Underground Detonations.	71
Aardvark Shot	73
Quantitative Interpretation of the Aardvark	
Results	75
Summary of Chapter IV	78
Chapter V - Application to Spontaneous Polarization	
Currents	80
Section I -S.P. Currents Caused by Thermoelectric	
Coupling.	81
Section II -S.P. Currents Caused by Electrochemical	
Coupling.	83
Electrochemical Coupling Coefficients	84
Dependence of the Chemical Potential	
on Depth.	86
Electrochemical Diffusion Potential	
across a Dike	90
Role of Metallic Conductors	93
Section III-Effect of Random Inhomogeneities	
on S.P. Currents.	100
Section IV -Other Causes of S.P.	105
Section V -Conclusions	106
Chapter VI - Suggestion's for Future Work.	108
Appendix A	110
Appendix B	115
Bibliography	117
Biography.	121

Lists of Tables and Figures

Tables

2.1	page	20
2.2		23
2.3		27
2.4		32
4.1		68
4.2		72
5.1		84
5.2		88

Figures

3.1, 3.2.	following page	40
3.3	"	45
3.4	"	46
3.5	"	47
3.6, 3.7, 3.8, 3.9.	"	49
3.10.	"	50
3.11.	"	54
3.12.	"	57
3.13.	"	57
3.14.	"	62
4.1	"	70
4.2, 4.3.	"	73
4.4	"	76
5.1	"	101

Table of Conversion Factors

Quantity	Common Units	M.K.S. Units
Conductivity	1 mhos/cm	= 10^2 mhos/m
Heat flux	1 cal/cm ² -sec	= 4.185×10^4 joules/ m-sec-°C
Magnetic field intensity	1 oersted	= $\frac{1}{4\pi} \times 10^3$ ampere-
Magnetic flux density	1 gauss	= 10^{-4} weber/turns/m ²
Permeability (at 20°C)	1 darcy	= 0.987×10^{-9} m ⁴ /sec-newton
	1 cm/sec (Hydraulic)	= 1.02×10^{-6} m ⁴ /sec-newton
Pressure	1 atmosphere	= 1.0133×10^5 Newtons/m ²
	1 psi	= 6.9×10^3 " "
	1 cm (water)	= 98 " "
	1 cm (Mercury)	= 1.33×10^3 " "
Streaming Potential	1 mv/atm	= 0.987×10^{-8} volts- m ² /newton

LIST OF SYMBOLS

a	radius of intercepted high temperature zone
a	spherical distance at which pressure is P_0
C, C_p, C_n, C_i	concentrations
$c, c_1, c_2, c_i, \bar{c}$	coupling coefficients
D	diffusivity
d	thickness of layer or dike
F	Faraday = 96500 coulombs/equivalent
f, f_i	total electric potential
h	depth to the center of the blast
\bar{J}	generalized flow
K.T.	Kiloton of TNT
K	heat conductivity
k	inverse of weathering depth
K'	permeability
L, L_{ij}, L'_{ij}, L_i	generalized conductivity coefficients
R_{21}	conductivity contrast = $\frac{\sigma_2 - \sigma_1}{\sigma_2 + \sigma_1}$
S_i, S_p, S_n	partial molal entropies
t	dike thickness
u_i, u^o, U_p, U_n, u^*	mobilities
Y_i	generalized driving potential
z_i	ith ion valence
$\alpha_i(x)$	gradient of coupling coefficient
κ	heat diffusivity
μ	chemical potential
σ	conductivity
ψ	autocorrelation function of
ϕ	electric potential
ϕ_{π}	autocorrelation function of the vertical contact potential

CHAPTER I

INTRODUCTION

Purpose

For some thirty years, thermodynamics of irreversible processes, as developed by Onsager and others, has been applied successfully to obtain important results for systems that are not in equilibrium and where there is an interaction of several processes. When two or more flows (e.g. heat flow, electrical current, etc.) are taking place simultaneously in the same system under the action of thermodynamic forces, such as temperature or concentration gradients, the rate of each flow is regarded as being proportional not only to the corresponding force, but also it is supposed to be dependent on the other forces as well. These phenomena, known as "coupling" of flows, give rise to several interesting effects. Among them, thermoelectricity, streaming potential, and electro-osmosis are well-known.

Here we shall apply the thermodynamics of irreversible processes to the study of coupling of electrical current with solvent flow, heat flow, or ionic flow which are caused by pressure, thermal, or concentration gradients. In particular, we shall apply the theory to a detailed study of the electrical after-effects of an underground nuclear blast and the currents generated across a dike or the contact between two media in the presence of a chemical potential gradient. This approach has the advantage of unifying several apparently unrelated phenomena

and giving quantitative results in each case once the relevant parameters of the medium are measured experimentally.

Underground Nuclear Blast

The first objective of this thesis is a theoretical study of the electrical aftereffects of a buried nuclear explosion and the manifestation of these effects at the surface. It is possible that measurements of blast-generated surface potentials could be used for an on-site inspection procedure.

One of the important aftereffects of an underground blast is the release of a large amount of heat. A one kiloton bomb releases about 5×10^{12} joules (Johnson and al., 1959), and assuming a specific heat of .2 cal/gm-°K and a density of rocks of 2.5 gm/cm³, it is easy to see that a 20KT bomb can heat to the boiling point temperature of water (100°C) all the rocks in a sphere of 175 feet radius and originally at 20°C. But if the explosion is totally contained, even though the released energy is enormous, no appreciable temperature rise will be observed at the surface in a reasonable time of months or even years due to the poor conductivity of the rocks. The dimensionless parameter (Carslaw and Jaeger, 1947) for heat conduction is

$$\Theta = \frac{Kt}{\gamma^2} \quad 1.1$$

where K is the thermal diffusivity and for rocks has a value of about 0.01 cm²/sec; γ is distance in cm; and t is time in seconds. For distances of the order of 100 meters or more, and expressing time in days, the heat diffusion parameter Θ is

$$\Theta \cong 10^{-5} \times t \quad (t \text{ in days})$$

and therefore at these distances, a time scale of years is involved. Consequently for all practical purposes, the thermal disturbances are completely masked at the surface (for an entirely contained explosion) and can not be used directly to detect the presence of a blast. However, studies by Madden and others (Madden and Marshall, 1959; Madden and Cantwell, 1962; see also table 2.4) have shown that rocks can couple efficiently fluid, thermal, and chemical potential gradients into electric potentials. Thermoelectric coupling coefficients for rocks can be as high as 1 mv/°C with average values of about .2-.4 mv/°C. Therefore, a temperature difference of 50 to 100°C can give rise to a very appreciable potential difference.

Another important aftereffect connected with the release of energy is a pressure build-up. Some of the released energy is used up mechanically to fracture the rocks or produce seismic waves; but the greater part of the energy goes into heating up the rocks and turning their pore fluids into steam. How large the pressure builds up and how long it lasts, depends on several factors such as the size of the bomb, the fluid content of the rocks, the permeability, the heat dissipation, and the extent of fracturing. If the blast is wholly contained and the fracturing does not open up large cracks, the only way this excess pressure can dissipate is through diffusion of heat and condensation of the steam, or outward flow of fluids. The first of these two mechanisms is probably unimportant, due to the slow rate of heat diffusion in rocks. But outward flow of fluids is expected to be a very important cause of pressure decrease in many shots. The rate of flow depends on the permeability coefficient which can vary

wildly from one situation to another by as much as seven orders of magnitude (see Table 2.3). Actually, the fracturing opens up many cracks, and increases the effective permeability. It is possible that in certain cases, cracking of the rocks opens up fissures reaching the surface and thus allowing all of the steam to escape into the air. Even in these cases, we can expect a pressure effect, because the pressure inside the cavity will be equal to the atmospheric pressure while the ambient hydrostatic pressure will be much higher. A backflow will then take place. For a shot buried at a depth of 200 meters, this backflow pressure is of the order of tens of atmospheres.

Due to all the various factors mentioned, it is extremely difficult to predict generally, the behaviour of pressure with time for any particular situation, but we can nevertheless get a rough idea of the time scales involved by using the following model. Assume that all the steam inside a spherical cavity of radius r_0 has been released to the air through fractures that reach the surface, and fluid starts flowing into the cavity under the action of a uniform hydrostatic pressure P_0 (we are neglecting the asymmetry due to gravity). This model, although very simple, will give an idea of the time scales involved, and is expected to be useful in certain cases.

The flow of incompressible fluid inside the earth is governed by

$$J = -k \nabla P \quad 1.2$$

$$\nabla^2 P = 0 \quad 1.3$$

where \vec{J} is the rate of flow and K is the permeability of the medium. Solution to 1.3 having spherical symmetry is

$$P = P_0 \left(1 - \frac{r_0^2}{r^2}\right) \quad 1.4$$

where P_0 is the hydrostatic pressure at large distances from the cavity. The total flux across the cavity boundary is

$$Q = - \oint \vec{J} \cdot d\vec{s} = - \kappa \oint \frac{\partial P}{\partial r} (r^2 d\Omega) = - 4\pi \kappa r_0^2 \left(\frac{\partial P}{\partial r}\right)_{r_0} \quad 1.5$$

Substituting from 1.4 into 1.5, we get for the rate of flow of fluid inside the cavity

$$Q = - 4\pi r_0 P_0 \quad 1.6$$

and the time it takes to fill up is approximately

$$t \approx \frac{V}{Q} = \frac{\frac{4}{3}\pi r_0^3}{4\pi \kappa r_0 P_0} = \frac{r_0^2}{3\kappa P_0} \quad 1.7$$

Taking some typical values of $r_0 = 50$ meters, $P_0 = 10$ atmospheres, and $\kappa = 10^{-11}$ MKS, we get

$$t = \frac{2500}{3(10^{-11})(1.01 \times 10^6)} \approx 2.1 \times 10^7 \text{ sec.} = 250 \text{ days}$$

This time constant can vary easily by a factor of 100, and the estimate given here is probably too high because we have neglected the effect of fracturing. This

calculation was done to show that time scales of a few days to even years are possible for the electrokinetic effect.

Rocks have rather large electrokinetic coefficients of the order of a few millivolts per atmosphere—sometimes as high as 30 mv/atm—and therefore a pressure difference of only ten atmospheres is sufficient to give potential differences of 50 millivolts or better.

Other after-effects such as gravity anomaly or seismic disturbances are not discussed here as they have no direct bearing on this thesis. A list of all possible effects and a brief discussion of the importance of each effect is given by T. R. Madden (Madden and Cantwell, 1960; p.7). In many ways the nuclear detection problem is very similar to mining geophysics problems because of the geometry and size of the target, and therefore conventional methods based on classical effects (gravity, resistivity, etc.) could be used. But it differs from mining problems because of the importance of streaming potential and thermoelectric phenomena. Mineralized areas, due to the rather long time scales involved, have reached equilibrium at least as far as temperature and pressure are concerned; but a blast area is far from having reached equilibrium and therefore these pressure and temperature effects play an important role in producing natural currents.

Spontaneous Polarization

The second objective of this thesis is a theoretical and quantitative study of the causes of certain types of spontaneous polarization currents. Spontaneous polarization effect or S. P., which can be produced by many different causes, are well-known and many authors

have discussed qualitatively several of the mechanisms responsible for these potentials (see Dobrin, 1952, p.289 and 378; Heiland, 1946, p.668; Mounce and Rust, 1945; Wyllie, 1949). Most of these explanations depend on oxidation-reduction reactions or concentration cells. One of the more quantitative explanations has been advanced by Sato who shows that the S. P. currents around a sulfide body are intimately connected with ore body, and that spontaneous polarization could take place even if the ore body itself did not undergo any changes and acted only as an inert conductor (Sato and Mooney, 1960). Others, studying the causes of S. P. in drill holes (Wyllie, 1949), attribute the polarization to the presence of a shale layer which acts as an almost perfect semi-permeable membrane and stops all negative ions from diffusing through, while it allows the positive ions to diffuse almost freely.

The methods of irreversible thermodynamics are used here to unify all the various explanations based on electrochemical or electrokinetic couplings. Shale barriers represent an extreme case and may give the largest potentials, but are not indispensable for causing S. P. currents. Any two materials in contact, with dissimilar diffusion rates, will tend to produce S. P. if there is a chemical potential gradient cutting across their common boundary. Oxidation-reduction problems are dealt with in much the same way as concentration diffusion problems. In particular the effects of geometry can be handled very nicely using this approach. Specifically, we have investigated the effect of vertical contacts and dikes on the magnitude of the S. P. anomalies.

Historical Review

The original ideas of this thesis, which are based

on principle of irreversible thermodynamics, were recently suggested by T. R. Madden in connection with the possibility of using electric methods for onsite detection of underground nuclear blasts (Madden and Cantwell, 1960.) Because of the non-equilibrium conditions in the near vicinity of the blast, and the large coupling coefficients of the rocks, it was thought that measurements of electrical aftereffects caused by the coupling of fluid and thermal gradients with electric potentials could be used to detect large underground nuclear blasts. However, it can be assumed that these gradients are confined to depth and vanish on the surface, and it is therefore necessary to undertake a theoretical study of the problem to find out the surface expression of the effects which are produced in the near vicinity of the source. As the research got underway, it became obvious that these same principles could be used to explain some of the causes of spontaneous polarization currents, and the effect of geometry on their magnitudes.

Many of these coupling phenomena have been known for some time but their description based on thermodynamics of irreversible processes is rather recent. Onsager developed his theory of irreversible thermodynamics in 1931 and applied it to the study of chemical monomolecular triangle reactions and heat flow in anisotropic crystals (DeGroot, 1961; Denbigh, 1951). Later on, the theory was applied by DeGroot and others to describe all kinds of coupling of flows such as electrochemical and thermoelectric effects.

Schlumberger and Leonardon (1934a and 1934b) studied the causes of S. P. potentials in bore holes and

concluded that they are due to electrofiltration and electrochemical couplings. They even made some laboratory studies that supported their view. But their theoretical explanation was rather qualitative and based on Nerst's equations for e.m.f. of reversible cells. These equations are of limited application in most cases of spontaneous polarization. Most other authors who have studied this problem, have systematically followed Schlumberger in explaining the cause of S. P. in boreholes.

Mounce and Rust (1945) studied the same problem and showed experimentally that currents can be set up in a system composed of two aqueous salt solutions of different concentrations and a shale layer which acts as a semi-permeable membrane. They supposed that a shale layer is essential to the creation of currents.

Wyllie (1949) took up the same problem but he came up with no new results. He discussed the role of the shale layer and stated that "action of a shale barrier is analogous to a glass membrane separating two acid solutions of different hydrogen ion concentrations. The shale behaves as a sodium electrode and is responsive to the activities of the sodium ions in the two solutions in such a way that the potential can be calculated by means of the Nerst equation." The shale membrane is an extreme case because it stops ions of one sign and only lets through ions of the other sign. Actually for creating electrochemical potential it is only necessary to have an asymmetry in the diffusion rates. Wyllie (1955) also underestimated the effect of geometry and inhomogeneities on S. P. potentials in drill holes and writes "These effects, though serious in electrical log

interpretation, are purely physical. They may be largely overcome...by the application of static (bucked current) S. P. logging techniques..."

Cagniard (1956) considered the role of electro-filtration as a source of spontaneous polarization. He states that this phenomenon is the cause of observed negative anomalies associated with topographic highs.

Kermabon (1956) made some measurements of the electrokinetic coupling and permeability coefficients of rocks and found that, in general, rocks have strong coupling coefficients.

Madden and Marshall (1959) made a systematic study of electrokinetic, thermoelectric, and electrochemical phenomena in connection with causes and background effects of induced polarization phenomenon. To the author's knowledge this is the first application of Onsager's theory to geophysical problems.

Since the importance of coupling phenomena in many geophysical problems has become well established, Madden and Cantwell (1962) have undertaken an extensive program of laboratory measurements of electrokinetic, thermoelectric, and electrochemical coefficients of rocks.

Outline of the Thesis

The Laboratory measurements show how efficiently rocks can couple fluid, thermal, and chemical gradients into electric potentials. This investigation was undertaken to understand better how these coupling phenomena which are confined to the near vicinity of the sources—where the gradients exist—manifest themselves on the surface, and what effects rock inhomogeneities have on the magnitudes of these couplings.

In the first part of Chapter I, the role of electrokinetic and thermoelectric couplings, produced by an underground nuclear blast, are discussed in view of their importance in producing electric currents around the blast area. It is shown that the time scales involved are always of the order of years for the thermoelectric effect and can be of the order of years for the electrokinetic effect. Furthermore, electrochemical and electrokinetic couplings are discussed as possible causes of the spontaneous polarization currents associated with sulfide ore bodies.

In Chapter II, Onsager's phenomenological relations are introduced without any attempt at justifying them. The connection between certain of the phenomenological coefficients and more familiar electrochemical and thermal quantities are discussed. Starting from Onsager's relations, it is shown that the same set of equations and boundary conditions govern the electrokinetic, thermoelectric, and electrochemical couplings in the earth. The effect of the driving pressure (or temperature, chemical potential, etc.) is shown to be equivalent to that of electric dipole sources distributed along the boundaries of the different rock zones.

In Chapter III, the equation governing the coupling of flows is solved for some simple geometries. The geometry is shown to have an essential role in creating spontaneous polarization currents detectable at the surface. It is shown that surface electrical signals arise whenever inhomogeneities in rock properties cut across the equi-pressure (or temperature or chemical potential) surfaces associated with the flow of fluid (or heat or ions). The relevant parameter, on which the

magnitude of the electric potential depends, is the ratio of the coupling coefficient of the rock to its electrical conductivity. Several geometries of horizontally and vertically layered earths are used to compute the thermoelectric, the electrokinetic, and the electrochemical potentials observed on the surface. The effect of geometry on the background S. P. noise is computed for a particularly simple model of vertically distributed random variations in rock properties.

Chapter IV is devoted to the applications of these results to the bomb detection problem. Maximum potentials to be expected from thermoelectric and electrokinetic couplings are computed to get the upper bound for these effects. It is shown that electrokinetic coupling is probably the most important cause of the potentials associated with underground nuclear blasts, while thermoelectric coupling might reinforce these potentials in certain cases. Computed magnitudes of the potentials are of the same order of magnitude as potentials measured during the Nevada underground test shots.

Chapter V is concerned with the spontaneous polarization currents associated with sulfide ore bodies, dikes, and other inhomogeneities. Electrochemical coupling is believed to be the most important cause of these currents at least for small scale effects, with thermoelectric and electrokinetic couplings may be important in certain cases. Coupling phenomena are examined for their role in producing S. P. noise.

Chapter VI is devoted to a brief discussion of some of the problems in electrochemistry and chemical properties of pore fluids which emerge from the investigations of this thesis.

CHAPTER II

REVIEW OF IRREVERSIBLE THERMODYNAMICS

In Chapter I, it was stated that the thermodynamics of irreversible processes can be used advantageously to study a whole host of apparently unrelated phenomena. Spontaneous polarization and electric currents generated by thermal gradients in non-mineralized areas are examples. In section I of this chapter, Onsager's theory of irreversible thermodynamics is introduced in a very qualitative way with emphasis on the meaning of the theory rather than the origin and proof of the theory.

The remaining sections of this chapter are concerned with the forces and flows in Onsager's theory and their application to study of coupling effects in the earth.

Section I - Onsager's Relations

Classical thermodynamics—which could more properly be called thermo-statics—deals with states of equilibrium, and modern irreversible thermodynamics as developed by Onsager, DeGroot, and others deals with states of non-equilibrium, when the system under consideration is displaced from equilibrium and flows are taking place. This theory has had its greatest successes in the study of steady-state time invariant systems, but it has been also useful in the study of slowly varying systems for small flow densities.

By analogy with dynamics, Onsager regards the processes of diffusion, heat flow, matter flow, and current flow as being representable in terms of velocities and "thermodynamic forces" which are the negative gradients of temperature

of chemical potential, etc., and depend on how far the system is displaced from equilibrium. For example, in the flow of electricity, the velocity is equal to the current density \vec{J} and the force is the negative gradient of the electric potential $-\nabla\phi$. When these flows take place separately, they are governed by the well-known empirical relations

$$J_Q = -K \nabla T \quad (\text{Fourier's Law}) \quad 2.1$$

$$J_s = -K' \nabla P \quad (\text{Darcy's Law}) \quad 2.2$$

$$J_M = -D \nabla C \quad (\text{Fick's Law}) \quad 2.3$$

$$J = -\sigma \nabla \phi \quad (\text{Ohm's Law}) \quad 2.4$$

where J_Q , J_s , J_M and J are flows of heat, solvent, matter, and current; ∇T , ∇P , ∇C and $\nabla \phi$ are gradients of temperature, pressure, concentration, and electric potential; K , K' , D and σ are generalized conductivities. Therefore, in general, if J is the rate of flow, X is the force, and L is a scalar quantity, there is an empirical linear relationship of the form

$$J = L X \quad 2.5$$

where L has the significance of "conductivity."

When two, three, or more flows take place simultaneously, there is interference and coupling between these flows. Peltier effect (evolution of heat at junctions of metals due to flow of an electric current) and the thermoelectric force (e.m.f. resulting from the maintenance of the junctions at different temperature) are well-known examples of such coupling between two flows. When several processes take place simultaneously,

equations of the form 2.5 are inadequate to describe the flows and in the absence of proof to the contrary, it must be assumed that each flow depends on all the forces

$$J_i = f_i(X_1, X_2, \dots, X_n) \quad 2.6$$

For a complete discussion of these coupling effects, the reader is referred to Callen (1960), DeGroot (1961), Denbigh (1951), Fitts (1962) and Prigogine (1955). Only the most important results are listed here.

The first postulate of thermodynamics of irreversible processes is that in a system in which several flows are taking place simultaneously due to the action of several forces X_i , it is possible to express each flow as a linear combination of all these forces:

$$J_i = \sum_j L_{ij} X_j \quad 2.7$$

These equations are called the phenomenological relations or thermodynamic equations of motion. Remembering that in the absence of all forces, the flows are zero, it is easy to see that the equation 2.7 is a Taylor's series expansion of equation 2.6 approximated to the first linear term. The assumption of linearity is by no means obvious, and needs to be verified in each case. In general, it is valid when the system is displaced only slightly from equilibrium, but terms of higher orders should be included when the system is far from equilibrium. An approach to include non-linear terms is indicated in Prigogine (1955, p.93). It seems, however, that except in the study of rates of chemical reactions, one is never too far from equilibrium and therefore the linear approximation is a

good one. Equation 2.7 states that each flow is caused by contribution of all forces through the phenomenological coefficients L_{ij} . The coefficients L_{ji} are for example the heat conductivity, the ordinary diffusion coefficient and the electrical conductivity. The coefficients L_{ij} with $i \neq j$ are the coupling or "drag" coefficients (DeGroot, 1961).

The second postulate is the principle of microscopic reversibility which is at the basis of Onsager's theorem. For a complete discussion of the principle of microscopic reversibility, the reader is referred to DeGroot (1961), Denbigh (1951) and Prigogine (1955). Onsager's theorem states that: If the forces and flows are chosen in such a way that the sum of the products $J_i X_i$ adds up to the rate of creation of entropy multiplied by the temperature, the matrix of phenomenological coefficients is symmetric

$$\text{If} \quad T \frac{dS}{dt} = \sum J_i X_i \quad 2.8$$

$$\text{Then} \quad L_{ij} = L_{ji} \quad 2.9$$

This result implies that there is a symmetry in the coupling of the various processes. The choice for these flows and forces will be indicated later on. Onsager's relations $L_{ij} = L_{ji}$ which have been proved in the case of fluctuations about equilibrium, are assumed to be valid in case of irreversible flows for small flow densities. Onsager's theory does not indicate whether or not the thermodynamic equations of motion are correct. In each case it has to be found by experiment whether or not these equations are a good approximation, and in particular it has to be shown that the forces X_i which

satisfy equations 2.7 and 2.8 are those to which the flows are in practice proportional.

Section II - Forces and Flows in Onsager's Relations

The two postulates of irreversible thermodynamics, leave a great latitude for the choice of flows and forces; as a matter of fact, there are differences among various authors in the choice of the various flows and forces. Here we shall follow Denbigh as modified by Eckardt and Callen (DeGroot, 1961, p.28; Madden and Marshall, 1951, p.23). For the processes which are of interest to us:

	<u>Flow</u>		<u>Force</u>
Heat	J_Q	calories/cm ² -sec	$-\nabla T$
Solvent	J_S	cm ³ /cm ² -sec	$-\nabla P$
Matter	J_3, J_4, \dots	mols/cm ² -sec	$\begin{cases} -\nabla\mu - Fz\nabla\phi & (\text{ionic}) \\ -\nabla\mu & (\text{non-ionic}) \end{cases}$

ϕ = electrical potential μ = chemical potential
 T = temperature F = Faraday's constant
 P = pressure z = ionic valence

The current flow is not shown explicitly in the above equations, because in electrolytic solutions, the current flow is not independent of the flow of matter, but is a linear combination of the anionic and cationic flows

$$I = F \sum_i z_i J_i \quad (i=3,4,\dots) \quad 2.10$$

In the above equations, we have followed Eckardt in defining the "heat flow" vector (DeGroot, 1961) as

$$J_Q = J_E - \mu J_M$$

where J_E is the total "energy flow" and J_m is the matter flow. In the absence of matter flow the distinction between heat flow and energy flow is irrelevant.

Assuming that the matter flow consists of only one cathionic flow J_p and one anionic flow J_n , we can write Onsager's relations in the following matrix form

$$\begin{bmatrix} J_Q \\ J_S \\ J_p \\ J_n \end{bmatrix} = \begin{bmatrix} L_{11} & L_{12} & L_{13} & L_{14} \\ L_{21} & L_{22} & L_{23} & L_{24} \\ L_{31} & L_{32} & L_{33} & L_{34} \\ L_{41} & L_{42} & L_{43} & L_{44} \end{bmatrix} \begin{bmatrix} -\nabla T/T \\ -\nabla P \\ -\nabla\mu_p - Fz_p \nabla\phi \\ -\nabla\mu_n - Fz_n \nabla\phi \end{bmatrix} \quad 2.11$$

The extension to the more general case of many ionic flows is straight-forward. From equations 2.11, the possible magnitudes of coupling effects can be deduced in terms of the coupling coefficients L_{ij} . As an example, consider a piece of some material in form of a rod, the two ends of which are kept at different temperatures and the sides are insulated. Neglecting dependance of $\nabla\mu$ on temperature and assuming all forces except ∇T and $\nabla\phi$ are zero, we get:

$$J_p = -L_{31} \frac{\nabla T}{T} - F(L_{33}z_p + L_{34}z_n) \nabla\phi \quad 2.12$$

$$J_n = -L_{41} \frac{\nabla T}{T} - F(L_{43}z_p + L_{44}z_n) \nabla\phi \quad 2.13$$

and current

$$I = -F(L_{31}z_p + L_{41}z_n) \frac{\nabla T}{T} - F^2[L_{33}z_p^2 + (L_{34} + L_{43})z_pz_n + L_{44}z_n^2] \nabla\phi \quad 2.14$$

when there is no current flow, we get

$$\left(\frac{\nabla\phi}{\nabla T}\right) = \frac{-1}{FT} \frac{L_{31}Z_p + L_{41}Z_n}{L_{33}Z_p^2 + (L_{34} + L_{43})Z_pZ_n + L_{44}Z_n^2} \quad 2.15$$

this is the thermoelectric power describing the potential per unit of temperature difference under the condition of zero electrical current.

Many of the coefficients L_{ij} have been measured in other studies. For instance, the solvent-electric current flow coupling coefficients are well known from studies by geophysicists of streaming potential and electro-osmosis because of their effects on self-potentials in drill-holes (Wyllie, 1955).

The coupling effects between solute flow and electric current known as diffusion potential are also well known because of their great importance in electrochemistry. The thermoelectric properties are less well known, but a great effort is being made to study them because of the possible application in direct energy conversion. Many measurements of electrokinetic and thermoelectric coefficients have been made by Madden and his group (Kermabon, 1956; Madden and Marshall, 1959; Madden and Cantwell, 1962).

Section III - Discussion of the Coefficients L_{ij}

In this section we discuss the physical significance of some of the phenomenological coefficients, and their relationship to the more familiar electrochemical and thermal quantities.

Section IIIa - Mobility

The mobility u^0 is defined as the speed of an ion

in infinite dilution under a unit electric field when all other forces are zero. The velocity of a positive ion is given by \bar{J}_p/C_p and that of a negative ion is given by $-\bar{J}_n/C_n$ where \bar{J}_p and \bar{J}_n are in moles/cm²-sec, and C_p and C_n are concentrations in moles/cm³. The minus sign for negative ions is necessary since they move in the opposite direction under the same electric field. From equations 2.11, we find

$$U_p = \left(\frac{\bar{J}_p}{C_p} \right)_{\substack{\nabla\phi=-1 \\ \nabla P=\nabla T=\nabla\mu=0}} = \frac{F(L_{33}Z_p + L_{34}Z_n)}{C_p} \quad 2.16$$

$$U_n = \left(\frac{-\bar{J}_n}{C_n} \right)_{\substack{\nabla\phi=-1 \\ \nabla P=\nabla T=\nabla\mu=0}} = \frac{-F(L_{43}Z_p + L_{44}Z_n)}{C_n} \quad 2.17$$

In practice for dilute solutions, the coupling coefficients L_{34} and L_{43} are small compared to coefficients L_{33} and L_{44} , and we have therefore

$$U_p \approx \frac{FL_{33}Z_p}{C_p} \quad U_n \approx -\frac{FL_{44}Z_n}{C_n} \quad 2.18$$

In Table 2.1 typical values of ionic mobility at 25°C at infinite dilution are listed (Glasstone, 1954; p.60):

Table 2.1 - Ionic Mobility u at 25°C (cm/sec)

H^+	36.2×10^{-4}	OH^-	20.5×10^{-4}
K^+	7.6×10^{-4}	SO_4^{--}	8.3×10^{-4}
B_a^+	6.6×10^{-4}	CP^-	7.9×10^{-4}
N_a^+	5.2×10^{-4}	NO_3^-	7.4×10^{-4}
L_i^+	4.0×10^{-4}	HCO_3^-	4.6×10^{-4}

These values of ionic mobilities indicate that, apart from hydrogen and hydroxyl ions, most other ions have comparable velocities around 4 to 8×10^{-4} cm/sec., therefore, one would expect that hydrogen and hydroxyl ions may contribute heavily to the current flow and electrochemical coupling. But as we shall see in Section IVd of this chapter, when several ionic flows are taking place simultaneously, the contribution of each ion to the current flow depends on its concentration gradient as well as its mobility. In general, the concentrations of hydrogen and hydroxyl ions are very low compared to other ions such as Ca^{++} , K^+ , Na^+ and therefore, contribute little to actual current flow.

Section IIIb - Electrical Conductivity

Electrical conductivity σ is the conductivity due to an electric field $-\nabla\phi$ when all other forces are zero, and it is given by equation 2.10. Inserting J_p and J_n from 2.11 into 2.10 and using Ohm's law

$$I = - \sigma \nabla \phi \quad 2.19$$

we get

$$\sigma = F^2 (L_{33} Z_p^2 + (L_{34} + L_{43}) Z_p Z_n + L_{44} Z_n^2) \cong F (Z_p C_p U_p - Z_n C_n U_n) \quad 2.20$$

Section IIIc - Thermal Conductivity

In the absence of all forces except for temperature gradient, the flow of heat is governed by Fourier's law which states that heat flow in cal/cm^2 is proportional

to the temperature gradient

$$J_Q = -K \nabla T \quad 2.21$$

Comparing equation 2.21 with equation 2.11, we see that for $\nabla P = \nabla \mu = \nabla \phi = 0$ we have

$$K = \frac{L_{11}}{T} \quad 2.22$$

but in general the chemical potential μ depends strongly on temperature and therefore the relationship is more complicated. Taking into account the dependance of μ on temperature and ignoring for the present time its dependance on pressure and concentration, we can write

$$\nabla \mu_i \cong \frac{\partial \mu_i}{\partial T} \nabla T = -TS_i \frac{\nabla T}{T} \quad 2.23$$

where S_i is the partial molal entropy. Inserting 2.23 in 2.11, we get for heat flow

$$J_Q = - (L_{11} - L_{13} TS_p - L_{14} TS_n) \quad 2.24$$

Therefore

$$K = + \left(\frac{L_{11}}{T} - L_{13} S_p - L_{14} S_n \right) \quad 2.25$$

Even though the thermal force in Onsager's equation is $-\nabla T/T$, we have assumed tacitly that the coefficient K rather than L_{11} is a constant. This is an agreement with the empirical equation 2.1. Actually, this assumption is not always true and for some material the coefficient K decreases with increasing temperature which

would indicate L_{11} is more nearly constant, but anyhow in our arguments, none of these coefficients are required to be strictly constant.

In Table 2.2, the thermal properties of some common substances are listed (Carslaw and Jaeger, 1947; p.382). Thermal conductivity K is given in calories/cm-sec-°C and thermal diffusivity κ ($= \frac{K}{\rho c}$ where ρ is the density and c is the specific heat) is given in cm²/sec.

Table 2.2 - Thermal Properties of Some Common Substances
(C.G.S. Units)

Substance	Conductivity K	Diffusivity $\kappa = \frac{K}{\rho c}$
Copper	0.93	1.14
Air	0.000058	0.187
Granite	0.006	0.011
Limestone	0.004	0.007
Sandstone	0.006	0.011
Soil (average)	0.0023	0.0046
Water	0.00144	0.00144

Thermal diffusivity is the parameter on which the rise in temperature depends. This is so because a material must not only have a high thermal conductivity, but it must also have a very low specific heat coefficient. Otherwise, much of the heat that is traversing a unit volume will be used to raise its temperature and very little will be passed to the next unit of volume. The values shown in Table 2.2 indicate that the diffusivity in rocks is very small and therefore the heat distribution in rocks is quasi-static when our length dimensions are of the order of 10^4 or 10^5 cm. A given picture of heat distributions is expected to remain essentially the same

over a period of days, months or even years as we already have shown in Chapter I. For instance, in the case of an underground nuclear blast, the zone of high temperature which might be 150 feet in radius will not change by more than a few per cent over a period of a year or two. This point is essential to the usefulness of the arguments presented in this thesis, otherwise, the effects would be so short lasting that they would be of no practical application.

For other equations relating diffusion coefficient, transport number, and Einstein's relation to phenomenological coefficients L_{ij} , the reader is referred to Madden (Madden and al., 1957, p.24-27).

Section IV - Application of Irreversible Thermodynamics to Study Coupling Effects in the Earth

Equation 2.11 is used in this section to derive specific equations for coupling of a pair of flows. Strictly speaking, it is impossible to isolate a pair of flows and their corresponding forces, because the presence of a gradient X will cause, through coupling, the establishment of other potential gradients and flows as well. Nevertheless, this assumption is believed to be a good one, because it allows us to isolate one effect at a time and study it in detail. Then for the case of several couplings, it is easy to superimpose the effects since equation 2.11 is linear.

In one-dimensional flow studies, the formal solution of the coupling equations is straight forward, and it is further simplified because one of the flows is usually assumed to be zero. In studying coupling effects in the earth, we are, in general, forced to work in three

dimensions, and furthermore, we are often interested in transient conditions. In what follows, we shall assume that the time scale for electric current is much shorter than the time scale for diffusion, heat, and solvent flow, so that the charge distribution is set up instantaneously. With this assumption, we have in the absence of electrical sources

$$\nabla \cdot \mathbf{I} = 0 \quad 2.26$$

Section IVa - Electrokinetic Coupling

To investigate the effect of electrokinetic coupling on currents generated in the earth, we shall assume all forces except the driving force $-\nabla P$ and the induced force $-\nabla \phi$ are zero. The dependance of μ on pressure can be neglected (Marshall, 1959; p.33). Combining J_p and J_n to give the current flow \mathbf{I} , we get

$$J_s = -L_{22} \nabla P - L'_{23} \nabla \phi \quad 2.27$$

$$\mathbf{I} = -L_{32} \nabla P - L'_{33} \nabla \phi \quad 2.28$$

where

$$\begin{aligned} L'_{22} &= L_{22} & L'_{23} &= L'_{32} = F(L_{23} Z_p + L_{24} Z_n) \\ L'_{33} &\equiv \sigma = F^2 (L_{33} Z_p^2 + 2L_{34} Z_p Z_n + L_{44} Z_n^2) \end{aligned} \quad 2.29$$

Here we have used Onsager's relations 2.9. The meaning of the coefficients in equations 2.27 and 2.28 are given here.

$$L'_{33} = \left(\frac{\mathbf{I}}{-\nabla \phi} \right)_{\nabla P=0} = \text{electrical conductivity } \sigma$$

$$L'_{22} = \left(\frac{J_s}{-\nabla P} \right)_{\nabla \phi = 0} = \text{permeability } K$$

$$-\frac{L'_{32}}{L'_{22}} = \left(\frac{\nabla \phi}{\nabla P} \right)_{I=0} = \text{streaming potential coefficient}$$

$$-\frac{L'_{23}}{L'_{22}} = \left(\frac{\nabla P}{\nabla \phi} \right)_{J_s=0} = \text{electro-osmotic coefficient}$$

Onsager's relation $L'_{23} = L'_{32}$ allows us to get both streaming potential and electro-osmotic coefficients from one single measurement of coupling effect.

Experimental data on streaming potential coefficients are scarce, but recently Madden and his group have made systematic measurements of streaming potential on rock samples (Kermabon, 1957; Madden and Marshall, 1959; Madden and Cantwell, 1962). In Table 2.3 are listed the summary of the measurements made on rocks by Kermabon, and Madden, and on clays by Olsen. These measurements were made using tap water. At the present time these studies are being continued to determine the effects of variations in salinity on the streaming potential in geologic materials.

From the magnitudes of the streaming potential coefficients in Table 2.3, we see that electrokinetic couplings can be very important in the earth. Streaming potential coefficients for geologic materials are as high as 10 or 20 mv/atm., and under favorable conditions even a pressure difference of only a few atmospheres can produce detectable differences of potentials of a few hundred millivolts. These favorable conditions depend largely on the geometry which will be discussed in the following chapter.

Table 2.3 - Electrokinetic Constants of Rock Samples and Natural or Artificial
Fine-Grained Materials (M.K.S. Units)

Rock Type	Sample Code*	Permeability L_{22}	Conductivity L_{33}	Streaming Potential (mv/atm.)	Investigator
Sedimentary Rocks Colorado Plateau	Y4	1.4×10^{-14}	Madden, Cantwell, Chapman, and Green "
	Y7	1.8×10^{-9}	3.0×10^{-3}	...	
	Y7B	8.6×10^{-10}	
	Y18	6.4×10^{-13}	
	Y34	9.0×10^{-11}	
	Y36	2.3×10^{-11}	
	Y38	3.1×10^{-14}	9.4×10^{-3}	...	
	Y41	2.4×10^{-14}	7.4×10^{-3}	...	
	Y49	2.6×10^{-14}	4.7×10^{-3}	...	
	Y52	3.0×10^{-10}	
Altered Volcanics Arizona	SA 7	1.6×10^{-10}	1.3×10^{-2}	...	"
	SA 8	5.9×10^{-15}	1.2×10^{-3}	...	"
	SA 9	1.8×10^{-10}	5.6×10^{-4}	...	"
	SA 14	9.4×10^{-13}	8.6×10^{-3}	...	"
	SA 24	2.5×10^{-11}	"
	SA 27	5.0×10^{-13}	"
	SA 29	1.2×10^{-11}	"
	SA 31	9.8×10^{-12}	4.3×10^{-3}	...	"
	SA 36	3.0×10^{-11}	"
	SA 40	2.1×10^{-12}	"
Quartz-Latite Porphyry, New Mexico	BC 3	1.1×10^{-15}	"
	BC 4	2.6×10^{-15}	"
	BC 9	3.2×10^{-15}	"
	BC 10	5.0×10^{-15}	"

Dakota Sandstone	S 2	...	8.9 X 10 ⁻¹³	1.7 X 10 ⁻²	8.8	"
	S 3	...	1.2 X 10 ⁻¹³	9.0 X 10 ⁻³	1.42	"
	S 7	...	2.0 X 10 ⁻¹²	2.7 X 10 ⁻³	22.6	"
	S 10	...	2.3 X 10 ⁻¹²	5.6	"
	S 21	...	2.1 X 10 ⁻¹⁴	3.5	"
	S 22A	...	9.3 X 10 ⁻¹⁴	1.7	"
Ophytic Trap Rock, Michigan	C&H A-4	...	4.2 X 10 ⁻¹⁵	1.0 X 10 ⁻³	3.87	"
	C-10	...	2.9 X 10 ⁻¹⁰	4.7	"
Metamorphics Ontario	N 7	...	2.0 X 10 ⁻¹⁴	1.4 X 10 ⁻³	12.0	"
	N 12	...	8.0 X 10 ⁻¹⁵	3.7 X 10 ⁻⁴	5.11	"
	N 18	...	1.9 X 10 ⁻¹⁴	2.6 X 10 ⁻⁴	11.7	"
	N 31	...	1.1 X 10 ⁻¹⁴	0.81	"
	N 37	...	4.6 X 10 ⁻¹²	15.	"
Quartz Sandstone Limestone Quartz Sandstone Red Sandstone Shale	3.8 X 10 ⁻¹⁴	1.9 X 10 ⁻³	8.	Kermabon
	1.9 X 10 ⁻¹⁵	1.3 X 10 ⁻³	2.	"
	1.7 X 10 ⁻¹¹	5.9 X 10 ⁻³	9.	"
	2.7 X 10 ⁻¹⁴	1.9 X 10 ⁻³	5.5	"
	3.0 X 10 ⁻¹⁶	1.7 X 10 ⁻³	1.	"
Kaolinite (dispersed, Na) Kaolinite (Natural flocculated, Ca) Kaolinite (flocculated, .1N NaCl)	30.	Olsen
	17.	"
	0.7	"

*These are the sample codes used by T. R. Madden.

The continuity equation for incompressible solvent flow is

$$\nabla \cdot \mathbf{J}_s = S(\vec{r}, t) \quad 2.30$$

This equation, which is valid for uncoupled flows, remains valid when couplings are present as long as \mathbf{J}_s , represents the total contributions due to all thermodynamic forces (DeGroot, 1961; p.95).

Equations 2.26, 2.27, 2.28, 2.30 and the boundary conditions on the continuity of potentials and normal components of flows are sufficient to solve for any geometry by standard techniques used in solving boundary-value problems. But this would cause unnecessary difficulties because we have two coupled partial differential equations with coupled boundary conditions. A great simplification can be obtained if we remember that ∇P is the cause and $\nabla \phi$ is the effect, and while we have to keep both terms on the right hand side of the equation 2.28, we can neglect the second term on the right hand side of equation 2.27 ($L'_{22} \nabla P \gg L'_{23} \nabla \phi$). A quick calculation will convince us of the validity of this assumption. Taking some typical values from Table 2.3, we have

$$\begin{aligned} L'_{22} &= 10^{-15} \text{ (MKS)} \\ L'_{23} &= L'_{32} = 10^{-10} \text{ (MKS)} \\ L'_{33} &= 10^{-3} \text{ (MKS)} \\ \Delta P &= 5 \text{ atm} = 5 \times 10^5 \text{ (MKS)} \\ \Delta \phi &= 50 \text{ mv} = 5 \times 10^{-2} \text{ volts (MKS)} \end{aligned}$$

therefore

$$L_{22}' \Delta P = 5 \times 10^{-10}$$

$$L_{23}' \Delta \phi = 5 \times 10^{-12}$$

$$L_{32}' \Delta P = 5 \times 10^{-5}$$

$$L_{33}' \Delta \phi = 5 \times 10^{-5}$$

From these calculations, it is clear that $L_{23}' \Delta \phi$ is much smaller than $L_{22}' \Delta P$ while $L_{32}' \Delta P$ is comparable to $L_{33}' \Delta \phi$. This amounts to uncoupling the solvent flow equation. We then get

$$J_s \cong - L_{22}' \nabla P \quad 2.31$$

$$I = - L_{33}' \nabla f \quad 2.32$$

where f is defined as the sum of electric potential ϕ and the potential induced through coupling

$$f = \phi + \left(\frac{L_{32}'}{L_{33}'} \right) P \quad 2.33$$

and using 2.26, we get the equation satisfied by f

$$\nabla^2 f = 0 \quad 2.34$$

Equation 2.31 for the solvent flow is separated and can be solved by straight forward methods. Equation 2.32 gives the current flow in terms of a potential f which we shall call the "total electric potential" and is made up of the ordinary potential ϕ and a contribution due to coupling $(L_{32}'/L_{33}')P$. Potential f satisfies the Laplace's equation in each medium, but its value on the

boundary depends on ϕ and P , which amounts to saying that f is caused by sources distributed along the boundaries. Equation 2.33 shows clearly the dependance of f on the streaming potential coefficient (L_{32}'/L_{33}').

In the next two sections of this chapter, similar equations are derived for the thermoelectric and electrochemical coupling cases and are shown to be identical to equations 2.32, 2.33, and 2.34.

Section IVb - Thermo-Electric Coupling

A similar analysis is used to investigate the thermoelectric coupling effect, but as we pointed out when discussing thermal conductivity K , the thermoelectric coupling is slightly more complicated because of the role played by the chemical potentials. Using equations 2.11 and 2.23, we can write

$$J_Q \cong -L_{11}' \nabla T - L_{13}' \nabla \phi \quad 2.35$$

$$I = -L_{31}' \nabla T - L_{33}' \nabla \phi \quad 2.36$$

where :

$$\begin{aligned} L_{11}' &= \left[\frac{L_{11}}{T} - L_{13} S_P - L_{14} S_n \right] \\ L_{13}' &= F [L_{13} Z_P + L_{14} Z_n] \\ L_{31}' &= F \left[\frac{L_{31} Z_P + L_{41} Z_n}{T} - (L_{33} Z_P + L_{43} Z_n) S_P - (L_{43} Z_P + L_{44} Z_n) S_n \right] \\ L_{33}' \cong \sigma &= F^2 [L_{33} Z_P + 2 L_{34} Z_P Z_n + L_{44} Z_n^2] \end{aligned} \quad 2.37$$

In this case the coefficients L_{13}' and L_{31}' are not equal, and, therefore, one single measurement of coupling effect is not enough to give us both coefficients, but rather

two distinct measurements of thermoelectric e.m.f. and Peltier heat are necessary

$$L'_{11} = \left(\frac{J_Q}{-\nabla T} \right)_{\nabla \phi = 0} = \text{thermal conductivity } K$$

$$-\frac{L'_{31}}{L'_{11}} = \left(\frac{\nabla \phi}{\nabla T} \right)_{I=0} = \text{thermoelectric e.m.f. } \Theta$$

$$-\frac{L'_{13}}{L'_{11}} = \left(\frac{J_Q}{I} \right)_{\nabla T=0} = \text{Peltier heat } \pi$$

In Table 2.4 are listed some of the measured thermoelectric coefficients for geologic materials (Madden, 1962). These measurements were made by comparing the voltage developed across the rock sample when a temperature gradient exists, to that developed across a tube of water to eliminate the temperature effect on the recording electrodes. Therefore, these values represent only the difference in the coupling coefficients of the rock and water, and the actual coefficients cannot be known without a knowledge of the thermoelectric properties of water. But as we shall see later on, we are only interested in the differences in coupling properties.

Table 2.4 - Measured Thermoelectric Coupling Differences

Rock Type	Code Sample*	Thermoelectric coefficient**
Sedimentary Rocks Colorado Plateau	Y4	.257
	Y7B	.475
	Y9	.002
	Y18	.152
	Y34	.107
	Y36	.135
	Y41	.068
	Y49	.228
	Y52	.158

	SA 7	.195
	SA 8	.196
	SA 9	.348
Altered Volcanics	SA 14	.120
Arizona	SA 27	1.36
	SA 29	.070
	SA 31	.076
	SA 37	.350
	SA 40	.449
	BC 3	.268
	BC 4	.150
Quartz-Latite	BC 5	.444
Porphyry, New Mexico	BC 9	.375
	BC 10	.184
	S 2	-.086
	S 3	.108
Dakota Sandstone	S 7	.081
	S 10	.243
	S 21	1.12

*Samples codes are those used by T. R. Madden

**Values listed represent the difference between the thermoelectric coefficients of rock samples and water.

From the data in the above table, it is obvious that the thermoelectric effect can be very important. A temperature difference of 100°C can produce sizeable anomalies of 20 to 100 millivolts. This explains why at the present time so much effort is spent in studying the thermoelectric effect for direct energy conversion. However, for the case of an underground nuclear blast, this effect is believed to be less important than the streaming potential effect because of the even larger electrokinetic coupling coefficients.

For similar reasons to those given in Section IVa, the continuity equation for heat flow

$$\nabla \cdot \mathbf{J}_q + \rho c \frac{\partial T}{\partial t} = Q(\vec{r}, t) \quad 2.38$$

remains valid when couplings are present. Furthermore, making the assumption $L'_{11} \nabla T \gg L'_{12} \nabla \phi$ when temperature T is the driving force, we get

$$J_Q \cong -L'_{11} \nabla T \quad 2.39$$

$$I = -L'_{33} \nabla f \quad 2.40$$

where f is related to T and ϕ by the relation

$$f = \phi + \left(\frac{L'_{31}}{L'_{33}} \right) T \quad 2.41$$

and satisfies the Laplace's equation

$$\nabla^2 f = 0 \quad 2.42$$

Clearly, equations 2.40 and 2.42, giving the current flow when thermoelectric couplings are present, are identical with equations 2.32 and 2.34 which give the current flow when electrokinetic couplings are present. A quick calculation will convince us that the assumption $L'_{11} \nabla T \gg L'_{12} \nabla \phi$ is a good one. Taking some typical values

$$\begin{aligned} L'_{11} &= 2.5 \text{ joules/m-sec-}^\circ\text{C} \\ L'_{12} &\cong L'_{21} T = \left(\frac{L'_{21}}{L'_{33}} \right) L'_{33} T = 1.75^\circ\text{C/volt} \\ \Delta T &= 80^\circ\text{C} \quad \Delta \phi = 0.1 \text{ volt} \end{aligned}$$

we get

$$L'_{11} \Delta T = 200 \quad \text{and} \quad L'_{12} \Delta \phi = .175$$

This last assumption is very helpful because it decouples the equations 2.38 and 2.39 for heat flow (but not the

equations 2.40 and 2.42 for current flow, because f depends on both ϕ and T .), and therefore, we can solve the heat flow problem by standard methods and use the results to obtain the induced current flow.

Section IVc - Electrochemical Coupling

In both electrokinetic and thermoelectric couplings, the flow of current depended on cross-coupling terms L_{31} and L_{31}' , but it is a quite different matter when diffusion of ions is taking place. This is because the ions themselves carry the electric current, so that the coupling is direct, concentration gradients and electrical potential gradients appear together as the driving force. We then have

$$J_p = -L_{33} \nabla \mu_p - L_{34} \nabla \mu_n - F(L_{33} Z_p + L_{34} Z_n) \nabla \phi \quad 2.43$$

$$J_n = -L_{43} \nabla \mu_p - L_{44} \nabla \mu_n - F(L_{43} Z_p + L_{44} Z_n) \nabla \phi \quad 2.44$$

As stated above the direct coupling effects are so important that the cross-terms can be neglected. We further assume $\mu_p \approx \mu_n$, since the concentrations of the positive and the negative ions can not be very different, otherwise, tremendous electric fields would be set up (this is true only when two kinds of ion, one positive and one negative are present). (The more general case is discussed later on.) With these assumptions, we have

$$I \approx -F(L_{33} Z_p + L_{44} Z_n) \nabla \mu - F^2(L_{33} Z_p^2 + L_{44} Z_n^2) \nabla \phi \quad 2.45$$

where the chemical potential μ is

$$\mu_i = \mu_{oi} + RT \ln C_i \quad 2.46$$

Using equation 2.26, we get

$$I = - L_{33} \nabla f \quad 2.47$$

where

$$f = \phi + \frac{L_{33}Z_p + L_{44}Z_n}{F(L_{33}Z_p^2 + L_{44}Z_n^2)} \mu \quad 2.48$$

and

$$\nabla^2 f = 0 \quad 2.49$$

The above equations are in essence identical to equations governing electrokinetic and thermoelectric couplings. The coefficient multiplying μ in equation 2.48 can be considered as the electrochemical diffusion coupling coefficient.

It is remarkable that the equations governing all three effects are identical and therefore all three effects can be studied together. The actual difference between the three effects is in the physics of the problem which results in different kinds of boundary conditions.

Section IVd - Several Ionic Flows

We can still neglect the cross-coupling terms when several ionic species are present. Using 2.46, we have

$$J_i \cong -L_i \nabla \mu_i - FL_i z_i \nabla \phi \quad 2.50$$

$$\nabla \mu_i \cong RT \frac{\nabla C_i}{C_i} \quad 2.51$$

$$L_i \cong \frac{u_i C_i}{F z_i} \quad 2.52$$

where

$$\begin{aligned} i &= \text{ion of the } i\text{th kind} & z_i &= \text{charge of } i\text{th ion} \\ u_i &= \text{mobility} & C_i &= \text{concentration} \\ L_i &= L_{ii} \quad (i = 3, 4, \dots, n) \end{aligned}$$

Current flow I is given by

$$I = -F \sum L_i z_i \nabla \mu_i - F^2 (\sum L_i z_i^2) \nabla \phi \quad 2.53$$

Using 2.51 and 2.52, we get

$$I = -F^2 (\sum L_i z_i^2) \left[\nabla \phi + \frac{RT}{F} \frac{\sum u_i \nabla C_i}{\sum u_i C_i z_i} \right] \quad 2.54$$

which indicates that the contribution to the current flow by each ion is a "weighted" average of its mobility and concentration gradient. The ion with the greatest mobility and concentration gradient contributes most of the current flow.

Section IVE - Summary of Coupling Equations

Starting from Onsager's relationships, we were able to derive a generalized equation for the current flow due to electrokinetic, thermoelectric, or electrochemical coupling. For each medium we have:

$$I = -L'_{33} \nabla f \quad 2.55$$

$$\nabla^2 f = 0 \quad 2.56$$

and the electric potential ϕ is given by

$$\phi = f - cY \quad 2.57$$

Using the boundary conditions for the continuity of electric potential ($\phi_1 = \phi_2$) and normal component of current flow ($\vec{J}_1 \cdot \vec{n} = \vec{J}_2 \cdot \vec{n}$) we can write the boundary conditions for f :

$$f_1 - f_2 = (c_1 - c_2) Y_{12} \quad 2.58$$

and

$$\sigma_1 \frac{\partial f_1}{\partial n} = \sigma_2 \frac{\partial f_2}{\partial n} \quad 2.59$$

where subscripts 1 and 2 refer to the two media in contact; Y is the generalized driving potential (P, T or μ); Y_{12} is the value of this potential at the boundary (P, T and μ are continuous at the boundary); f is the "total electric potential" giving rise to current flows; σ ($= L'_{33}$) is the conductivity; and c is the ratio of the cross-term to electrical conductivity. We shall call c the "coupling coefficient."

Potential f is uniquely determined by the equation 2.56 and the two boundary conditions 2.58 and 2.59. It is important to note that the driving potential Y enters only in the boundary condition 2.58 through its value at the boundary Y_{12} , and its value inside each medium is immaterial. In other words, the generation of currents depends essentially on interaction between the equipotential surfaces and the boundaries. This interaction creates a series of "sources" at the boundaries. Therefore, we can expect that the geometry of the coupling differences will play a dominant part in the magnitude and the distribution of the observed effects, while other factors such as the geometrical distribution of conductivities will influence much less the electric potential picture.

CHAPTER III

THEORETICAL SOLUTIONS FOR SOME SIMPLE GEOMETRIES

In the previous chapter, using the principles of the thermodynamics of irreversible processes, we derived the equations for the potential distribution due to the coupling of flows. In this chapter, these equations are solved analytically in terms of the driving potential (or rather, its value at the boundaries) for the particularly simple geometries of horizontal and vertical layering. The problem of random distribution of inhomogeneities is solved for one-dimensional variations. Numerical computations are carried out for concentrated heat and pressure sources buried in a horizontally layered half space; concentrated heat sources in the presence of a buried slab; and depth dependent chemical potentials in the presence of vertical contacts and dikes.

The laboratory measurements discussed in the previous chapter show how efficiently rocks can couple pressure, temperature, and chemical potential gradients into electric potential. At the earth's surface, it can be assumed that these gradients do not exist or are negligible, either because the air acts as a short circuit for these gradients (for example, air has an essentially infinite permeability, and as a result, the fluid pressure at the surface of the earth will be the same everywhere), or else because the flows are confined to the near vicinity of the underground source. However, surface currents are possible if there is coupling at depth as will be shown shortly.

Section I - Horizontally Layered Earth

To begin with, we consider the idealized but realistic case of a layered earth. Our model (Fig. 3.1) consists of homogeneous, conductive layers overlying a homogeneous half space. Each layer has a thickness d_i , electrical conductivity σ_i , and coupling coefficient C_i . For such a layered earth composed of n layers, we have:

$$\nabla^2 f_i = 0 \quad (i = 1, 2, \dots, n) \quad 3.1$$

and boundary conditions

$$\sigma_i \frac{\partial f_i}{\partial n} = \sigma_{i+1} \frac{\partial f_{i+1}}{\partial n} \quad 3.2$$

$$f_i - f_{i+1} = (C_i - C_{i+1}) \chi_{i,i+1} \quad 3.3$$

Because of the axial symmetry, it is convenient in this case to use cylindrical coordinates (r, z, ϕ) with the z -axis pointing downward. We shall treat in detail three cases—homogeneous half space, one layer over a half space, and two layers over a half space—to give a clear idea of the anomalies to be expected at the surface.

Homogeneous Half Space - Air is a very poor conductor of electricity compared to the earth, and therefore the conduction currents in the air are negligible. The only boundary condition that the potential f must satisfy is therefore:

$$\frac{\partial f}{\partial z} = 0 \quad \text{at } z = 0 \quad 3.4$$

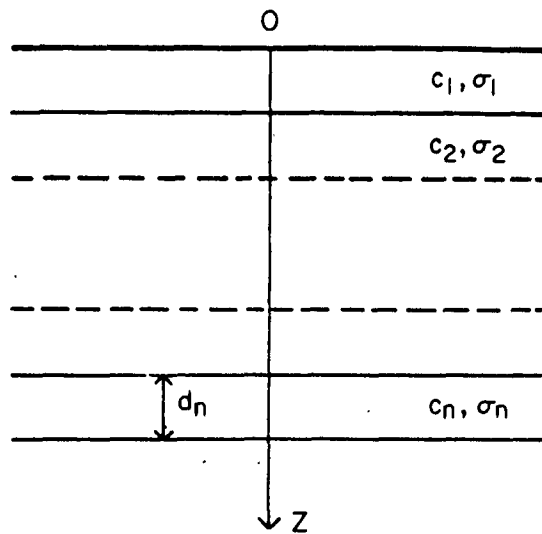


FIGURE 3.1 HORIZONTALLY LAYERED
HALF SPACE

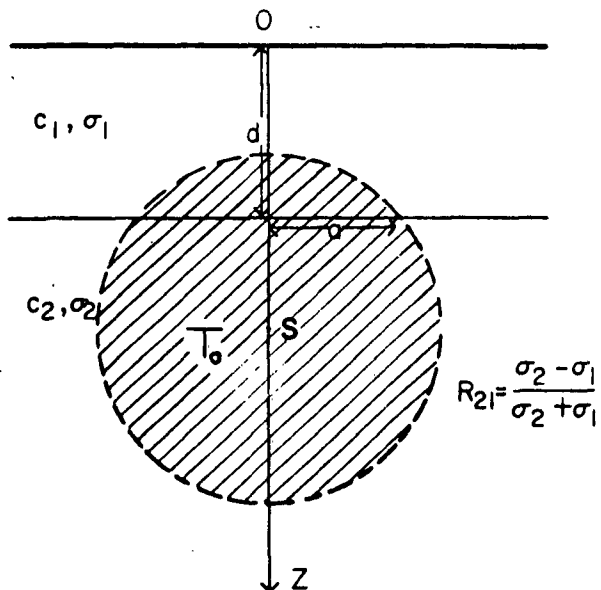


FIGURE 3.2 ONE LAYER OVER HALF SPACE
GEOMETRY FOR THE THERMO-
ELECTRIC CASE

f satisfies Laplace's equation, and by 3.4 its normal derivative must vanish on the boundary. One possible solution satisfying these two conditions is $f = \text{constant}$, and using the uniqueness of solutions theorem (Ramsey, 1959; p.117, problem 2), we see that f must be constant everywhere in the half-space; therefore, there are no currents generated. The electric potential ϕ which is what we try to measure (see Appendix B) is given by

$$\phi = f - c\gamma \quad 3.5$$

where γ is essentially constant on the surface. For instance if γ represents temperature rise, it is zero on the surface because the rocks are poor conductors of heat, and as a consequence, the zone of high temperature is confined to the near vicinity of the underground source. Even if the temperature rise reached the surface, air which is a very good conductor of heat (compared to the rocks) would act as a short circuit to bring the temperature everywhere on the surface to its background value. If the driving force is the pressure P , it will be zero everywhere on the surface of the ground because air has infinite permeability. The chemical potential μ is also constant on the surface, or we hope so, because its value depends on temperature, pressure and concentration of ions which depends on the oxidation conditions at the surface. As long as one is making measurements in the same medium, the chemical potential μ should not change laterally. Therefore, according to 3.5, the electric potential ϕ is the same everywhere, and no variations can be detected.

The above negative result is of tremendous importance, because it indicates that even though there is a driving force in the medium, and there is coupling between the flows as predicted by Onsager's relations, the homogeneity of the medium cancels on the surface any effect that may be produced at depth. This is because there is no boundary cutting across the equipotential surfaces and inducing electrical sources. The following cases will show that effects detectable at the surface arise whenever inhomogeneities in rock properties cut across the equipotential surfaces associated with the various driving forces.

Incidentally, equation 3.5 implies that as long as both potential electrodes used in measuring ϕ are in the same medium, it is impossible to distinguish between the potential difference $\Delta\phi$ and the "total potential" difference Δf (we are assuming $\Delta\gamma = 0$ on the surface). The two potential differences are distinct whenever the electrodes are in different media. We then have

$$\Delta\phi = \Delta f - (\Delta C)\gamma \quad 3.6$$

where ΔC is the difference in coupling coefficients.

One Layer Over a Half Space - For the case of a layer of thickness d overlying a half space, we have the following boundary conditions

$$\frac{\partial f_1}{\partial z} = 0 \quad \text{at } z=0 \quad 3.7$$

$$\left. \begin{aligned} \sigma_1 \frac{\partial f_1}{\partial z} &= \sigma_2 \frac{\partial f_2}{\partial z} \\ f_1 - f_2 &= (C_1 - C_2) \gamma_{12} \end{aligned} \right\} \text{at } z=d \quad 3.8$$

Using cylindrical coordinates (Morse and Feshbach, 1953), the solution can be written in the following form

$$f = \int_0^{\infty} (A_1 e^{-\lambda z} + B_1 e^{\lambda z}) J_0(\lambda r) \lambda d\lambda \quad 3.9$$

and using the boundary conditions 3.8 and 3.7, we get (see Appendix A)

$$A_1 = B_1 = \frac{1}{2} (1 + R_{21}) (C_1 - C_2) \left[\frac{e^{-\lambda d} \bar{Y}_{12}(\lambda)}{1 + R_{21} e^{-2\lambda d}} \right] \quad 3.10$$

where R_{21} is the electrical reflection coefficient, so familiar to people using resistivity methods, and $\bar{Y}_{12}(\lambda)$ is the Fourier-Bessel transform of the driving potential $Y(r, z)$ evaluated at $z = d$.

$$R_{21} = \frac{\sigma_2 - \sigma_1}{\sigma_2 + \sigma_1} \quad 3.11$$

$$\bar{Y}_{12}(\lambda) = \int_0^{\infty} Y(r, d) J_0(\lambda r) r dr \quad 3.12$$

Therefore, we get for the potential f in Medium I

$$f_1(r, z) = \frac{1}{2} (1 + R_{21}) (C_1 - C_2) \int_0^{\infty} \frac{e^{-\lambda d} \bar{Y}_{12}(\lambda)}{1 + R_{21} e^{-2\lambda d}} (e^{-\lambda z} + e^{\lambda z}) J_0(\lambda r) \lambda d\lambda \quad 3.13$$

where

$$\Delta = 1 + R_{21} e^{-2\lambda d} \quad 3.14$$

Clearly enough the value of $f_1(r, z)$ in equation 3.13 depends only on the value of the driving potential evaluated at the boundary between the layer and the

conductive half space. The effect of denominator Δ is to give rise to multiple reflections (series of images) due to contrast in conductivity between the two media. If the resistivity contrast is zero ($R_{21} = 0$, $\Delta = 1$), the equation 3.13 giving f is slightly simplified but remains essentially unchanged.

Assume that the boundary between the layer and the half space does not cut across any equipotential surface connected to the driving force. In this case

$$Y_{12}(r, d) = Y_0$$

where Y_0 is a constant. Using equation 3.12, we have

$$\overline{Y}_{12}(\lambda) = Y_0 \int_0^\infty J_0(\lambda r) r dr = Y_0 \frac{\delta(\lambda)}{\lambda} \quad 3.15$$

Substituting from 3.15 into 3.13, we get:

$$f_1(r, z) = (c_1 - c_2) Y_0 \quad 3.16$$

and $\Delta f_1 = 0$

This is in agreement with what was stated while discussing the case of a homogeneous half space. If the boundary does not cut across equipotential surfaces, as it is the case here, no effect can be observed on the ground. This result has nothing to do with our choice of horizontal layering.

Application to Buried Heat Source - One of the long lasting aftereffects of an underground nuclear blast is the release of a large amount of heat, and therefore creation of a temperature gradient. The heat released is roughly

5×10^{12} joules/kiloton of TNT (Johnson and al., 1959), and since the rocks are poor conductors of heat, this energy will be confined to the near vicinity of the shot for an extremely long period of time if aeration and ground water movements are negligible. Most of the energy goes into raising the temperature of the water present to its boiling point and turning some of it into steam. This steam will be in equilibrium with water, and therefore, its temperature will be the boiling point temperature of water at the prevailing pressure. In this manner no part of the high temperature zone will be above the boiling point of water (Johnson and al., 1959), but rather there will be a roughly spherical zone at a uniformly high temperature and a surrounding medium at ambient temperature. The radius of the high temperature zone for 20 KT blast can be as much as 150 to 200 ft.

In our model (Fig. 3.2) the spherical heat source at temperature T_0 is centered at S , and a is the radius of the high temperature zone cut by the boundary at $z=d$. The background temperature is assumed to be zero degree, because assuming a background temperature different of zero will not change anything, as only the differences in temperature are important. The assumed temperature distribution along the boundary $z=d$ is shown in Fig. 3.3

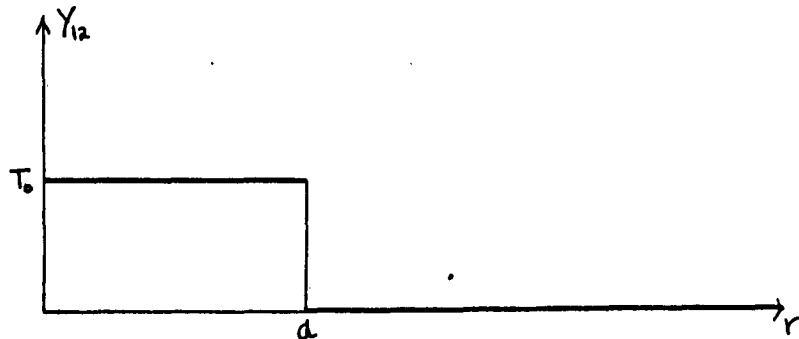


Fig. 3.3 - Temperature distribution along the boundary a short time after the explosion.

With this idealized picture of the temperature distribution we get:

$$\overline{Y}_{12}(\lambda) = T_0 \int_0^a J_0(\lambda r) r dr = T_0 \frac{a J_1(a\lambda)}{\lambda}$$

and

$$f_1(r,0) = (1+R_{z1})(C_1 - C_2) T_0 \left(\frac{a}{d}\right) \int_0^\infty \frac{e^{-\xi}}{1+R_{z1}e^{-2\xi}} J_1\left(\frac{a}{d}\xi\right) J_0\left(\frac{r}{d}\xi\right) d\xi \quad 3.17$$

In going from 3.13 to 3.17, we have made a slight change of variable for computational purposes.

The product $(C_1 - C_2) T_0$ in the above equation represents the strength of the induced electrical sources, and depends on the temperature difference T_0 and the coupling difference $(C_1 - C_2)$. According to this equation, it is possible to have media with strong coupling properties and still observe no surface effect, if the coupling coefficients are equal. An asymmetry of the coupling properties is essential to the generation of electric currents.

The ratio $f_1(r,0)/[(C_1 - C_2) T_0]$, which we shall call the "geometric factor," is a dimensionless number and represents the effect of distance r , thickness of the layer d , size of the shot a , and the conductivity contrast R_{z1} . A high speed computer has been used to calculate this geometric factor for several values of $(\frac{a}{d})$, $(\frac{r}{d})$ and R_{z1} . The results are shown in Fig. 3.4. To get specific answers in millivolts, one has to multiply the ordinates in the figure by the appropriate temperature rise T_0 and the difference of coupling $(C_1 - C_2)$. It is important to note the strong dependence of the geometric factor on conductivity contrast R_{z1} , as well as the thickness d of the overlying layer. This is because the

thermoelectric effect is highly localized, i.e., the sources stop abruptly at distance a .

Application to Buried Pressure Source - When a nuclear charge is detonated underground it acts as a pressure source as well as a heat source, and a differential pressure of tens or even hundreds of atmospheres is probably the case over a period of days or months. We now apply the equation 3.13 to predict the instantaneous potential distribution due to a concentrated pressure source.

In our model (Fig. 3.2) the spherical pressure source is centered at S at a depth h from the surface. We shall assume that the earth has a homogeneous permeability. From equations 2.30 and 2.31, we get:

$$-L_{11} \nabla^2 P = S_0 \delta(\vec{r} - \vec{r}_0)$$

and remembering that the fluid pressure must be zero on the surface, we get the solution

$$P(r, z) = \frac{P_0 a}{R} - \frac{P_0 a}{R'}$$

where

$$R = [r^2 + (z-h)^2]^{1/2}$$

and

$$R' = [r^2 + (z+h)^2]^{1/2}$$

and the Bessel transform of $P(r, z)$ evaluated at the boundary $z = d$ is

$$\overline{P}_{12}(\lambda) = P_0 a \left[\frac{e^{-\lambda(h-d)} - e^{-\lambda(h+d)}}{\lambda} \right]$$

Substituting this value of $\overline{P}_{12}(\lambda)$ in equation 3.13, we

get on the surface $z=0$

$$f_1(r,0) = (1+R_{21})(c_1-c_2)\left(\frac{a}{d}\right)P_0 \int_0^\infty \frac{e^{-\frac{h}{d}\xi} - e^{-\left(\frac{h}{d}+2\right)\xi}}{1+R_{21}e^{-2\xi}} J_0\left(\frac{r}{d}\xi\right) d\xi$$

Expanding the denominator and integrating, we get

$$f_1(r,0) = (1+R_{21})(c_1-c_2)\left(\frac{a}{d}\right)P_0 \left[\frac{d^2}{\sqrt{r^2+h^2}} - (1+R_{21}) \sum_{m=0}^{\infty} (-)^m R_{21}^m \frac{d^2}{\sqrt{r^2+(h+(2m+2)d)^2}} \right] \quad 3.18$$

where h is the depth to the pressure center, d is the thickness of the layer, r is the distance along the surface, R_{21} is the conductivity contrast, and a is the radius at which the pressure is measured to be P_0 .

Figure 3.5 shows the values of the dimensionless factor $f_1(r,0)/[(c_1-c_2)(\frac{a}{d})P_0]$ computed for several values of $(\frac{r}{d})$, $(\frac{h}{d})$, and R_{21} . Pressure does not drop off as abruptly as temperature, and consequently the streaming potential sources are ^{not} quite as localized as the thermoelectric sources. This is indicated by the slight dependence of the geometric factor on conductivity contrast R_{21} (see Fig. 3.5).

Two Layers Over a Half Space - The only interest in this problem is to show what happens to the coupling potentials when more than one boundary cuts across the equipotential surfaces. See Figure 3.6.

Using the equations and the boundary conditions 3.1, 3.2, and 3.3, we get (See Appendix A)

$$f_1(r,0) = (1+R_{21}) \int_0^\infty \left[\frac{\Delta_1 e^{-\lambda d_1}}{\Delta} (c_1-c_2) \overline{Y}_{12}(\lambda) + \frac{\Delta_2 e^{-\lambda(d_1+d_2)}}{\Delta} (c_2-c_1) \overline{Y}_{23}(\lambda) \right] J_0(\lambda r) \lambda d\lambda \quad 3.19$$

where

$$\Delta_1 = (1+R_{32}e^{-2\lambda d_2}) \quad \Delta_2 = (1+R_{32})$$

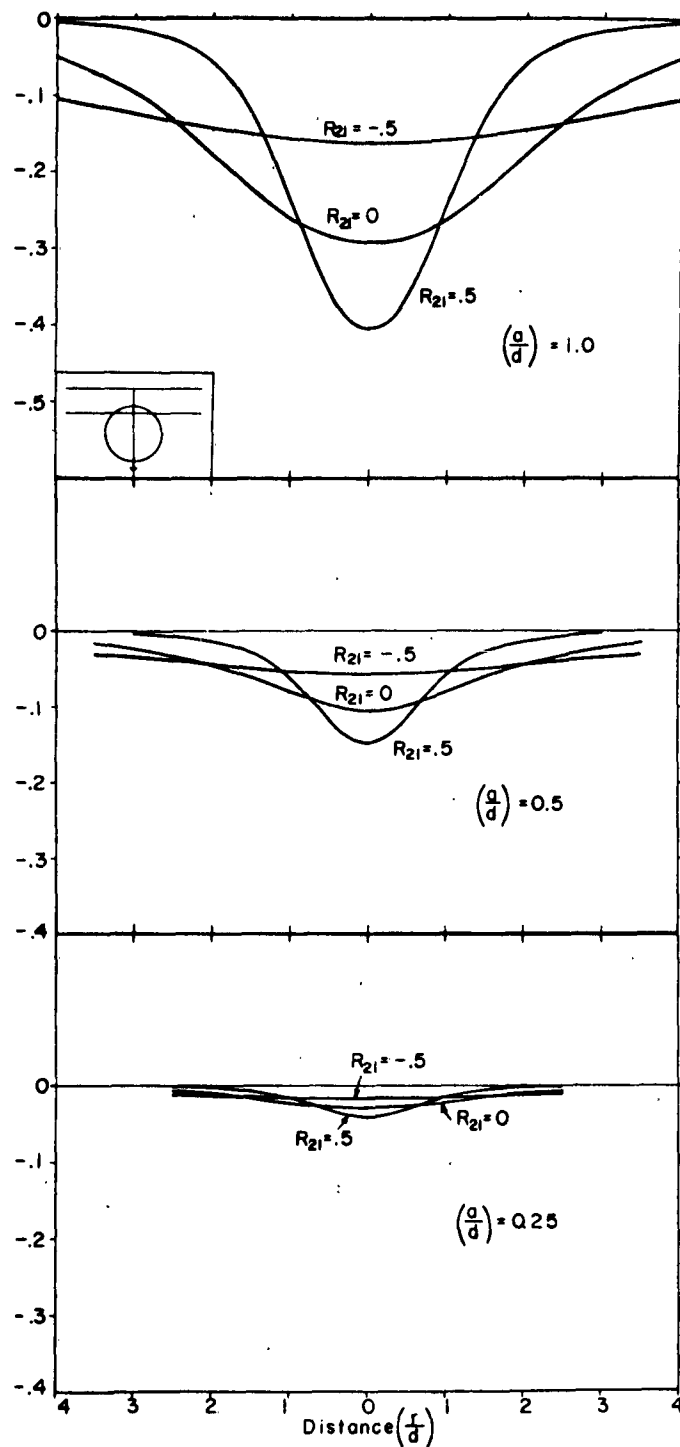


FIGURE 3.4 PLOTS OF THERMOELECTRIC POTENTIAL $f_1(r)/[(c_1 - c_2) T_0]$ vs. (r/d) (SEE FIG. 3.2 FOR EXPLANATIONS)

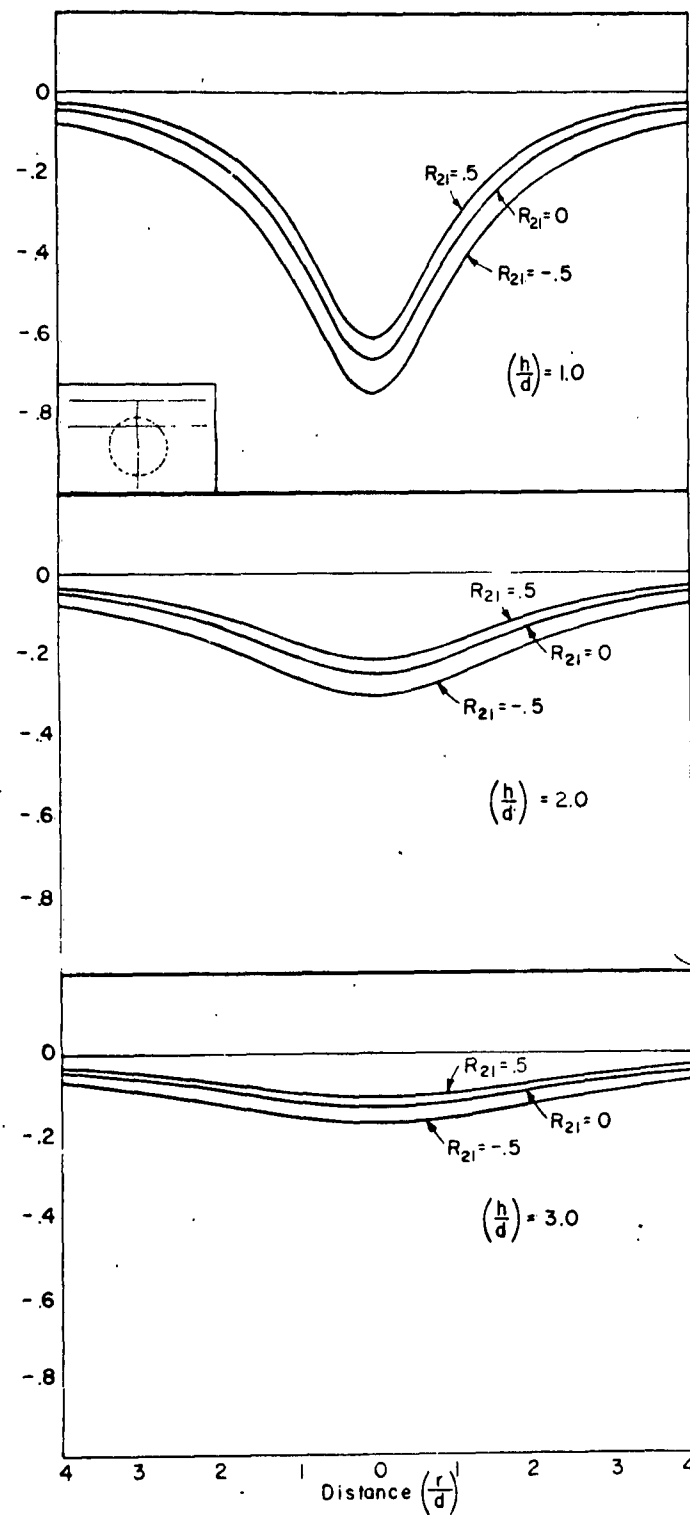


FIGURE 3.5 PLOTS OF STREAMING POTENTIAL $f_1(r)/[(c_1 - c_2)(\frac{a}{d})P_0]$

and

$$\Delta = (1 + R_{32} e^{-2\lambda(d_1 + d_2)}) + R_{21} e^{-2\lambda d_1} (1 + R_{32} e^{-2\lambda(d_2 - d_1)})$$

Comparing equation 3.19 and 3.13, we conclude therefore, that as a first approximation (i.e., $R_{21} = 0$) the coupling effect in this case can be considered as the sum of two independent effects due to χ_{12} and χ_{23} . Of course, for sources of equal strength, this superposition is weighted by the distance from the surface. The effect from the source nearer to the surface is the more important (this is suggested by the terms $e^{-\lambda d_1}$ and $e^{-\lambda(d_1 + d_2)}$ under the integral sign). Consequently, we shall restrict ourselves to the simple cases, because we can get a rough idea of the more complicated situations by superimposing the results for one layer.

Section II - Buried Slab

In this section we shall compute the induced thermoelectric potential when a spherical heat source interacts with an inhomogeneity in shape of a buried slab. A semi-infinite slab of thickness $2w$ is embedded at a depth d in an otherwise homogeneous half space. A high temperature spherical zone of radius R is located at the same depth at a distance a away from the slab (see Fig. 3.7). Dipole sources are induced along the portion of the boundary which is intercepted by the high temperature zone.

Due to the very complicated boundaries, this problem cannot be solved analytically, but when the contrast in conductivity is zero ($R_{21} = 0$), the solution can be obtained by assuming a boundary distribution of dipole sources and integrating numerically. Indeed, for $\sigma_1 = \sigma_2$, we have:

$$\nabla^2 f_1 = \nabla^2 f_2 = 0 \quad 3.39a$$

$$\frac{\partial f_1}{\partial n} = \frac{\partial f_2}{\partial n} \quad 3.39b$$

$$f_1 - f_2 = (c_1 - c_2) Y_{12} \quad 3.39c$$

According to these equations the potential f satisfies the Laplace's equation in each medium and the current is continuous everywhere, while the potential f is discontinuous when crossing the boundary. This means that the thermoelectric potential is due to dipole sources distributed along the boundary. The dipole strength is $(c_1 - c_2) Y_{12}$ per unit area. The dipole potential of a small area ΔA located at (x_0, y_0, z_0) , and having the orientation \vec{n} is

$$\Delta f_1(x, y, 0) = \frac{(\Delta A)}{2\pi} (c_1 - c_2) T_{12} \cdot \frac{(\vec{R} \cdot \vec{n})}{r^3} \quad 3.40$$

where $\vec{R} = (x_0 - x)\vec{i} + (y_0 - y)\vec{j} + (z_0 - z)\vec{k}$
The total potential f_1 is obtained by summing up the contribution to all the dipoles. This problem has been solved on an IBM 709 and the results for several values of w , a , and d are shown in Fig. 3.10. These curves show some interesting behaviours, but the most important feature is the smallness of the geometric factor in this case as compared with the case treated in Section I (Fig. 3.4).

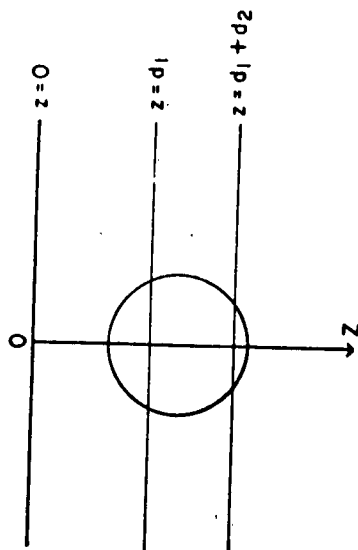


FIGURE 3.6 TWO LAYERS OVER HALF SPACE
AND A CONCENTRATED HEAT SOURCE

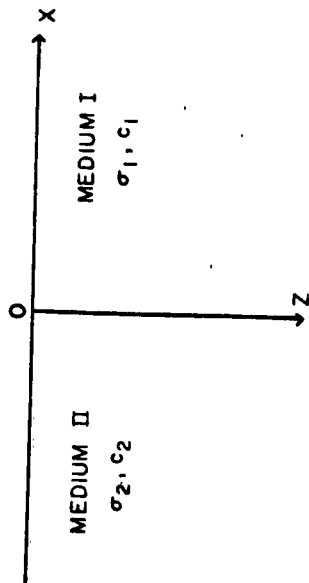


FIGURE 3.8 TWO QUARTER SPACES SEPARATED
BY A VERTICAL CONTACT

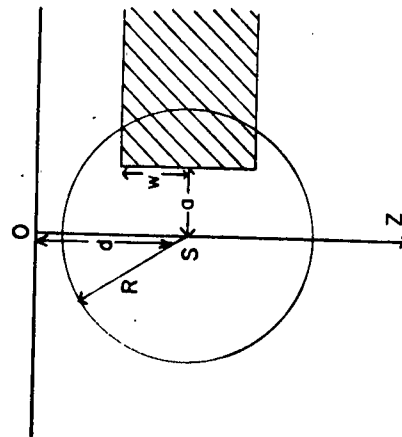


FIGURE 3.7 A BURIED SLAB AND A CONCENTRATED
HEAT SOURCE

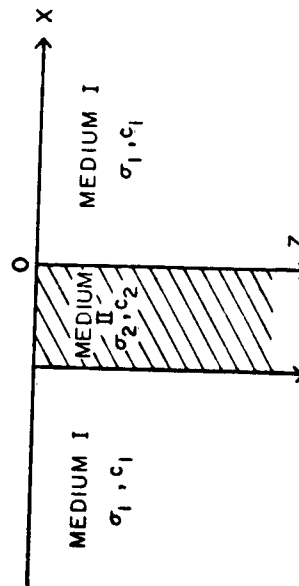


FIGURE 3.9 VERTICAL DIKE EMBEDDED IN A
HALF SPACE

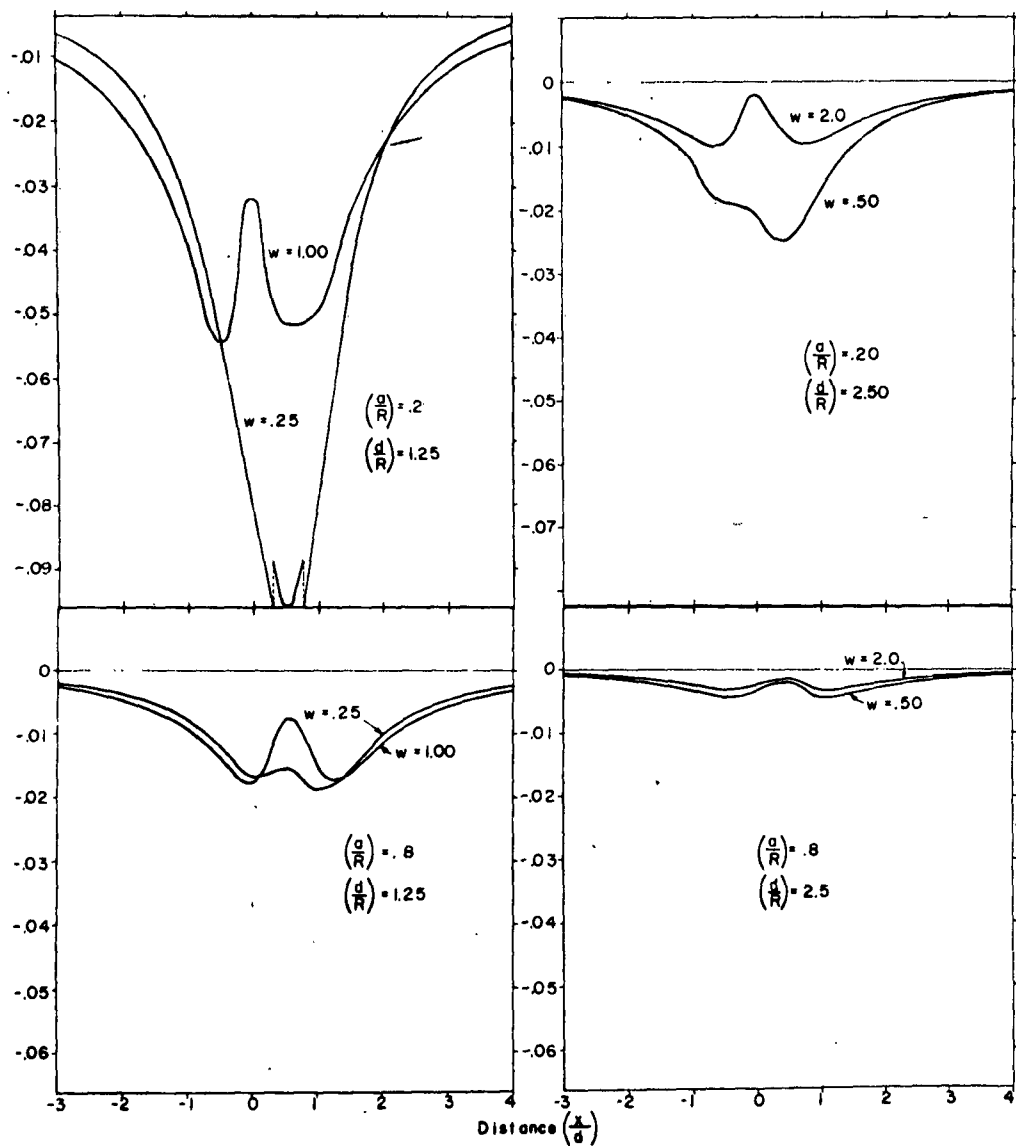


FIGURE 3.10 THERMOELECTRIC POTENTIAL $t_1(x) / [(c_1 - c_2)T_0]$ OVER A BURIED SLAB FOR $R_{21} = 0$ (SEE FIG 3.7 FOR EXPLANATION)

Section III - Vertically Layered Earth

Another idealized but useful model is a vertically layered earth. It can be treated analytically and it is geologically useful as a model for vertical contacts and dikes (see Fig. 3.8 and 3.9).

Geophysicists have observed many spontaneous polarization anomalies that can not be associated with any oxidizing sulfide ore bodies or graphite lenses. We shall use our model of a vertically layered earth to show how these spontaneous potentials can be associated with the presence of a contact or a dike through the phenomenon of electrochemical coupling. It will be sufficient to use a two dimensional model with the z-axis pointing vertically downward along one of the boundary planes and the x-axis pointing to the right (Fig. 3.8) along the surface of the ground. We shall treat separately the vertical contact and the dike problems.

Vertical Contact Problem - For the case of two quarter spaces separated by a vertical boundary at $x = 0$, we use rectangular coordinates (x, z) and assume that the driving potential Y is independent of y-coordinate. We can then write (see Appendix A)

$$f_1 = \int_0^{\infty} A_1 e^{-\lambda x} \cos \lambda z d\lambda \quad x > 0 \quad 3.20$$

$$f_2 = \int_0^{\infty} A_2 e^{\lambda x} \cos \lambda z d\lambda \quad x < 0 \quad 3.21$$

Using the boundary conditions, we get

$$A_1 = \frac{1}{2} (1 + R_{21}) (c_1 - c_2) \bar{Y}_{12}(\lambda) \quad 3.22$$

$$A_2 = -\frac{1}{2} (1 - R_{21}) (c_1 - c_2) \bar{Y}_{12}(\lambda) \quad 3.23$$

where R_{21} has the same meaning as before and $\bar{Y}_{12}(\lambda)$ is the Fourier Cosine transform of the driving potential evaluated at $x = 0$,

$$\bar{Y}_{12}(\lambda) = \frac{1}{2\pi} \int_0^{\infty} Y(0, z) \cos \lambda z dz \quad 3.24$$

Therefore, for potentials f_1 and f_2 we get

$$f_1 = \frac{1}{2} (1 + R_{21}) (c_1 - c_2) \int_0^{\infty} \bar{Y}_{12}(\lambda) e^{-\lambda x} \cos \lambda z d\lambda \quad 3.25$$

$$f_2 = -\frac{1}{2} (1 - R_{21}) (c_1 - c_2) \int_0^{\infty} \bar{Y}_{12}(\lambda) e^{+\lambda x} \cos \lambda z d\lambda \quad 3.26$$

Equations 3.24, 3.25, and 3.26 illustrate once more that the potential f depends only on the value of $Y(z, 3)$ at the boundary. In this case, the horizontal variations of Y are unimportant to the generation of currents, but it is not so for the potential ϕ which is given by

$$\phi(x, z) = f(x, z) - c Y(x, z) \quad 3.27$$

Furthermore, the above equations show that f is discontinuous across the boundary, while ϕ is continuous. To prove that ϕ is continuous, we have only to calculate ϕ_1 and ϕ_2 on both sides of the boundary:

$$\begin{aligned}\phi_1(o, z) &= f_1(o, z) - c_1 Y(o, z) = \frac{1}{2}(1+R_{21})(c_1 - c_2)Y - c_1 Y \\ &= - \frac{\sigma_2 c_2 + \sigma_1 c_1}{\sigma_2 + \sigma_1} Y(o, z)\end{aligned}$$

$$\begin{aligned}\phi_2(o, z) &= f_2(o, z) - c_2 Y(o, z) = -\frac{1}{2}(1-R_{21})(c_1 - c_2)Y - c_2 Y \\ &= - \frac{\sigma_2 c_1 + \sigma_1 c_2}{\sigma_2 + \sigma_1} Y(o, z)\end{aligned}$$

We should not be disturbed by the discontinuity of f because only ϕ has any physical significance and can be measured (see Appendix B).

Again if the boundary does not cut across equipotential surfaces, we have

$$Y(o, z) = Y_o \quad (\text{a constant})$$

and therefore

$$f_1(x, z) = \frac{1}{2}(1+R_{21})(c_1 - c_2)Y_o$$

$$f_2(x, z) = -\frac{1}{2}(1-R_{21})(c_1 - c_2)Y_o$$

Consequently the potential f is constant in each

medium and there is no current generated as predicted earlier.

Application to Electrochemical Diffusion Potential - In order to get some numerical results, we shall apply equations 3.25 and 3.26 to the study of currents generated across a contact through electrochemical coupling. This is the problem commonly encountered in drill hole electrical logging. Here we shall assume that the chemical potential is a function of depth z (it may also be a function of x-coordinate, but we are only interested in its value at $x=0$). We assume that its z-dependence can be written

$$\mu = (\Delta\mu_0) e^{-kz} \quad 3.28$$

This choice of μ , although arbitrary is applicable to a physical problem that will be discussed in Chapter V. The chemical potential decreases from a value $\mu = (\Delta\mu_0)$ at $z=0$ to $\mu = (\Delta\mu_0) e^{-1}$ at a depth $z = 1/k$ which might be called the "effective" depth of weathering, after which the chemical potential remains roughly the same. We have implicitly assumed in 3.28, that at great depth the chemical potential is zero, because adding a constant value does not affect the current distribution or the potential difference.

Using equations 3.24 and 3.25 we get (Erdelyi, 1954)

$$\overline{\mu}_{12}(\lambda) = \frac{2(\Delta\mu_0)}{\pi} \frac{K}{\lambda^2 + k^2} \quad 3.29$$

$$f_1(x, z) = \frac{1}{\pi} (c_1 - c_2) (1 + R_{21}) K \Delta\mu_0 \int_0^\infty \frac{e^{-\lambda x} \cos \lambda z}{\lambda^2 + k^2} d\lambda \quad 3.30$$

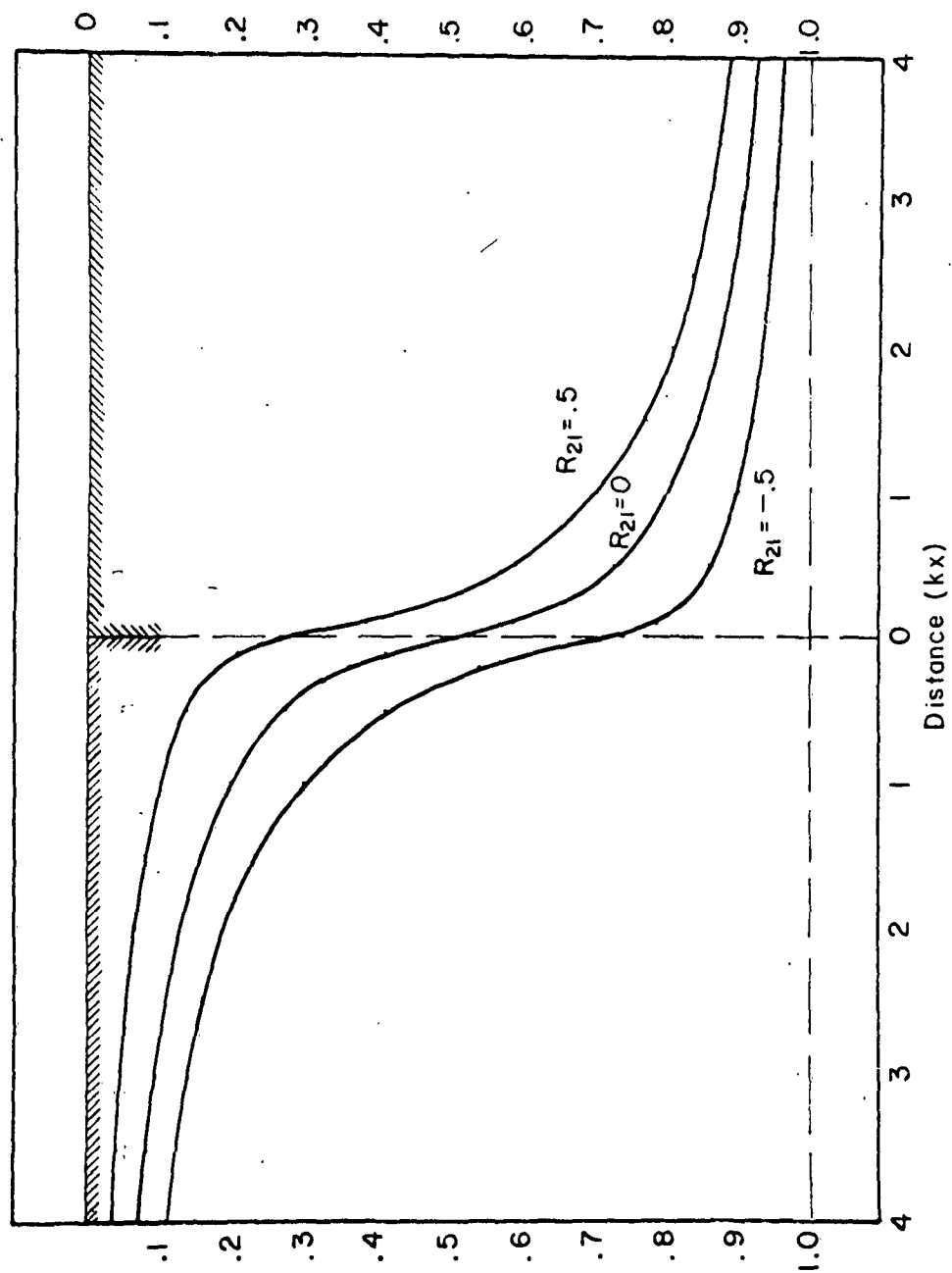


FIGURE 3.11 ELECTROCHEMICAL POTENTIAL $\phi(x) / [(c_1 - c_2)(\Delta\mu)]$ FOR A VERTICAL CONTACT

This solution can be evaluated in terms of exponential integrals with complex arguments. For $z=0$, the solution is very much simplified and we get (Erdelyi, 1954)

$$\phi_1(x, 0) = \frac{1}{\pi} (1 + R_{21}) (C_1 - C_2) \Delta\mu_0 \left[\sin(kx) \text{Ci}(kx) - \cos(kx) \text{Si}(kx) \right] \quad 3.31$$

where

$$\text{Ci}(kx) = - \int_{kx}^{\infty} \frac{\cos u}{u} du$$

and

$$\text{Si}(kx) = - \int_{kx}^{\infty} \frac{\sin u}{u} du$$

Figure 3.11 shows the behaviour of ϕ on the surface. It is interesting to note that far from the common boundary the electrical potential ϕ is not zero. The two media are at different potentials and the maximum potential difference is

$$(\Delta\phi)_{\max} = (C_1 - C_2) \Delta\mu_0 \quad 3.32$$

For the current flow across the boundary separating the two media, we have

$$J_{12}(0, z) = - \sigma_1 \left(\frac{\partial \phi_1}{\partial z} \right)_{x=0} = \frac{1}{\pi} (1 + R_{21}) (C_1 - C_2) (k\sigma) (\Delta\mu_0) \int_0^{\infty} \frac{\cos \lambda z}{\lambda^2 k^2} \lambda d\lambda$$

$$J_{12}(0, z) = \frac{1}{2\pi} (1 + R_{21}) (C_1 - C_2) (k\sigma) (\Delta\mu_0) \left[e^{kz} E_1(kz) - e^{-kz} E^*(kz) \right] \quad 3.33$$

where

$$E_1(kz) = \int_{kz}^{\infty} \frac{e^{-u}}{u} du$$

and

$$E^*(kz) = - \int_{-kz}^{\infty} \frac{e^{-u}}{u} du$$

Vertical Dike - A more realistic case is that of a vertical dike of conductivity σ_2 and coupling coefficient C_2 embedded in a homogeneous medium (see Fig. 3.8). The boundary conditions are

$$\frac{\partial f_1}{\partial z} = \frac{\partial f_2}{\partial z} = 0 \quad \text{at } z=0 \quad 3.34a$$

$$\left. \begin{aligned} \sigma_1 \frac{\partial f_1^+}{\partial z} &= \sigma_2 \frac{\partial f_2}{\partial z} \\ f_1^+ - f_2 &= (C_1 - C_2) Y_{12} \end{aligned} \right\} \quad \text{at } x=0 \quad 3.34b$$

$$\left. \begin{aligned} \sigma_1 \frac{\partial f_1^-}{\partial z} &= \sigma_2 \frac{\partial f_2}{\partial z} \\ f_1^- - f_2 &= (C_1 - C_2) Y_{23} \end{aligned} \right\} \quad \text{at } x=-d \quad 3.34c$$

The two media on both sides of the dike are identical and therefore $Y_{23} = Y_{12}$. The potentials f_1 and f_2 are of the following forms

$$f_1^+ = \int_0^{\infty} A_1 e^{-\lambda x} \cos \lambda z d\lambda \quad 3.35a$$

$$f_2 = \int_0^{\infty} (A_2 e^{-\lambda x} + B_2 e^{\lambda x}) \cos \lambda z d\lambda \quad 3.35b$$

Substituting from 3.34b and 3.34c into 3.35a, and 3.35b we get (see Appendix A)

$$A_1 = \frac{1}{2}(1+R_{21})(C_1-C_2) \frac{1-e^{-\lambda d}}{1-R_{21}e^{-\lambda d}} \bar{Y}_{12}(\lambda)$$

$$A_2 = -\frac{1}{2}(1-R_{21})(C_1-C_2) \frac{e^{-\lambda d}}{1-R_{21}e^{-\lambda d}} \bar{Y}_{12}(\lambda)$$

$$B_2 = -\frac{1}{2}(1-R_{21})(C_1-C_2) \frac{1}{1-R_{21}e^{-\lambda d}} \bar{Y}_{12}(\lambda)$$

and finally we have

$$f_1 = \frac{1}{2}(1+R_{21})(C_1-C_2) \int_0^{\infty} \left(\frac{1-e^{-\lambda d}}{1-R_{21}e^{-\lambda d}} \right) \bar{Y}_{12}(\lambda) e^{-\lambda x} \cos \lambda z d\lambda \quad x > 0 \quad 3.36a$$

$$f_2 = -\frac{1}{2}(1-R_{21})(C_1-C_2) \int_0^{\infty} \left(\frac{e^{-\lambda(x+d)} + e^{-\lambda x}}{1-R_{21}e^{-\lambda d}} \right) \bar{Y}_{12}(\lambda) \cos \lambda z d\lambda \quad -d < x < 0 \quad 3.36b$$

Assuming once more that the driving potential is of the form 3.28, we get for the potentials on the surface

$$f_1(x,0) = \frac{1}{\pi}(1+R_{21})(C_1-C_2)(kd)(\Delta\mu) \int_0^{\infty} \frac{(1-e^{-\xi})e^{-\frac{x}{d}\xi}}{(1-R_{21}e^{-\xi})(\xi^2+(kd)^2)} d\xi \quad 3.37a$$

$$f_2(x,0) = -\frac{1}{\pi}(1-R_{21})(C_1-C_2)(kd)(\Delta\mu) \int_0^{\infty} \frac{e^{-\frac{(1+x)}{d}\xi} + e^{-\frac{x}{d}\xi}}{(1-R_{21}e^{-\xi})(\xi^2+(kd)^2)} d\xi \quad 3.37b$$

Potential ϕ is plotted in Fig. 3.12 for several values of d and R_{21} .

Current flow across the boundary is given by

$$J_{1z}(0, z) = \frac{1}{\pi} (1 + R_{21}) (c_1 - c_2) (K\sigma) (\Delta\mu) \int_0^\infty \frac{(1 - e^{-\xi}) \cos(\frac{z}{d}\xi)}{(1 - R_{21}e^{-\xi}) (\xi^2 + (kd)^2)} \xi d\xi \quad 3.38$$

and is plotted in Fig. 3.13. Near the surface the current flows from medium II into medium I (for $c_1 > c_2$) and the current density is high. At a depth nearly equal to the effective depth of weathering $1/k$, the current reverses its direction and remains that way for increasing depth but the current density goes rapidly to zero.

These graphs of ϕ and J_x for our hypothetical model show striking resemblance with self-potential field data and have all the characteristics usually associated with spontaneous polarization and current flow around oxidizing sulfide veins.

Section IV - Random Distribution of Inhomogeneities

We shall assume, as in Section II, that the half-space has a uniform conductivity σ . Therefore, the potential ϕ is due to distributions of dipoles of strength $(c_1 - c_2)Y$ at each boundary. Assuming for the present that the coupling coefficient C is a continuous function of coordinates, we get

$$\begin{aligned} 2\pi\phi &= \sum_i \iint [c(x_i^*) - c(x_i)] \frac{x_i - x}{R^3} Y(x_i) dy_i dz_i \\ &+ \sum_i \iint [c(y_i^*) - c(y_i)] \frac{y_i - y}{R^3} Y(x_i) dx_i dz_i \\ &+ \sum_i \iint [c(z_i^*) - c(z_i)] \frac{z_i - z}{R^3} Y(x_i) dx_i dy_i \end{aligned} \quad 3.41$$

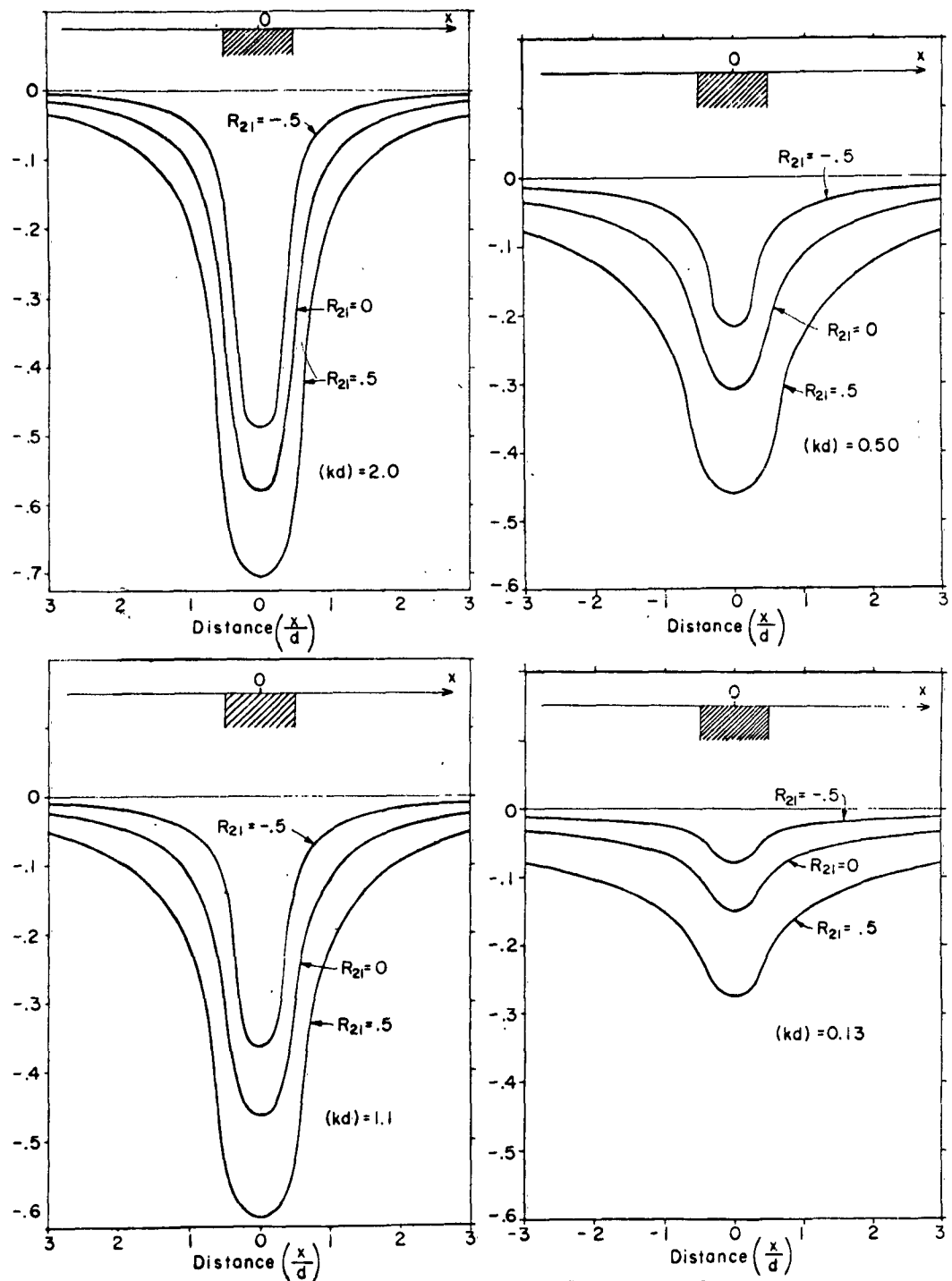


FIGURE 3.12 ELECTROCHEMICAL POTENTIAL $\phi(x)/[(c_1 - c_2)(\Delta\mu)]$ FOR A VERTICAL DIKE

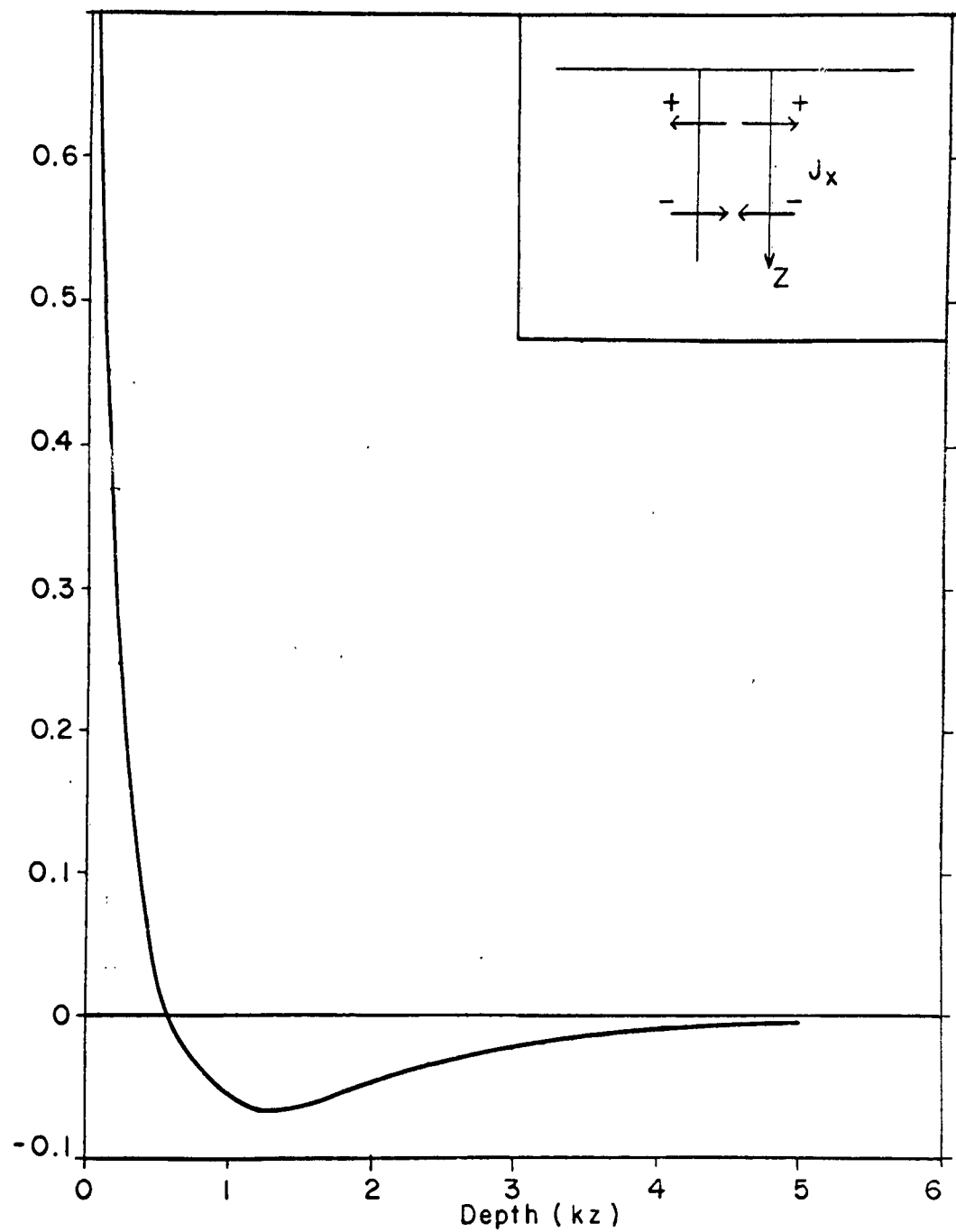


FIGURE 3.13 CURRENT FLOW $J_{ix}(z) / [(c_1 - c_2)(k\sigma_1)(\Delta\mu)]$ ACROSS THE DIKE BOUNDARY

Clearly we can write

$$C(x_i^+) - C(x_i^-) = \left(\frac{\partial C_i}{\partial x} \right)_{x_i} \Delta x_i \quad 3.42$$

and similar relations for y and z variations of C . As the number of boundaries tends to infinity, the summation over index i must be replaced by an integration and we finally get

$$2\pi f = \iiint \left[\vec{\nabla} C \cdot \vec{\nabla} \left(\frac{1}{R} \right) \right] Y(z) dV \quad 3.43$$

Equation 3.43 is the exact form for finding f when C is known as a function of coordinates. Its main merit is that it expresses f in terms of a volume distribution of dipoles.

As a simple model of random medium, we shall assume that C is a random function and its variation depends only on the x -coordinate. This is a rather drastic simplification, but it can be used as a model for a series of vertical dikes of arbitrary thicknesses and coupling coefficients. Therefore, we can write

$$(\vec{\nabla} C)_x = \alpha_i(x)$$

We shall assume that α_i is a member of an ensemble for which the ergodic theorem holds, i.e. the average over the ensemble is equal to the average over the x -coordinate. Furthermore, since $\alpha_i(x)$ is the gradient of the coupling coefficient $C(x)$, we can assume

$$\overline{\alpha_i(x)} = 0 \quad 3.44$$

Substituting 3.44 in 3.43, we get

$$\overline{f_i} = \frac{1}{2\pi} \iiint \overline{\alpha_i(x)} \frac{x'-x}{R^3} Y(z) dV' \equiv 0$$

This means that the induced potential oscillates about a zero average value. Taking the second moment to find out the RMS value of the fluctuations, we get

$$\overline{f_i^2} = \frac{1}{4\pi^2} \iiint \iiint \overline{\alpha_i' \alpha_i''} \frac{x'-x}{R^3} \frac{x''-x}{R''^3} Y(z') Y(z'') dV' dV'' \quad 3.45$$

In the above equation $\overline{\alpha_i' \alpha_i''}$ represents the auto-correlation function of and we shall write it

$$\overline{\alpha_i' \alpha_i''} = \psi_{\alpha\alpha}(|x'-x''|) \quad 3.46$$

Using the result

$$\int_{-\infty}^{\infty} \frac{dy'}{R^3} = \int_{-\infty}^{\infty} \frac{dy'}{[(x'-x)^2 + (y'-y)^2 + z'^2]^{3/2}} = \frac{2}{(x'-x)^2 + z'^2}$$

we can integrate 3.45 with respect to y' and y'' to get

$$\overline{f_i^2} = \frac{1}{4\pi^2} \iiint \psi_{\alpha\alpha}(|x'-x''|) \frac{(x'-x) Y(z')}{(x'-x)^2 + z'^2} \frac{(x''-x) Y(z'')}{(x''-x)^2 + z''^2} dx' dx'' dz' dz'' \quad 3.47$$

To get any farther we need to make specific assumptions on $Y(z)$ and $\psi_{\alpha\alpha}(|x'-x''|)$. Since we are going to use the model to predict background noise due to electro-

chemical diffusion, we shall follow Section III and put

$$Y(z) = (\Delta\mu) e^{-Kz}$$

Making a shift of variables $x'x \rightarrow \xi'$ and $x''x \rightarrow \xi''$ and using the result (Erdelyi, 1954)

$$F(k\xi) \equiv \xi \int_0^{\infty} \frac{e^{-kz}}{\xi^2 + z^2} dz = [\sin(k\xi) \operatorname{Ci}(k\xi) - \cos(k\xi) \operatorname{Si}(k\xi)]$$

we get

$$\overline{f_A^2} = \frac{(\Delta\mu)^2}{\pi^2} \iint \psi_{\alpha\alpha}(|\xi' - \xi''|) F(k\xi') F(k\xi'') d\xi' d\xi''$$

3.48

Function $F(k\xi)$ is a tabulated function. We already have used this function in Section II of this chapter. The above result can be put in a still simpler form by making the change of variable $\xi' \rightarrow \tau + \xi''$. We then get

$$\overline{f_A^2} = \frac{(\Delta\mu)^2}{\pi^2 K} \int_{-\infty}^{\infty} \psi_{\alpha\alpha}(\tau) \varphi_{FF}(k|\tau) d\tau \quad 3.49$$

where

$$\varphi_{FF}(k|\tau) = K \int_{-\infty}^{\infty} F(k\xi'') F(k(\xi'' + \tau)) d\xi'' \quad 3.50$$

The function $\varphi_{FF}(k(\tau))$ is the autocorrelation function of $F(k\xi)$ which represents, except for a constant coefficient, the potential due to a single vertical contact. According to 3.49, the rms value of the background noise is a weighted function of $\varphi_{FF}(k/\tau)$, the weighting function being $\psi_{\alpha\alpha}(|\tau|)$. The autocorrelation function $\varphi_{FF}(k/\tau)$ is plotted in Fig. 3.14.

To get specific answers for $\overline{f_\lambda^2}$, one has to compute $\psi_{\alpha\alpha}(|\tau|)$ from the field measurements of $\alpha(x) = \frac{\partial C}{\partial x}$. No such extensive measurements have been undertaken as yet. Here, we shall assume that the autocorrelation function $\psi_{\alpha\alpha}(|\tau|)$ can be written

$$\psi_{\alpha\alpha}(|\tau|) = \frac{(\Delta C)^2}{t} [2\delta(\tau) - \delta(\tau-t) - \delta(\tau+t)] \quad 3.51$$

This choice of $\psi_{\alpha\alpha}(|\tau|)$, although arbitrary, will be justified in Chapter V. $(\Delta C)^2$ is the rms value of the coupling difference $\overline{\Delta C_\lambda^2}$ between two adjacent dikes; t is the average thickness of the dikes;

With this choice of $\psi_{\alpha\alpha}(|\tau|)$, we get

$$\overline{f_\lambda^2} = \frac{(\Delta C)^2 (\Delta \mu)^2}{\pi^2} \left[\frac{\varphi_{FF}(0) - \varphi_{FF}(kt)}{kt} \right] \quad 3.52$$

which clearly indicates that the noise level is a function of the average dike thickness t as well as the chemical potential $\Delta \mu$ and average variation in coupling $(\Delta C)^2$. Application of these equations to S. P. noise will be taken ^{up} in Chapter V.

The function $\varphi_{FF}(k|\tau|)$ is the autocorrelation function of $F(k\xi)$ which represents, except for a constant coefficient, the potential due to a single vertical contact. According to 3.49, the rms value of the background noise is a weighted function of $\varphi_{FF}(k|\tau|)$, the weighting function being $\psi_{\alpha\alpha}(|\tau|)$. The autocorrelation function $\varphi_{FF}(k|\tau|)$ is plotted in Fig. 3.14.

To get specific answers for $\overline{f_k^2}$, one has to compute $\psi_{\alpha\alpha}(|\tau|)$ from the field measurements of $\alpha(x) = \frac{\partial C}{\partial x}$. No such extensive measurements have been undertaken as yet. Here, we shall assume that the autocorrelation function $\psi_{\alpha\alpha}(|\tau|)$ can be written

$$\psi_{\alpha\alpha}(|\tau|) = \frac{(\Delta C)^2}{t} [2\delta(\tau) - \delta(\tau-t) - \delta(\tau+t)] \quad 3.51$$

This choice of $\psi_{\alpha\alpha}(|\tau|)$, although arbitrary, will be justified in Chapter V. $(\Delta C)^2$ is the rms value of the coupling difference $\overline{\Delta C_x^2}$ between two adjacent dikes; t is the average thickness of the dikes;

With this choice of $\psi_{\alpha\alpha}(|\tau|)$, we get

$$\overline{f_k^2} = \frac{(\Delta C)^2 (\Delta \mu)^2}{\pi^2} \left[\frac{\varphi_{FF}(0) - \varphi_{FF}(kt)}{kt} \right] \quad 3.52$$

which clearly indicates that the noise level is a function of the average dike thickness t as well as the chemical potential $\Delta \mu$ and average variation in coupling $(\Delta C)^2$. Application of these equations to S. P. noise will be taken ^{up} in Chapter V.

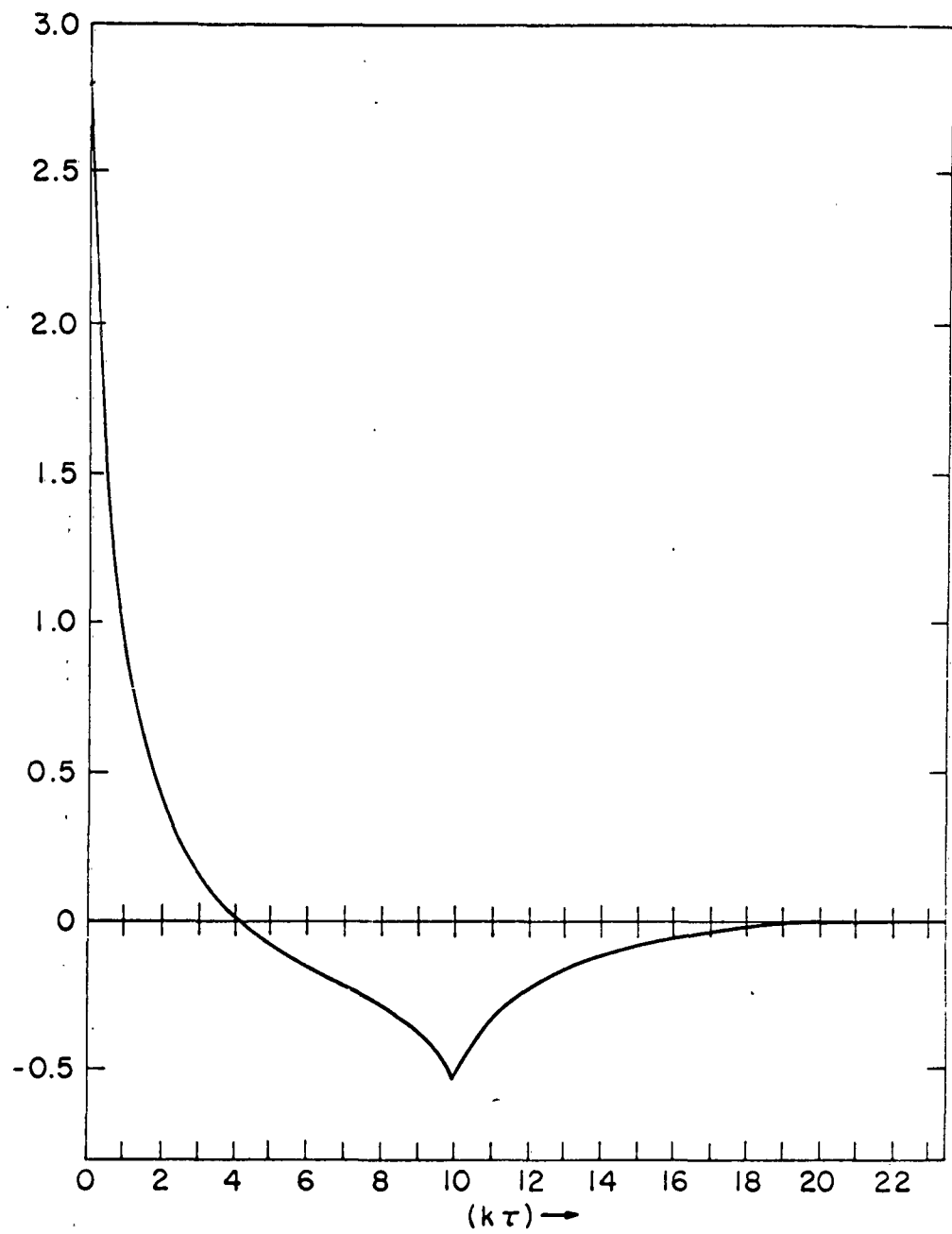


Figure 3.14 - Plot of Autocorrelation Function $\varphi_{FF}(k|\tau|)$

CHAPTER IV

APPLICATION TO THE DETECTION OF UNDERGROUND NUCLEAR BLASTS

Purpose

Having derived the equation governing the distribution of potentials induced by the coupling of flows and studied the effect of geometry on these coupling currents, we now proceed to the applications of the theory. In this chapter, the potentials generated by the electrokinetic and thermoelectric couplings are computed to show the applicability of these couplings to the detection of an underground nuclear blast by its electrical aftereffects. In the next chapter, the problem of spontaneous polarization near inhomogeneities is discussed in detail. No attempt will be made to cover every geophysical application.

Temperature and Pressure Changes

When a nuclear charge is detonated underground, some of the released energy serves to fracture rocks, produce seismic waves, etc., but most of the energy remains confined in the near vicinity of the blast in form of heat and serves to raise the temperature of the pore fluids and create steam under pressure in equilibrium with the fluids. The earth acts essentially as an infinitely large fluid reservoir, and therefore the steam temperature never rises above the boiling point temperature. This point is confirmed by drill hole temperature measurements made a few days after the Rainier shot (Johnson and

al., 1959), and which indicated a maximum temperature of 85°C in the blast area. Incidentally, this is nearly equal to the boiling point temperature of water for the atmospheric pressure at those elevations (The mesa in which the charge was detonated is several thousand feet above the sea level).

If the explosion is totally contained and no extensive fracturing takes place, the only way the steam can escape is by forcing the surrounding fluid out. Under these conditions, the high pressure source should exist for a long time as shown in Chapter I. But it is expected that, even though the blast may take place at depths of several thousand feet, extensive fracturing should take place which would increase the permeability of the medium, and speed up the release of pressure. Also if the gas should channel its way out, we could expect an even faster release of pressure. The actual situation is difficult to predict.

When the shot is not buried too deeply, the fracturing may open up fissures reaching to the surface, and thus release the excess steam until the pressure inside the blast cavity is reduced to the atmospheric pressure. But, as we have already pointed out in Chapter I, even in this case the pressure effect would not be lost, because the excess of the hydrostatic pressure over the cavity pressure would cause a backflow of fluids into the cavity. For a shot buried at 200 meters, this excess back pressure can be of the order of 20 to 50 atmospheres.

While the temperature picture we presented here has been confirmed by drill hole temperature measurements after the Rainier shot, no direct evidence exists to confirm our pressure model. But there is indirect

evidence to suggest that our pressure reversal model can be applied in certain cases. For instance, the potentials measured over Aardvark shot showed an abrupt change in sign that could be easily explained by our model.

Chemical reactions that follow the blast could possibly add to the complexity of the picture. They are little understood except that the time scales involved are very long, and therefore, the role of electrochemical diffusion as a source of currents can not be evaluated at this point. However, the temperature and pressure effects are understood enough to attempt to predict the magnitudes of thermoelectric and electrokinetic potentials to be expected, and compare them with the potentials measured at some of the underground nuclear detonations.

Thermoelectric Effect of a Bomb

As we have already shown, the temperature in the blast area can not be above the boiling point temperature of water at the prevailing pressure. Let us assume that the pressure is atmospheric and therefore this boiling point temperature is about 100°C. Assuming an ambient temperature of 20°C, we get a temperature difference $\Delta T \approx 80^\circ\text{C}$. If the shot were completely contained, the pressure would build up, and consequently, this estimate of 80°C would be far too low.

The thermoelectric coefficients of rocks (or rather the difference between the coefficients for rocks and that for water) are seen from Table 2.4 to have any value between 0 and 1.36 mv/°C, with typical values of .2 to .5 mv/°C. Therefore, a typical value for the difference of coupling ($C_1 - C_2$) would be about .2—.3 mv/°C. This is only an order of magnitude and it could be as large as

one millivolt per degree or as little as zero.

To get the geometric factor from Fig. 3.4, let us assume that a 20KT bomb is exploded inside a half space at a depth of 100 feet below a homogeneous layer as shown in Fig. 3.2. If the thickness of the overlying layer is 300 feet and the radius of the high temperature cavity is about 180 feet, the radius a of the high temperature zone intercepted at the boundary between the layer and the half space would be

$$a \cong \sqrt{180^2 - 100^2} \cong 150 \text{ ft}$$

and the ratio $\left(\frac{a}{d}\right) = .5$. Assuming a conductivity contrast $R_{21} = 0$, and using the data of Fig. 3.4, equation 3.17 gives us

$$\Delta f_{\max} = (0.3 \text{ mv}/^{\circ}\text{C})(80^{\circ}\text{C})(.11) \cong 2.6 \text{ mv} \quad 4.1$$

The factor (.11) in 4.1 is the geometric factor and it indicates that although the induced thermoelectric potential is 24 millivolts, the maximum potential observed at the surface is only about eleven per cent of that value.

This estimate of 2.6 mv is too small to be easily detectable. A refinement of the present exploration techniques along with a thorough study of the nature of the background noise would be necessary to develop techniques for detecting such potentials.

This small voltage indicates that the thermoelectric coupling is not, in general, very important in producing electric potentials from a nuclear blast. Under very favorable conditions, i.e., half space much more conductive

than difference of couplings, $(C_1 - C_2) \geq 0.5 \text{ mv}/^\circ\text{C}$; a ratio $(\frac{q}{d}) = 1.0$; and a temperature difference $\Delta T = 200^\circ\text{C}$; we would get

$$\Delta f_{\text{max}} \cong (0.5 \text{ mv}/^\circ\text{C})(200^\circ\text{C})(.5) \cong 50 \text{ mv} \quad 4.2$$

which is a quite large potential difference and can be easily measured with the present techniques and instruments. However, coupling differences of $0.5 \text{ mv}/^\circ\text{C}$ and temperature differences of 200°C can be considered unreasonably high in most cases, and therefore thermoelectric effects of 50 mv should not be expected.

We conclude this section with a comment on Fig. 3.4 showing the geometric factor for the thermoelectric effect. Over the shot, the geometric factor $f_1(r)/[(C_1 - C_2)T]$ is greater for positive values of R_{z1} (i.e., half space more conductive than the layer); but, at large distances, the reverse is true. This means that—assuming thermoelectric potentials, are large enough to be detected—a bomb can be more easily detected if the overlying layer is a relatively good conductor, because the effect persists over a larger area.

Electrokinetic Effect of a Bomb

Streaming potential measurements shown in Table 2.3 indicate that there are large variations in the electrokinetic coupling coefficients of the rocks, with the smaller coefficients corresponding usually to more tightly packed rocks. Table 4.1 summarizes these results:

Table 4.1. Summary of Streaming Potential Measurements Made on Rock Samples

Rock Type	Number of Samples	Streaming Potential (mv/atm.)	
		Average Value	Standard Deviation
Sedimentary Rock, Colorado Plateau	9	13.8	13.5
Dakota Sandstone	6	7.3	7.5
Altered Volcanics, Arizona	10	8.4	7.5
Metamorphic Rocks, Ontario	5	8.9	5.2
Ophytic Trap Rocks, Michigan	2	4.3	0.4
Quartz-Latite Porphyry, New Mexico	4	.40	.16

We already have discussed briefly what happens when a large charge is detonated underground. The pressure build-up that follows is influenced by several factors, and the resulting pressure picture is difficult to predict theoretically.

If the blast were completely contained and no gases were allowed to escape, the pressure inside the cavity would be definitely greater than the ambient pressure. A simple calculation will give us the order of magnitude of this excess pressure. Assume that the rocks are saturated with water, and the volume increase due to outflow is negligible. Therefore, any steam produced will have the same specific volume as water ($18 \text{ cm}^3/\text{mole}$). Using a temperature of 373°K and assuming that steam at this temperature behaves like an ideal gas, we get

$$P = \frac{RT}{v} = \frac{8.32 \times 373}{18 \times 10^{-6}} \approx 172 \times 10^6 \text{ newtons/m}^2$$

or $P = 1700$ atmospheres.

This estimate will be too high, partly because rock porosity is always greater for gases than for fluids and the resulting steam occupies a larger volume than the original fluid, and partly because steam at 100°C is far from being an ideal gas, and its pressure will be far below that predicted by the perfect gas law.

For a particularly simple model of a blast creating extensive cracks and allowing the gases to escape into the air, the pressure inside the cavity would be the atmospheric pressure. If the center of the blast is located at a depth of 400 feet below the surface, the back flow pressure due to gravity would be about 12 atmospheres.

Let us compute the streaming potential for back flow conditions, using a value of 10 mv/atm. for the difference in coupling ($C_1 - C_2$). We assume again that the blast area has a radius $a = 180$ ft., and is buried at a depth $h = 400$ feet; the overlying layer has a thickness $d = 300$ ft., and the conductivity contrast is zero. We then have $(\frac{a}{d}) = .6$, $(\frac{h}{d}) = 1.33$, and from Fig. 3.5, we get an approximate value of 0.5 for the geometric factor $f_1(r)/[(C_1 - C_2)(\frac{a}{d})P.]$ right over the shot ($r=0$). Thus the maximum potential difference is

$$\Delta f_{\max} = (10 \text{ mv/atm.})(0.6)(12 \text{ atm.})(0.5) \approx 36 \text{ mv} \quad 4.3$$

This is a sizeable anomaly and could be detected.

Under very favorable conditions, the backflow pressure can be much higher; pressures of 50 atm. or better are possible. Using a drastically large value of 20 mv/atm. for the coupling difference, we get

$$\Delta f_{max} = (20 \text{ mv/atm}) (0.6) (50 \text{ atm}) (0.5) = 300 \text{ mv} \quad 4.4$$

This represents a very large anomaly and should be considered as an upper limit of the potentials to be expected. The actual potentials measured at some of the underground nuclear detonations are only of the order of a few millivolts (See Fig. 4.2, 4.3, and Table 4.2).

From these results and those of the previous section we should not conclude that the streaming potential is necessarily the more important effect. That would depend on the local geologic conditions which could, for instance, produce large thermoelectric and small electrokinetic coupling differences at the same time. It is important to note that only differences in coupling are involved. It is possible to have two layers with large coupling coefficients and yet observe no streaming potential effect because the difference in coupling is small. Another possibility is to have a situation in which a thin layer separates two media of comparable coupling effects. In this case the differences ($c_1 - c_2$) and ($c_2 - c_3$) are of opposite sign and therefore the induced potentials tend to cancel each other (see equation 3.19). The above results indicate, however, that in principle, the electrokinetic coupling can be the more important of the two. At least, the results of Nevada underground tests tend to confirm this view.

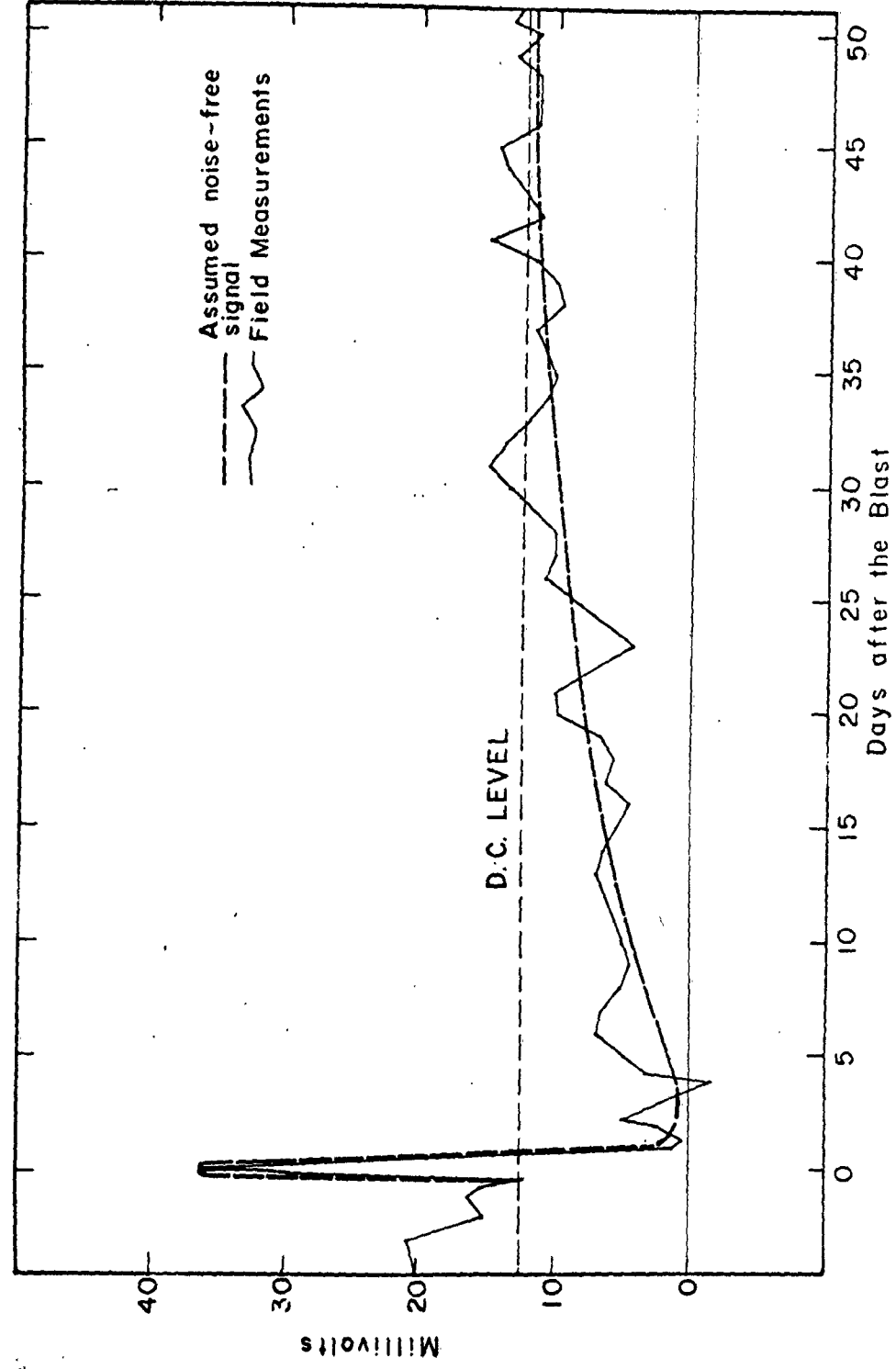


FIGURE 4.1 ELECTRIC POTENTIAL DECAY FOR AARDVARK SHOT, PROJECT NOUGAT

Nevada Underground Detonations

As part of an investigation of the feasibility of using surface electrical measurements to detect underground nuclear detonations, extensive field measurements were undertaken in conjunction with Project Gnome and some events of Project Nougat (Glaser and Kruszyna, 1962; Kruszyna, 1962). There were noticeable potential changes of 10 to 30 mv. in many cases. The results from these shots are summarized in Table 4.2.

The observed potentials at the Gnome event showed a sharp rise over a period of 36 hours followed by a gradual decay toward the pre-shot noise level. The decay was complete after eight days. If our pressure model is applicable here, it would suggest the no degassing took place and the observed effects were due to streaming potentials created by out-flowing fluid.

The results of the Hardhat event show as sharp potential rise over a period of two days followed by an abrupt drop within a few hours, after which the potential started to rise again above the pre-shot level, and it was still rising seven days after the detonation when the recording ceased. The potential reversal in this case could be explained by our model of pressure release but it would be difficult to explain why the potential continued to rise again above the ambient level.

The Ardvark event was the most conclusive of the six tests. A large and sharp potential rise of about 24 mv. was followed by an abrupt reversal to a value well below the ambient level (Fig. 4.1), after which the potential decayed over a period of 45 days to its pre-shot level. This behaviour fits very well our model of flow reversal caused by degassing. The A. C. noise level was relatively

Table 4.2 - Summary of Potential Measurements from
Projects Gnome and Nougat

Event						
	Gnome	Hardhat	Black	Aardvark	Eel	Marshmallow
Yield	Low 5 KT	Low 5 KT	Low	Medium 37 KT	Low	Low
Depth (feet)	1200'	950'		1434'		1200'
Magnitude of Potential use (mv)	15	40	10	24		3?
Magnitude of Potential reversal (mv)		30	30?	35	10	13?
Decayed to Pre- shot Value?	yes	no	?	yes	yes	?
Approximate Decay time (days)	8	?	50?	45	16?	?
Noise Level	Low	Moder- ate	High	Low	Low	Moder- ate

low during this event and good enough records are available to attempt a quantitative interpretation of the results. It is possible that the good quality of the records was due to the large size of the blast. This was the only medium yield shot of the series.

In the case of the Black event, even though relatively large potential changes were observed, no definite conclusion can be drawn due to the large variations in the noise level.

The Eel event did not show any potential rise, but rather the potential dipped some 10 mv. below the background level and gradually recovered in about two weeks.

In the marshmallow event, a very modest potential rise of 3 mv. occurred over a period of two days. A potential reversal followed, and at the end of 3 days, the observed potential was some 13 mv. below the pre-shot level. The recording was stopped after seven days making it impossible to decide whether the readings were due to blast induced potential changes or erratic telluric currents.

Aardvark Shot

Aardvark event was a 37 ± 7 KT detonation buried at a depth of 1434 ft. inside a tuff layer overlain by alluvium. The thickness of the alluvial layer is not known exactly but it is of the order of 1000 ft. Five potential measuring electrodes were located radially at 250 ft. intervals, the nearest being located about 500 ft. from ground zero. All potential measurements were made relative to a reference electrode R located at 4000 ft. from ground zero. Measurements were made starting 4 days before and continuing to 53 days after the blast. A potential change between each of the five electrodes and the reference electrode was observed. A sharp potential

rise was followed in each case by an abrupt drop to a value below the natural D. C. level. Figure 4.1 shows the potential difference between electrode 1 (the nearest to the shot) and the reference electrode R . The line marked "D. C. Level" is an estimate of the background potential that was not completely bucked out. The broken line indicates the measured potentials, while the heavy line represents the probable signal due to the blast. The large potential reversal and the decay time of about 45 days are two very important features that will be discussed in the next section.

The measurements from the other electrodes have the same general features, although the magnitudes of the observed potentials are systematically smaller. In each case there was a positive potential peak followed abruptly by a negative potential peak and a gradual decay over seven or eight weeks. Figure 4.2 shows the positive peaks by a series of bars. The length of each bars indicates the uncertainty in the interpretation due to the presence of noise. Fig. 4.3 presents similar results, except that here we have plotted the observed negative peaks. Both graphs show clearly that the induced potential decreases with increasing distance from ground zero as predicted by the theory. However, they differ drastically among themselves in exhibiting different rates of decrease.

The time scale of 45 days and the sign reversal as shown in Fig. 4.1 suggest that electrokinetic coupling is responsible for the observed electric potentials. We showed in Chapter I, that the time scale for thermal effect is always of the order of years, while shorter time scales could be expected for the pressure effects. A time scale of 45 days is very compatible with the calculations made in Chapter I for the fluid backflow case, but it is com-

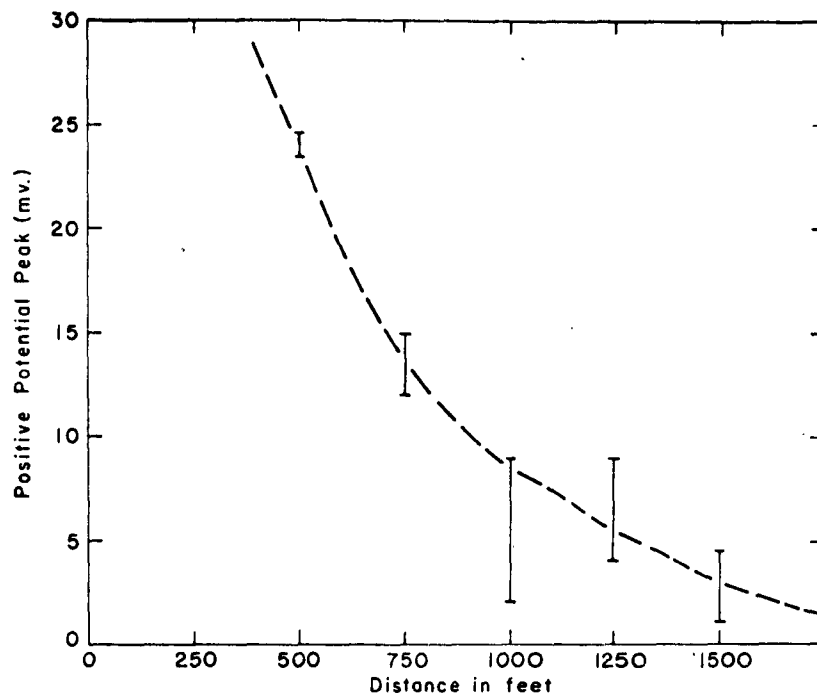


Figure 4.2 - Observed Positive Potential Peak vs. Distance from Ground Zero for Aardvark Shot

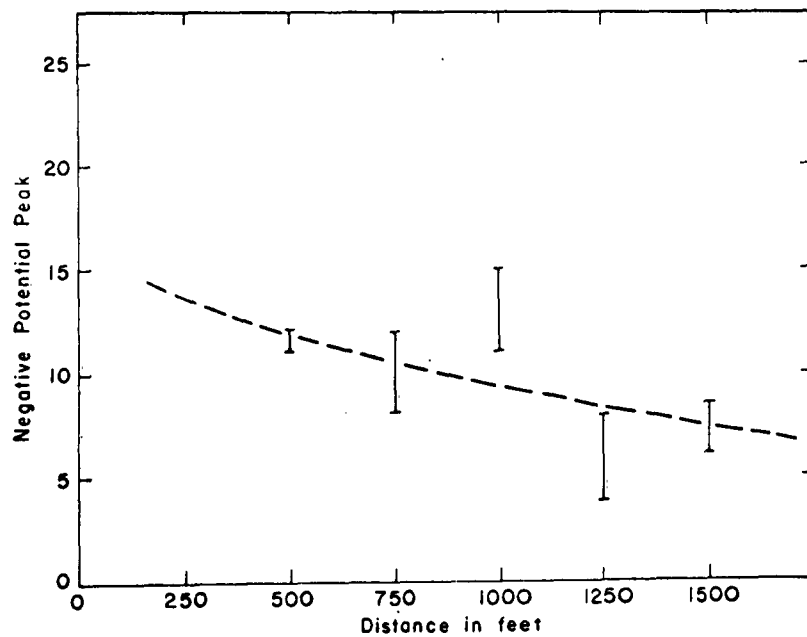


Figure 4.3 - Observed Negative Potential Peak vs. Distance from Ground Zero for Aardvark Shot

pletely unrealistic for thermal dissipation. The sign reversal is still a more positive indication of the importance of the streaming potential in this case. The temperature effect cannot be expected to reverse, but if the effect were due to electrokinetic coupling, the sign reversal could be explained by a reversal in the direction of flow following a pressure release due to the outgassing of the cavity. Thus in Fig. 4.1, the positive peak would be interpreted as being due to streaming potentials induced by the steam pressure forcing the fluids out. But in a matter of hours, all of the excess steam would have leaked to the surface, resulting in a slower back flow which would be responsible for the negative potentials.

Quantitative Interpretation of the Aardvark Results

As we have already seen, the general features of the Aardvark shot can be explained on the basis of a reasonable model involving electrokinetic coupling and flow reversal. We wish to examine more carefully the check between the field data and the theoretical streaming potentials for our simple model assuming one layer over half space geometry (Figures 3.2 and 3.5). In particular, we would like to predict the depth of the shot and the thickness of the overlying layer.

One unusual feature of the observed data is the rate of decrease of the potentials with increasing distance. The maximum positive peaks, shown in Fig. 4.2, decrease rapidly with increasing distance indicating a shallow source, while the negative peaks, shown in Fig. 4.3, decrease much more slowly indicating a more deep seated source. Furthermore, the positive potential peaks last for only a few hours and therefore represent transient

conditions of very short duration. The plot of the negative peaks would represent the more stable conditions following the short period transient behaviour, and thus, would be more reliable for quantitative interpretation. The positive potentials could be caused by upward channeling of the steam. The blast could have opened up many cracks, allowing the steam to push its way upward and thus produce a shallow and short-lasting streaming potential effect. The reversed potentials that followed would represent the streaming potential created by the backflow of fluids into the blast cavity.

The theoretical streaming potentials for one layer over half space (Fig. 3.5) have been replotted in Fig. 4.4 using the depth of the shot h rather than the thickness of the layer d as the constant parameter. These plots show a great resemblance in their rates of fall-off with horizontal distance. The thickness of the overlying layer affects the magnitude of the potentials slightly, but it does not affect the shape of the curves. This indicates that the depth estimates will not be greatly influenced by the particular geometry that is assumed, the paramount factor being the depth of the shot.

The observed data from the Aardvark event have been superimposed on each of the three plots in Fig. 4.4. The circled points represent the potential estimates read from Fig. 4.3. It can be seen that field data and the computed curves fit as well as the accuracy of the data permits. The match of the field data with the streaming potential curve for $(\frac{d}{h})=1.0$ gives $h = 1400$ ft. and $d = 1400$ ft. Using the plot for $(\frac{d}{h})=\frac{1}{2}$, we get $h = 1650$ ft. and $d = 825$ ft.; and finally, the plot for $(\frac{d}{h})=\frac{1}{3}$ gives $h = 2000$ ft. and $d = 670$ ft. The Aardvark shot was actually detonated in a tuff layer at a

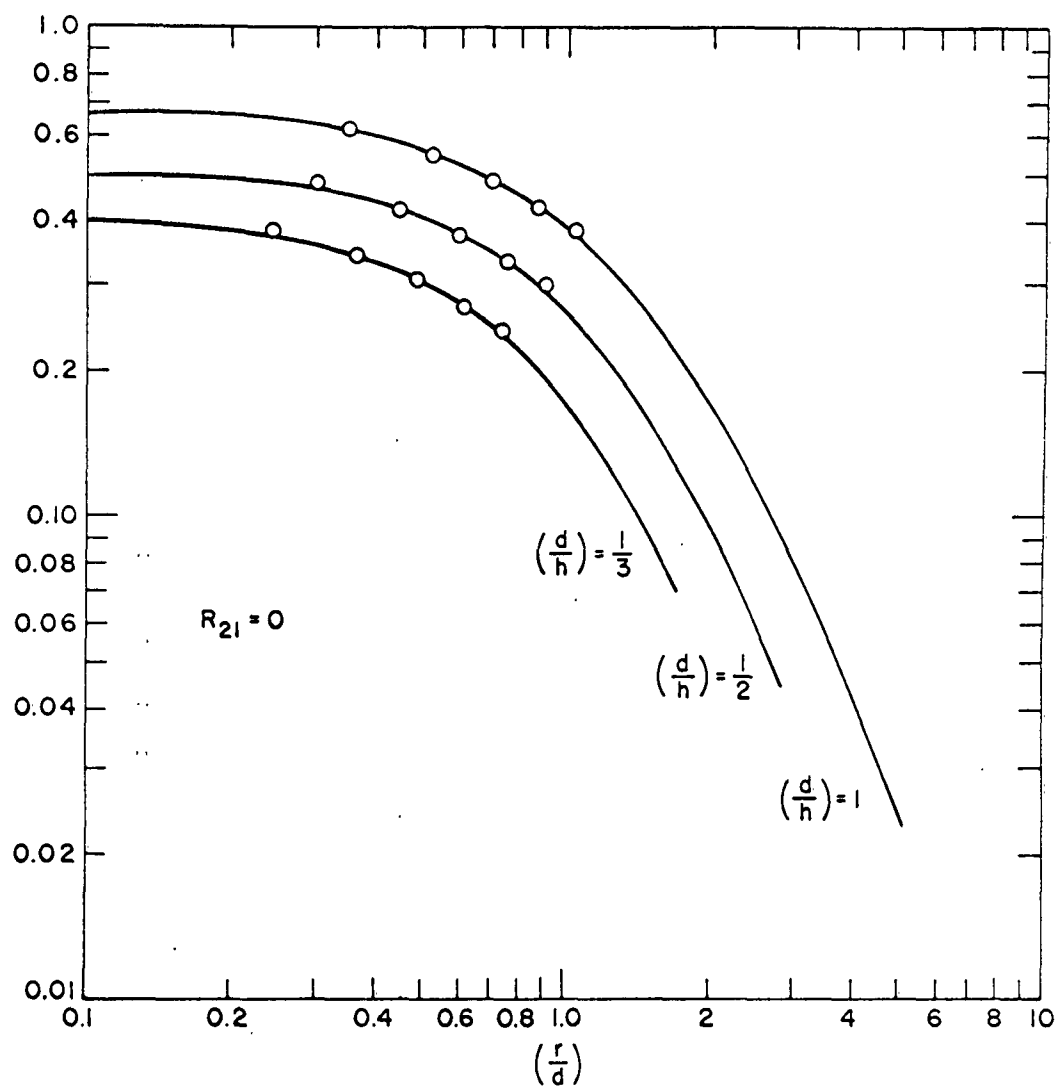


Figure 4.4- Match of Observed Data with Theoretical Streaming Potential Curves for One Layer over Half Space

depth of 1434 feet. The thickness of the overlying alluvium is not known exactly, but it is of the order of 1000 feet. Considering the accuracy of the data, these estimates of h and d are not too far off. One disturbing fact is that these estimates of the depth tend to be too high. Estimates that fall short of the actual depth can be due to the rock fracturing and upward funneling that follow the detonation and have the effect of moving up the center of the blast after-effects. On the other hand, estimates that are too high could hardly be explained, and would be looked upon with suspicion.

Estimates of the coupling coefficients suggest that our pressure model for the Aardvark shot is very reasonable. According to equation 3.18, the streaming potential is given by

$$f = (c_1 - c_2) \left(\frac{a}{d} \right) P_o G(r, h, R_u) \quad 4.5$$

where $G(r, h, R_u)$ is the dimensionless "geometric factor" plotted in Fig. 3.5, and P_o is the driving pressure. The geometric factor $G(r, h, R_u)$ is a positive number, therefore, the sign of the potential f is given by the sign of the product $(c_1 - c_2)P_o$. In our model of the Aardvark shot, we said that the negative potentials were caused by a backflow pressure. Therefore, in our case, P_o is negative and the coupling difference $(c_1 - c_2)$ is positive, indicating that the overburden has a larger coupling coefficient than the tuff layer. Indeed, it is found that, in general, the loosely packed rocks inhibit higher coupling effects. Using a shot depth of 1400 ft. (the top curve in Fig. 4.4), we get for the geometric factor $G = 0.62$, and from Fig. 4.1, we get $\Delta f = 12 \text{ mv}$. The radius a of the area affected by a 37 KT blast is around 200 ft. giving a

ratio $\left(\frac{a}{d}\right) \approx 0.14$. Assuming that at 1400 ft. of depth, the hydrostatic pressure is about 42 atm., we get for the coupling difference

$$(c_1 - c_2) = \frac{\Delta f}{\left(\frac{a}{d}\right) P_0 G} = \frac{12}{(0.14)(42)(0.62)} \approx 3.3 \text{ mv/atm. } 4.6$$

This estimate of 3.3 mv/atm. is very realistic and provides an additional check of our pressure model.

Summary of Chapter IV

While a host of irreversible effects may follow the detonation of an underground nuclear blast, theoretical estimates of the expected potentials as well as the observed data indicate that the streaming potential is the most important after effect. It can generate potentials of sufficient magnitude to be detected by present exploration techniques.

Comparison between the field data and the theoretical streaming potentials for one layer over a half-space indicate the feasibility of quantitative interpretation of the field measurements. The match between the observed potentials and three different theoretical curves gave a fair estimate of the depth of the shot, the error being attributed mostly to the large noise level. Some of the negative potential peaks read from the field records might be off by as much as 100 per cent.

A simple model of pressure release and flow reversal was found to explain all of the features of the potentials created by the Aardvark shot. However, this model is not expected to be universally applicable. Indeed, the data recorded at Gnome shot did not show any reversal of potential. More field measurements taken with improved

recording techniques are necessary before definite conclusions can be drawn on the applicability of the streaming potential model to on site detection of underground explosions.

CHAPTER V

APPLICATION TO SPONTANEOUS POLARIZATION CURRENTS

Spontaneous polarization currents or self-potentials, refer to natural earth currents that are relatively stable in time—both in direction and magnitude. They are commonly associated with the weathering of sulfide ore bodies, the movement of underground water, variations in rock properties across geologic contacts, the bioelectric activity of plant roots, and a host of lesser important phenomena such as corrosion of pipe lines. Electrochemical action arising from concentration differences of electrolytes in contact with metallic conductors, spontaneous polarization of two dissimilar metals in contact with solutions, electrofiltration, and topographic effect due to the normal atmospheric electric gradient have been proposed to be the most important mechanisms of generation of these currents.

The electrochemical and electrokinetic mechanisms of self-potentials have been discussed in detail by various authors (Heiland, 1946; Mounce and Rust, 1945; Sato and Mooney, 1960), but no serious attempts have been made to evaluate the effect of geometry on the magnitude of the induced potentials. We shall attempt to apply the results of Chapter II and III to an evaluation of the role of various couplings in producing self-potentials as well as an estimation of the effect of geometry on these potentials. In particular, we shall examine the importance of the geothermal gradient in producing large scale S. P. currents through thermoelectric coupling, the role of electrochemical coupling in producing small scale S. P. currents, and the effect of geometry on the magnitude of S. P. noise produced by electrochemical coupling.

Section I - S. P. Currents Caused by Thermoelectric Coupling

In Section III of Chapter III, we proved that when vertical boundaries cut across the equipotential surfaces associated with a depth-dependent driving potential, spontaneous polarization currents are generated. The general features of these currents are shown in Fig. 3.11, 3.12, and 3.13. It is believed that the same type of currents could be induced in the earth's crust where large lateral changes of rock properties and a vertical temperature gradient exist at the same time. Indeed, it has been proposed in the past that thermoelectric currents through the mantle and the crust might be responsible, at least in part, for the earth's magnetic field.

In computing the thermoelectric currents in the earth, we shall limit ourselves to currents generated in the crust, because in the mantle the conditions are vastly different. The experimental data on thermoelectric coupling coefficients listed in Table 2.4 are for porous rocks where the conductivity is mainly electrolytic, and the coupling coefficients for the rocks in the mantle, where the mode of condition is very different, are not known.

It is well known that there is a geothermal gradient of about $30^{\circ}\text{C}/\text{km}$ which can be assumed to exist at least as far as the base of the crust. This will give an appreciable temperature difference of some 1000°C between the top and the bottom of the crust which we shall assume to be about 35 km in thickness. Such a large temperature difference can create sizeable potential difference over distances of several kilometers.

Let us compute the magnitude of the potential difference along the surface, assuming that the lateral crustal changes in coupling properties can be represented

approximately by a vertical discontinuity. Furthermore, we shall assume that the dependence of temperature on depth can be approximated by an equation of the form 3.28, where now the "depth" $\frac{1}{K}$ is of the order of 20 to 30 km. We can then use the equations 3.31 and 3.33 derived for a two-dimensional vertical contact model. The conductivity contrast R_{21} can be put to zero without loss of generality. As it can be seen from Fig. 3.11, the potential difference $\Delta\phi$ across the contact is very little affected by variations in conductivity. This difference of potential $\Delta\phi$, for two points on opposite sides of the contact and a distance $(Kx) = 1.0$ away from it, is found from Fig. 3.11 to be about 0.6 and we have to multiply this value by the coupling difference $(C_1 - C_2)$ and the temperature difference ΔT to get the value of the potential difference in millivolts. Using a typical value of $0.2 \text{ mv}/^\circ\text{C}$ for the coupling difference, we get

$$\Delta\phi = (0.2 \text{ mv}/^\circ\text{C})(1000^\circ\text{C})(0.6) = 120 \text{ mv} \quad 5.1$$

This rather large potential difference is developed, as we said above, over a dimensionless distance $(Kx) = 2.0$; using the value of 25 km for $1/K$, we get for the actual distance $x = 50 \text{ km}$. Therefore, the potential drop is no more than 2 or 3 mv/km. From the point of view of the mining geophysicist, this would represent a rather small noise that would not influence his studies.

It is obvious that the contribution of the thermoelectric currents in the crust to the earth's magnetic field will be negligible. Using a potential gradient of 3 mv/km and a crustal conductivity of 10^{-4} mhos/m , the current density is

$$\vec{J}_x = -\sigma \nabla V \cong (10^{-4})(3 \times 10^{-6} \text{ volts/m}) = 3 \times 10^{-10} \text{ amps/m}^2 \quad 5.2$$

Assuming that the current forms an infinite sheet of 20 km thickness, the magnetic field is

$$H \cong \frac{1}{2} (J_z) (h) \cong \frac{1}{2} (3 \times 10^{-10}) (2 \times 10^4 m) = 3 \times 10^{-6} \text{ amp turns/m}$$

$$H \cong 4 \times 10^{-8} \text{ Oersteds (gauss)}$$

This field is completely negligible. However, it is possible that the thermoelectric currents are much more important inside the mantle due to its high conductivity, but then our assumptions concerning the geothermal gradient and magnitude of the coupling coefficients are untenable.

Section II - S. P. Currents Caused by Electrochemical Coupling

Electrochemical action is believed to be by far the most important mechanism of generation of self-potential currents that are commonly associated with ore bodies or other inhomogeneities in rock properties. These currents are assumed to arise from concentration differences of electrolytic solutions in contact with metallic conductors (such as sulfide ores), from the chemical differences of the materials coming in contact with solutions or from differences in diffusion properties of materials. Because many of the large anomalies that have been observed are associated with sulfide ore bodies, nearly all the proposed theories of the electrochemical origin of self-potentials depend heavily on the oxidation-reduction reactions involving sulfides. Then theories are mainly concerned with the mechanism of generation of self-potentials, and few of them consider the effect of geometry on the magnitude of these potentials.

In Chapter II, we studied the role of electrochemical diffusion in producing self-potentials, and in Chapter III, it was shown that whenever inhomogeneities in rock properties cut across the surfaces of equal chemical potential, electric currents are generated through diffusion. The magnitude of the currents depends on the differences in coupling properties and the chemical potentials of the ions.

Electrochemical Coupling Coefficients - Few measurements of electrochemical coefficients can be found in the literature, but at the present time the Geophysical Laboratory at M. I. T. is undertaking such measurements on rock samples. The few results that are presently available are shown in Table 5.1.

Table 5.1 - Electrochemical Coefficients of Rock Samples (NaCl Solutions)

Rock Type	Sample Code	Electro-chemical Coefficient (mv/decade)	Effective transference ⁺	Investigator
Sedimentary Rocks Colorado Plateau	Y3	7.8	.57	Heath
	Y18	4.0	.53	"
	Y34	-2.2	.48	"
	Y36	-5.6	.45	"
	Y38	6.8	.56	"
	Y41	3.6	.53	"
	Y46	5.8	.55	"
	Y52	8.8	.57	"
Altered Volcanics Arizona	SA 28	3.8	.53	"
	SA 31	-3.1	.47	"
	SA 34	8.8	.57	"
	SA 35	9.5	.58	"
	SA 36	6.8	.56	"
Quartz-Latite Porphyry, New Mexico	BC 4	6.0	.55	"
	BC 5	4.8	.54	"
	BC 9	8.8	.57	"

Metamorphics,	N 12	5.8	.55	"
Ontario	N 16	5.8	.55	"
	N 37	6.8	.56	"
Dakota Sandstone	S 22A	-0.7	.49	"
Dense Sandstone	G 2	6.8	.56	"
tuff		1.2	.51	Marshall
tuff		26.0	.72	"
Tremolite				
Sandstone		43.7	.87	"
Sandstone, med. grained		-2.4	.48	"
Sandstone, med. grained		-1.2	.49	"
Sandstone, fine grained		46.1	.89	"
Sandstone, dirty		11.8	.60	"

The measurements were made by placing the samples between two aqueous NaCl solutions of strength .001N and .03N, and measuring the difference of coupling between the rock sample and water. The results reported here are in millivolts per decade of concentration (decade is the logarithm to the base ten of the ratio of concentrations), and have been corrected for the coupling effect of water.

It is interesting to compare these measurements with the maximum coupling coefficient possible for a uni-univalent salt solution. From 2.46 and 2.48, the coupling effect for a two-ion system is

$$\bar{C}\mu = \frac{L_{33}Z_P + L_{44}Z_n}{L_{33}Z_P^2 + L_{44}Z_n^2} \frac{RT}{F} (2.3 \log_{10} C) \quad 5.4$$

Using 2.18 and the definition of transference numbers t^+ and t^- , the diffusion coefficient, as used in Table 5.1, is at 25°C given by

$$\bar{C} = 2.3 \frac{RT}{F} (t^+ - t^-) \quad 5.5$$

or $\bar{C} = 59.1 (t^+ - t^-) \text{ mv/decade}$

The maximum value of the coupling coefficient, for $t^+ = 1$ and $t^- = 0$, is therefore 59 mv/decade. Equation 5.5 has been used to compute the transference numbers listed in Table 5.1. The largest reported values of t^+ are close to unity (for clays) corresponding to coupling values of slightly less than 59 mv/decade.

Dependence of the Chemical Potential on Depth - The chemical potential of an ion in solution is essentially a function of temperature pressure, and concentration. Near the surface of the earth, these conditions are found to be very much dependent on depth. The temperature and the pressure can be considered to vary almost linearly with depth. The dependence of concentrations on depth is not so simple, due to the large number of controlling factors. The lateral variations of these factors are so great that they tend to mask the dependence of concentrations on depth.

There are very few data on the composition and chemical properties of pore fluids at depth. Most analysis of rocks give the total ion content (solid + dissolved) and thus provide no information on the composition of the pore fluids. However, there are many analysis of shallow ground waters and of oil field brines because of their obvious applications. Table 5.2 lists a few analysis of surface ground waters (Hawkes and Webb, 1962) and oil field brines from Illinois Basin (Meents and al., 1952). Although the data presented here is very incomplete, it gives an idea of the wide range of variations. It is obvious from these data that the concentration of each ion as well as the total salinity can vary by as much as a 10^3 or 10^4 from one condition to a different one.

We are here interested in variations over depths of a few hundred feet or a few thousand feet, and for these

depths, the most important factor controlling the concentrations is the weathering. It is important to realize that it is not necessary to know how these changes are brought about, in order to apply the electrochemical diffusion theory. All that is required is to have a gradient of chemical potential that will induce ionic flows. As a matter of fact, we can assume that the chemical potential varies very rapidly over a certain depth (the weathering zone) and then varies more slowly or remains the same below that depth (depth environment). A study by Sato (Sato, 1960a; Sato and Mooney, 1960) of oxidation potential Eh and hydrogen concentration pH of natural waters in several mines indicates that the Eh and pH vary over wide ranges in the weathering zone (corresponding to changes of concentration for Fe^{++} and H^+ as high as 10^{13} and 10^8) while they are restricted to much narrower ranges in the depth environment. This result would tend to confirm our picture of the depth dependence of the chemical potential.

When the system contains only two kinds of ions of equal valency, one positive and one negative, there is only one chemical potential to consider because the concentrations of positive and negative ions can never be very different ($\mu_p \approx \mu_n$). In this case, the coupling coefficient for the medium is essentially constant and is given by 5.5. The dependence on depth of the chemical potential can be represented by

$$\mu = (\Delta\mu) e^{-kz} \quad 5.6$$

where $1/k$ is related to the depth of weathering (this choice of z-dependence is prompted by its analytic simplicity). We have arbitrarily assumed that at depth the chemical

Table 5.2 - Composition of Ground Waters and Oil Field Brines
Total Ions and Major Constituents (ppm) (Data from
Hawkes & Webb, 1962; Meents and al., 1952)

	Depth (feet)	Total	Ca ⁺⁺	Mg ⁺⁺	Na ⁺ +K ⁺	HCO ₃ ⁻	SO ₄ ⁼	CP ⁻
Surface Ground- waters	{1}	1168	30	31	279	445	303	80
	{2}	283	40	22	1.6	213	4.9	2.0
	{3}	120	12	6.6	10.3	85	4.4	1.2
	{4}	110	19	5.1	7.6	39	30	5.8
Illinois Oil Field Brines	176 {5}	44323	1026	541	14765	44	12	26157
	267 {6}	10561	58	89	3971	2286	7	5128
	495 {7}	4359	24	25	1618	636	7	2235
	320 {8}	26640	214	145	9940	881	0	15632
	2950 {9}	113226	2806	1054	38578	141	973	66736
	2960 {10}	98182	2483	1356	32204	709	87	57514
	2970 {11}	122300	3165	1060	41748	114	235	72851
	3150 {12}	125280	6005	1130	40576	78	1909	75104
{1}	Well in sandstone formation, New Mexico							
{2}	{7} McDonough formation							
{3}	{8} Coles formation							
{4}	{9} Cypress (clay) formation							
{5}	{10} Richland member, cypress formation							
{6}	{11} Wayne formation							
	{12} AuxVases (Edwards) formation							

potential is zero; adding a constant value will not affect the induced currents. $(\Delta\mu)$ represents the difference in chemical potential and is given approximatively by

$$(\Delta\mu) = RT \ln \frac{C(z_0)}{C(0)} \quad 5.7$$

where $C(z_0)$ and $C(0)$ are the concentrations at depth and at the surface respectively. We have here neglected the variations of μ due to temperature and pressure changes. Subject to these restrictions, the equations derived in Section III of Chapter III can be used to compute the electrochemical diffusion potentials of solutions containing only two kinds of ions (or when two ions predominate).

When several ions are present in appreciable quantities, the concentrations are not necessarily equal, and we can not speak anymore of the variations of a single chemical potential. Starting from equation 2.53, giving the current flow in a multi-ion system, the potential is defined now as

$$f = \phi + \frac{F \sum L_i z_i \mu_i}{(F^2 \sum L_i z_i^2)} \quad 5.8$$

The electric potential ϕ and the chemical potentials μ_i must be continuous across any boundary, therefore, using 2.18 and 2.20, we get for the boundary condition on f

$$f_2 - f_1 = \sum_i \left(\frac{u_i^{(2)} C_i^{(2)} \mu_i}{\sigma_2} - \frac{u_i^{(1)} C_i^{(1)} \mu_i}{\sigma_1} \right) \quad 5.9$$

where $\sigma = F \sum_i u_i C_i z_i$

u_i , C_i , and μ_i are the mobility, the concentration, and the chemical potential of each ion, respectively; subscripts and superscripts 1 and 2 refers to the two media in contact. This equation replaces the boundary equation 2.58.

The above expression cannot be separated into the product of a coupling difference and a driving potential as we did in the case of a dissociated salt. In principle we can compute its value from a knowledge of the mobilities and the concentrations of all the ions present. Since the mobilities and the concentrations depend on depth, we can still assume that the depth-dependence of the expression on the right hand side of 5.9 is given by 5.6.

Electrochemical Diffusion Potential across a Dike - In the absence of metallic conductors, the electric potential is due to diffusion of ions, very much similar to a junction potential. But when metallic conductors such as sulfide ore bodies are present, some complications are introduced which will be discussed in the next section.

The general features of the electrochemical diffusion potential across a dike were computed in Chapter III, and are shown in Figs. 3.12 and 3.13. The parameter $1/\kappa$ represents roughly the depth of weathering or the depth associated with large changes in concentrations; therefore, the product (κd) represents the ratio of the dike thickness d to the weathering depth. In Fig. 3.12 the geometric factor $\phi(x)/[(C_1 - C_2)(\Delta\mu)]$ has been plotted as a function of $(\frac{x}{d})$ where x is the distance along the surface. These plots show a great similarity in amplitude and the rate of decrease with distance. Clearly, the maximum value of the geometric factor is only slightly

dependent upon the parameter (κd) of the dike (i.e. the thickness of the dike). In going from a thick dike, (κd) = 2.0, to a thin dike, (κd) = 0.5, the maximum value of the potential changes only by a factor of two.

The dependence of the potentials on conductivity contrast R_{21} is much more important, especially for thin dikes. For a dike of thickness (κd) = 0.13, the maximum potential changes by a factor of four in going from a conductive dike, $R_{21} = 0.5$, to a more resistive dike, $R_{21} = -0.5$. The changes are even more dramatic for larger conductivity contrasts. For a highly resistive dike ($R_{21} \approx -1.0$), the electrochemical coupling effect is almost negligible as it can be seen from equations 3.37a and 3.37b, while for a very conductive dike ($R_{21} \approx +1.0$), the maximum value of the geometric factor is almost equal to unity and is not affected appreciably by the thickness of the dike. This is one of the reasons for the larger potentials associated with conductive ore veins.

Figure 3.12 shows that the half-power width of the anomaly, for thin dikes computed cases, is almost independent of the parameter (κd), implying that for these cases, the half-power width depends on the thickness of the dike. For very thick dikes the vertical contact case (Fig. 3.11) is applicable.

The magnitude of the electrochemical potential can be computed from a knowledge of the mobilities and the concentrations of the ions present. Unfortunately, the pore fluids of rocks represent multi-ion systems whose coupling properties have not been measured. The coupling coefficients listed in Table 5.1 have been measured using a NaCl solution.

As a first approximation, we can assume that only two kinds of ions (e.g. Na^+ and Cl^-) are present. This is

very often a good approximation as can be seen from the data in Table 5.2. Therefore, we can use equations 5.6 and 5.7 which are valid for a two-ion system. The concentration C in 5.7 would refer, for instance, to the concentration of sodium or chlorine or the total concentration. From Table 5.2, it is seen that the total ion concentration can vary easily by a factor of 10^2 over a depth of two or three hundred feet, giving rise to a driving potential $\Delta\mu = RT \ln 10^2$. Corresponding to this choice of concentration difference, the depth parameter $1/\kappa$ of equation 5.6 would be about 100 ft. or more.

From Table 5.1, typical values of the coupling difference ($c_1 - c_2$) are seen to be about 5 to 15 mv/decade. Assuming a dike thickness of 100 ft. ($kd = 1.0$), a conductivity contrast of three ($R_{21} = 0.5$), and a coupling difference of 15 mv/decade, we get for the maximum diffusion potential (see Fig. 3.12)

$$\Delta\phi = (15 \text{ mv/decade})(\log 10^2)(0.6) = 18 \text{ mv} \quad 5.10$$

This can be considered as a typical maximum value of the potentials induced by electrochemical coupling. It is rather difficult to produce much larger potentials by diffusion.

It can be seen from 5.9 that the driving potential is a weighted average of all μ 's and the weighting factors are proportional to the concentrations of the ions. If the concentration of an ion goes to zero, it is true that its chemical potential becomes infinitely large, but the product

$C_i \mu_i$ in equation 5.9 goes to zero. This point is very important in understanding why huge potential differences are never produced by diffusion coupling.

Role of Metallic Conductors - Most of the observed self-potentials are less than 100 mv in magnitude. This certainly is true of the background noise in S. P. surveys. However, larger potentials of several hundred millivolts are often observed over sulfide ores and graphite zones that form massive bodies or continuous veins. These large self-potentials, that can attain 500 mv in magnitude, can not be caused by electrochemical diffusion alone. In the preceeding section, we found that the largest anomalies induced by simple diffusion can not be more than tens of millivolts unless rather unreasonably high value of are assumed. When metallic conductors are present, such an increase in the driving potential is produced.

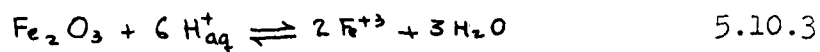
We shall see farther, that in the presence of electronic conductors, the driving potential is essentially determined by the concentrations of the minor elements capable of undergoing oxidation-reduction reactions, such as iron and manganese. Among these minor constituents, iron occurs in rocks in fair quantities, however, its solubility is very low. From a knowledge of all the reactions and the free energies involving iron we can compute its ionic concentration. These well-known methods of chemical thermodynamics need not be repeated here, and the interested reader is referred to R. M. Garrels (1960) and M. J. N. Pourbaix (1949) for detailed treatments. We shall confine ourselves to a brief discussion of the results.

It is found that any chemical reaction in aqueous solutions can be represented in terms of the reacting species, the pH, and the Eh of the solution. The pH, defined as $-\log (H^+)$, determines the influence of the hydrogen ion, and E_h , the oxidation potential, determines the influence of electrons. For instance, the activities of ferrous and ferric ions in equilibrium with each other are determined by (Sato and Mooney, 1960, p. 232)



Therefore, a change of 0.12 volts in the Eh value changes the ratio of ferric to ferrous ions by two orders of magnitude.

If the equation 5.10.1 represents the only important reaction, the concentrations of ferric and ferrous ions are independent of the pH. But, in general, there are other competing reactions such as



$$\text{Log} [\text{Fe}^{3+}] = 0.72 - 3 \text{pH} \quad 5.10.4$$

Equation 5.10.4 implies that at constant Eh, a change of unity in the value of the pH corresponds to a change of 10^3 in the concentration of Fe^{3+} ions. Actually because of the many competing reactions the concentrations of ferrous and ferric ions are determined by the combination of both pH. It is found that in very oxidizing environment values of Eh = 0.7 volts and pH = 2 are possible; while, in very reducing conditions values of Eh = -0.3 volts and pH = 8 are possible. Using these values of Eh and pH in conjunction with the data presented by R. M. Garrels (Garrels, 1960, Figs. 6.5a and 6.5d), we see that the concentrations of Fe^{3+} and Fe^{2+} vary respectively from 10^{-7} and 10^{-5} at the surface to 10^{-24} and 10^{-6} at depth. When electronic conductors such as sulfide ores or graphite are present it will be shown that the magnitude of the S. P. currents are controlled by the chemical potentials of the reacting species (i.e. Fe^{3+} and Fe^{2+}) and with such large variations in the concentration, large S. P. anomalies are possible.

Many sulfide ores such as pyrite and chalcophrite are good electronic conductors, and when present in a massif form or as continuous veins, they provide a conducting path for electrons between the surface where oxidizing conditions prevail and the zone below the water table where reducing

conditions are prevailing. The presence of this conducting path facilitates the oxidation-reduction reactions. Let us specifically consider the ferric-ferrous ion pair. Below the water table, the reaction taking place is

$\text{Fe}^{++} \rightarrow \text{Fe}^{+++} + e^-$ which gives off an electron that travels up through the ore body. In the weathering zone above the water table the opposite reaction takes place:

$\text{Fe}^{+3} + e^- \rightarrow \text{Fe}^{++}$. As a net result of then two reactions, a Fe^{++} ion disappears at depth and reappears near the surface, while a Fe^{+3} ion disappears from near the surface and reappears at depth. This gives the Fe^{++} and Fe^{+3} ions apparent mobilities that are much higher than the mobilities of the diffusion ions. We shall designate these apparent mobilities as U^* . Of course, inside the ore body itself the other ions have zero mobility.

If other reacting species are present (e.g. Manganese), they behave in very much the same way as the $\text{Fe}^{++}\text{Fe}^{+3}$ pair. Sato and Mooney (1960) have studied the chemical reactions taking place around sulfide ore bodies, and their study confirms the importance of the ferrous-ferric electron exchange reaction.

According to equation 5.9, the driving force is a weighted average of the chemical potentials μ_i of all the ions present, the weighting factors being dependent on the mobilities. Inside the conducting ore body, only the reacting species have large apparent mobilities and all other ions have zero mobility (it is obvious that the ore body does not influence, for instance, the diffusion of Ca^{++}). Therefore, if the ferrous-ferric pair represents the only important reacting species, the driving force Y_2 in the ore zone (medium²) is

$$Y_2 = \frac{U_{\text{Fe}^{+3}}^* C_{\text{Fe}^{+3}} \mu_{\text{Fe}^{+3}} + U_{\text{Fe}^{++}}^* C_{\text{Fe}^{++}} \mu_{\text{Fe}^{++}}}{\sigma_2} \quad 5.11a$$

where

$$\sigma_2 = F [U_{Fe^{+3}}^* C_{Fe^{+3}} Z_{Fe^{+3}} + U_{Fe^{+2}}^* C_{Fe^{+2}} Z_{Fe^{+2}}] \quad 5.11b$$

~~The driving force~~ and The conductivity σ_2 seem to be dependent on the concentrations of ferrous and ferric ion. This is an apparent inconsistency that can be easily removed. For one thing, we know that inside the ore body, the conductivity is electronic and should not depend on the ferrous-ferric pair. Furthermore, while the Fe^{+3} and Fe^{+2} ions have essentially infinite mobilities through the ore body (we are neglecting the reaction impedance), their concentrations are zero, which implies that the products $U_{Fe^{+3}}^* C_{Fe^{+3}}$ and $U_{Fe^{+2}}^* C_{Fe^{+2}}$ are constant and independent of the mobilities and the concentrations. Finally the ferrous and ferric ions are coupled through the reaction $Fe^{+2} \rightleftharpoons Fe^{+3} + e^-$ for every ferric ion transferred, a ferrous ion is transferred in the opposite direction—which means that the mobilities and concentrations inside the ore are related by

$$U_{Fe^{+3}}^* C_{Fe^{+3}} = - U_{Fe^{+2}}^* C_{Fe^{+2}} \quad 5.12$$

Substituting from 5.12 and 5.11b into 5.11a, we get
($Z_{Fe^{+3}} = 3$, $Z_{Fe^{+2}} = 2$)

$$Y_2 = \frac{2.3RT}{F} \log \frac{[Fe^{+3}]}{[Fe^{+2}]} \quad 5.13a$$

$$Y_2 = 59.1 \log \frac{[Fe^{+3}]}{[Fe^{+2}]} \quad (\text{in millivolts}) \quad 5.13b$$

This above expression represents the driving potential

inside the ore body (medium 2) when the ferrous-ferric pair represents the only important reacting species.

Outside the ore body, the driving potential is still given by 5.9

$$Y_1 = \sum_i \frac{v_i^{(n)} c_i^{(n)} \mu_i}{\sigma_i} \quad 5.14$$

where all the ions have finite mobilities. If the concentration of a particular ion is very small, its contribution to the driving potential will be equally small because

$c_i \mu_i \xrightarrow{c_i \rightarrow 0} 0$. The magnitude of the driving potential is determined mainly by the ions that are most abundant (e.g. Na^+ , Cl^- , Ca^{++} etc.), and the concentrations of these ions vary only slightly with depth. From the data in Table 5.2, it is obvious that at best these concentrations vary by two or three orders of magnitudes which can only produce small anomalies. Therefore, the variations of with depth are essentially negligible, and we can write for the total driving potential

$$f_2 - f_1 = 59.1 \log \frac{[Fe^{+3}]}{[Fe^{++}]} \quad 5.15$$

This last equation is similar to the Nerst's equation for reversible cell reactions, however, the two situations are not quite equivalent. In the reversible cell the concentrations are constant throughout the cell and the e.m.f. is determined by the equilibrium between ferrous and ferric ions. In our case, equation 5.15 represents a variable boundary condition as both Fe^{+3} and Fe^{++} are functions of depth.

It is by now clear why such minor constituents as iron that are normally unimportant in determining the electrochemical properties of the soil, suddenly become so important in the presence of a metallic ore body. Another feature of this explanation is that it does not require the ore body to undergo oxidation or reduction. The ore body provides only a conducting path for the electrons. This last conclusion is consistent with the arguments advanced by Sato and Mooney.

The equation 5.15 is in the form of the product of a coupling difference ($c_1 - c_2 = 59.1$ mv/decade) and a driving potential ($\Delta\mu = \log \frac{[Fe^{+3}]}{[Fe^{+2}]}$). Therefore, we can still use the equations 3.28, 3.27a, 3.27b, and the Fig. 3.12.

From a knowledge of the Eh and pH values around the ore body, we can obtain the concentrations of ferrous and ferric ions, and using 5.15 and Fig. 3.12, we can compute the S. P. anomalies to be expected. Values of Eh = 0.6 and pH = 4 are typical for the near surface conditions (Sato and Mooney, 1960; Fig. 4), while values of Eh = -0.2 and pH = 8 are typical of the conditions at depth. Using these values of Eh and pH, it is found (Garrels, 1960; Figs. 6.5a, 6.5d, and 6.6) that in going from the oxidizing conditions near the surface to the reducing conditions at depth, the ferric ion concentration decreases approximatively by 10^{12} while the ferrous ion concentration increases by about 10^2 . Therefore, the driving potential difference is

$$\Delta\mu = \log \frac{10^{-10}}{10^2} = \log 10^{-12}$$

Assuming a weathering depth of 500 ft. ($1/K = 500$ ft.) and a conductive dike ~~of~~ 250 ft. thick ($R_s = 0.5$, $\kappa_d = 0.5$),

the geometric factor is seen to be about 0.6. Using these values, the maximum S. P. anomaly observed over the ore body is

$$\Delta\phi_{\max} = (59.1)(\log 10^{12})(0.6) \cong 425 \text{ mv}$$

This certainly is a very large self-potential and compares favorably with some of the largest observed S. P. anomalies. Most S. P. anomalies are below 500 mv, but occasionally larger S. P. anomalies have been observed. Sato mentions some unusually large values reported by Shibato (1.0 volt, graphite) and Fujita (1.3 volts).

Assuming extremely oxidizing reducing conditions near the surface ($E_h = 0.7$ volts, $pH = 2.5$) and extremely reducing conditions at depth ($E_h = -0.3$ volts, $pH = 9$), the ferric ion concentration decreases by 10^{19} and the ferrous ion concentration decreases by 10^3 in going from the oxidizing zone to the depth environment. If the ore body is extremely conductive ($R_{21} = 1.0$), the geometric factor is near unity (see equation 3.37a which for $R_{21} = 1.0$ and $x \neq 0$, gives $f_1(x) = (c_1 - c_2)(\Delta\mu)$). Therefore, the maximum anomaly is

$$(\Delta\phi)_{\max} \cong (59.1)(\log \frac{10^{19}}{10^3})(1.0) \cong 950 \text{ mv}$$

This is just about the largest anomaly we can get through the oxidation-reduction reactions of the ferrous-ferric ion pair. If the larger observed S. P. anomalies are controlled by oxidation-reduction reactions, other ions must be involved. $Mn^{+4} - Mn^{+2}$ pair is one possibility, however, it is not clear under what conditions, the manganese ions become important. This point needs to be investigated

further. It is also possible that some of the larger anomalies are combinations of electrochemical S. P. potentials and topographic effects due to electrofiltration.

Section III - Effect of Random Inhomogeneities on S. P. Currents

Although the diffusion coupling properties of rocks do not seem capable of producing the large S. P. anomalies observed over certain ore zones. They can still give rise to some S. P. variations which must be considered as noise when S. P. surveys are being conducted. In this section, we shall evaluate the effect of a random distribution of inhomogeneities in producing such S. P. noise, when the variations in coupling properties are function of the x-coordinate only.

The general expression for the rms value of the noise $\overline{f_A^2}$ was derived in Section IV of Chapter III. From 3.49, we have

$$\overline{f_A^2} = \frac{(\Delta\mu)^2}{\pi^2 K} \int_{-\infty}^{\infty} \psi_{\alpha\alpha}(|\tau|) \varphi_{FF}(k|\tau|) d\tau \quad 5.17$$

where $\varphi_{FF}(k|\tau|)$ is the autocorrelation of the potential due to a vertical contact; $\psi_{\alpha\alpha}(|\tau|)$ is the autocorrelation of the gradient $\alpha(x)$ of the coupling parameter C ; and $1/K$ is essentially the depth of weathering.

The particularly simple model, that we shall use to compute $\psi_{\alpha\alpha}(|\tau|)$ is that of an earth composed of an infinite number of dikes, each having a thickness t_A and a coupling

coefficient C_i that we only know by their statistical properties.

As we cross each dike boundary, the coupling coefficient changes by a finite amount ΔC_i which can be positive or negative. Thus, the gradient $\alpha(x)$ of coupling is represented by a series of impulses. The variation of $\alpha_i(x)$ across a dike is shown in Fig. 5.1. The average value of the coupling difference $\overline{\Delta C_i}$ is obviously zero, but its rms value is not. We then have

$$\begin{aligned}\overline{\Delta C_i} &= 0 \\ \overline{\Delta C_i^2} &= (\Delta C)^2\end{aligned}\tag{5.18}$$

where (ΔC) is the rms value of the fluctuations in coupling properties.

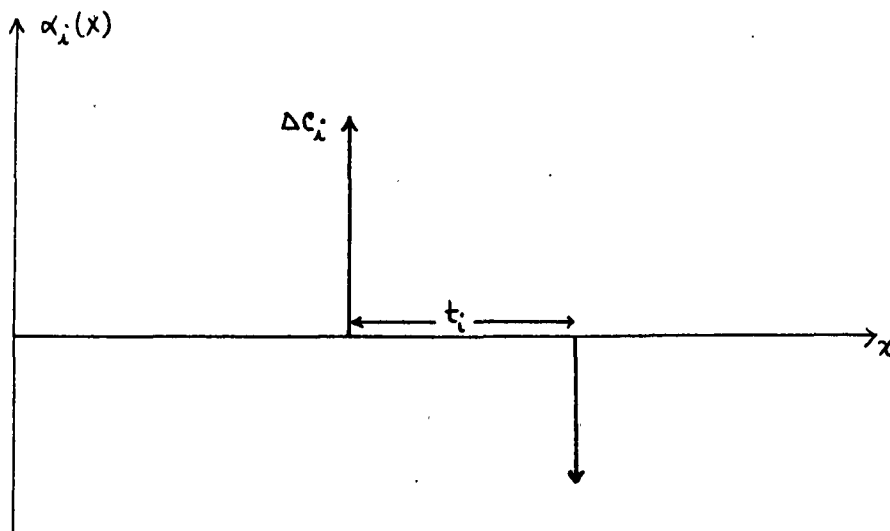


Figure 5.1 - Typical variations of coupling gradient $\alpha(x)$ across a dike.

The distribution of the random pulses along the surface

depends on the random distribution of the dikes. From a well-known theorem in communication theory, the random function $\alpha_i(x)$ can be represented as a convolution of a transient function $r(x)$ and white noise function $\delta_i(x)$

$$\alpha_i(x) = \int_{-\infty}^{\infty} r(u) \delta_i(x-u) du \quad 5.19$$

We shall assume that in our model, $r(x)$ can be represented by analogy with Fig. 5.1, by an impulse function

$$r(x) = (\Delta M) [\delta(x) - \delta(x-t)] \quad 5.20$$

where t is related to the average dike thickness and (ΔM) is related to the rms fluctuations in coupling properties ($\overline{\Delta M_i} = 0$).

With these assumptions, the autocorrelation is given by

$$\begin{aligned} \overline{\alpha_i(x) \alpha_i(x+\tau)} &= \iint_{-\infty}^{\infty} r(u') r(u'') \overline{\delta_i(x-u') \delta_i(x+\tau-u'')} du' du'' \\ &= \iint_{-\infty}^{\infty} r(u') r(u'') \left[\frac{1}{L_0} \delta(u''-u'-\tau) \right] du' du'' \\ &= \frac{1}{L_0} \int_{-\infty}^{\infty} r(u') r(u'+\tau) du' \end{aligned}$$

$$\text{or} \quad \psi_{aa}(|\tau|) = \frac{1}{L_0} \overline{\Phi_{rr}}(\tau) \quad 5.21$$

$\frac{1}{L_0}$ indicates the number of dikes per unit length, and $\overline{\Phi_{rr}}(\tau)$ is the autocorrelation of $r(x)$. From 5.20, we get for $\overline{\Phi_{rr}}(x)$

$$\overline{\Phi}_{rr}(\tau) = (\Delta M)^2 [2\delta(\tau) - \delta(\tau-t) - \delta(\tau+t)] \quad 5.22$$

and substituting from 5.21 and 5.22 into 5.17, we get for the S. P. noise

$$\overline{f_i^2} = \frac{(\Delta M)^2 (\Delta \mu)^2}{\pi^2 K L_0} [\varphi_{FF}(0) - \varphi_{FF}(kt)] \quad 5.23$$

The dimensionless parameter (kt) in the above equation is a measure of the ratio of the dike thickness to the depth of weathering. We finally have to relate $(\Delta M)^2$ to the rms fluctuations of the coupling.

If equation 5.20, giving $\lambda(x)$, represents the typical change of the coupling gradient $\alpha_\lambda(x)$, the typical change in the coupling itself would be

$$\Delta C_\lambda = (\Delta M) U(x) \quad 5.24$$

where $U(x)$ is a pulse of finite width t and height of unity. Therefore, the variations of ΔC_λ along the surface can be represented in our model by

$$\Delta C_\lambda = \int_{-\infty}^{\infty} (\Delta M) U(u') \lambda_\lambda(x-u') du' \quad 5.25$$

and its autocorrelation is given by

$$\begin{aligned} \overline{\Delta C_\lambda(x) \Delta C_\lambda(x+\tau)} &= \iint_{-\infty}^{\infty} (\Delta M)^2 U(u') U(u'') \overline{\lambda_\lambda(x-u') \lambda_\lambda(x+\tau-u'')} du' du'' \\ &= \frac{(\Delta M)^2}{L_0} \int_{-\infty}^{\infty} U(u') U(u'+\tau) du' \end{aligned}$$

The rms value of fluctuations is obtained by putting $\tau = 0$

$$(\Delta c)^2 \equiv \overline{\Delta c_i^2} = \frac{(\Delta \mu)^2}{\omega_0} t \quad 5.26$$

Substituting from 5.26 into 5.23, we get the final expression

$$\overline{f_i^2} = \frac{1}{\pi^2} (\Delta c)^2 (\Delta \mu)^2 \left[\frac{\varphi_{FF}(0) - \varphi_{FF}(kt)}{kt} \right] \quad 5.27$$

For very thick dikes ($kt \rightarrow \infty$) the numerator in the brackets remains finite while the denominator becomes infinitely large, and thus, the rms value of the noise approaches zero. At the other end, when the dike becomes infinitely thin ($kt \rightarrow 0$) the noise level $\overline{f_i^2}$ approaches a limiting value given by

$$\overline{f_i^2} \xrightarrow{kt \rightarrow 0} \frac{1}{\pi^2} (\Delta c)^2 (\Delta \mu)^2 \varphi'_{FF}(0) \quad 5.28$$

where $\varphi'_{FF}(0)$ is the derivative of the autocorrelation function shown in Fig. 3.14. In this case, the rms fluctuations $(\Delta c)^2$ of the coupling properties becomes small in amplitude, since the adjacent dikes cannot be very different in their properties. The noise will consist essentially of high frequency components. For large values of the thickness t , the same high frequency components may be present, but there are also some broad variations in coupling properties which will give rise to low frequency components in the noise.

Using a coupling difference of 10 mv/decade, a concentration ratio of 10^2 , and a thin dike ($kt=1$), we get

$$\overline{f_i^2} \cong \frac{(10)^2 (\log 10^2)^2}{\pi^2} \left[\frac{2.8 - 0.9}{1.0} \right]$$

and a rms value

$$\left(\overline{f_a^2}\right)^{\frac{1}{2}} \cong 9 \text{ mv}$$

Although this value of 19 mv should be considered as the upper bound of typical diffusion noise to be expected, it is large enough to account for much of the observed noise.

Section IV - Other Causes of S. P.

Electrofiltration and bioelectrical currents are also believed to be important in producing self-potentials. For instance, the topographic effect observed in S. P. surveys is believed to be due to the streaming potential of water seeping into the ground. We already have seen that rocks have large electrokinetic coupling coefficients of several millivolts per atmosphere. Therefore, flow of water under a small pressure head is sufficient to induce measurable potential differences. Cagniard (1956) reports the results of a S. P. survey in Yugoslavia over a very porous quartz hill, where an unusually large observed anomaly of -300 mv was attributed to electrofiltration.

Some authors have attributed the topographic effect to uphill currents caused by the atmospheric electric gradient. Although there is a large vertical gradient of about 100 volts/m, these currents are negligible due to the extremely low conductivity of the air. Using a typical value of 10^{-14} mhos/m for the conductivity of the air, the induced current density is 10^{-12} amps/m², and the ohmic potential drop inside the ground with an average conductivity of 10^{-4} mhos/m is therefore 10^{-6} volts/m or 0.1 mv per 100 meters, a potential drop too small to affect S. P. results.

Streaming potentials induced by flow of mud under pressure are also responsible for the self-potentials

observed in well loggings.

Currents of bioelectric origin are also believed to be very important in producing large S. P. noise in wooded areas. Scott (1962) reports potential differences of 20 mv or more across plant roots. A series of field studies of S. P. noise by Madden, Cantwell, Sill, and Maher (Madden and Cantwell, 1962) showed that the micro-structure of the self-potentials (noise level) was higher in the woods than in open areas. Several traverses run from an open field into the adjacent woods gave large negative anomalies that were greatest right at the edge of the woods (50—100 mv). Bioelectric currents are believed to travel down the main root and return through the earth, as one would expect for any conductor extending from the surface to any depth.

Section V - Conclusions

The results of this chapter are in general agreement with the observed facts as well as the other proposed mechanisms of S. P. currents (Heiland, 1946; Sato and Mooney, 1960; Wyllie, 1955). Many of the results we have obtained are similar to the results obtained by Sato and Mooney using the electrochemical approach. However, our approach through the use of irreversible thermodynamics is superior in certain respects.

First of all, using Onsager's relations as our starting point, we were able to include the effect of geometry in our equations. It is generally assumed that the maximum anomaly to be expected in a self-potential survey would be one half of the total potential difference. The computed geometric factors for a dike (Fig. 3.12) show that this rule of thumb is not necessarily true and the actual magnitudes depend very much on the ratio of the dike thickness

to the weathering depth and on the conductivity contrast. For very thin dikes, the observed anomaly is only two to three tenths of the total potential difference, while for very thick and highly conductive dikes the observed anomaly is nearly equal to the total potential difference available.

Furthermore, our approach shows that S. P. anomalies can be also caused by pure electrochemical diffusion. These diffusion potentials are small compared to the anomalies observed over certain sulfide or graphite bodies, however, they are of sufficient magnitude to account for much of the background S. P. noise.

Finally, our treatment includes the ore bodies with electronic conductivity as a special case. By using the irreversible thermodynamics approach, we have introduced the concentrations of the reacting species (i.e. the Eh and the pH of the solution) rigorously. It is true that the Eh of a solution containing, for instance, ferric and ferrous ions is determined by the concentrations of these two ions, but in the approach through classical chemistry it is not quite clear why the Eh is related to the observed anomalies. Our approach, not only shows clearly the relationship between the activities of the ions in solution and the observed potentials, but it clearly shows the limitations. Briefly these limitations are: (a) the ore body must provide a continuous path for electrons; (b) the coupling coefficient of 59.1 mv/decade is only valid when large concentration variations of one reacting species are involved. When several reacting species are present, equation 5.15 is no longer valid, and new equation including all the reacting species has to be derived.

CHAPTER VI

SUGGESTIONS FOR FUTURE WORK

In this thesis, the principles of irreversible thermodynamics were applied successfully to a study of the broad features of S. P. anomalies associated with underground nuclear detonations and sulfide ore bodies, however, several difficulties were encountered that need to be investigated further.

Interpretation of the Underground Detonation Data - The available field data contained larger amount of noise that made the depth interpretation difficult. As a matter of fact, fair fits were obtained using the curves computed for several $(\frac{h}{a})$ ratios, and it looked as if the data would fit the theoretical curves for other thickness to depth ratios. Furthermore, the depth estimates were systematically too high. This problem needs to be further studied along two different lines. First of all, better field recording techniques are needed to minimize the effect of S. P. noise and tellurics. Secondly, theoretical curves for many more thickness to depth ratios $(\frac{d}{h})$ and conductivity contrasts R_{21} need to be computed to evaluate unambiguously the usefulness of the theoretical model in predicting the depth of the shot.

Chemical Properties of Pore Fluids - Very little is known of the actual chemical properties of pore fluids. The estimates of concentrations used in computing the S. P. anomalies over the ore bodies were obtained from simple theoretical consideration. The actual concentrations of the ions in the pore fluids may be very different from

the theoretical values because many reacting species may be involved. An investigation of the chemical properties of pore fluids is required to obtain actual estimates of the concentrations of the reacting species. Occasionally anomalies of one volt or better have been observed, but these can not be explained on the basis of the available data on the solubility of ferric and ferrous ions. However, they can be explained if the $Mn^{+4} - Mn^{+2}$ pair is the dominating reacting species. The solubility of manganese in pore fluids in the presence of iron and other ions needs to be investigated.

Multi-Component Oxidation-Reduction Reactions - In our treatment of the self-potentials over metallic ore bodies, we assumed that ferrous-ferric ion pair is the only important reacting species, and the equation 5.15 that was derived to compute the potentials is only valid under these conditions. The form of this equation for a system containing several reacting species needs to be investigated.

Extension to Disseminated Ore Bodies - In our treatment of the self-potentials over metallic ore bodies, we assumed that the ore was present in massiff form or as a continuous vein. However, in most cases of interest the ore is present in disseminated form. The reacting species may still have large apparent mobilities and dominate over the other ions. This problem needs to be investigated because of its practical applications.

Appendix A

Solution of the Boundary Value Cases

I. One Layer over a Half-Space.

Boundary conditions are

$$\frac{\partial f_1}{\partial z} = 0 \quad \text{at } z = 0$$

$$\left. \begin{aligned} \sigma_1 \frac{\partial f_1}{\partial z} &= \sigma_2 \frac{\partial f_2}{\partial z} \\ f_1 - f_2 &= (c_1 - c_2) Y_{12} \end{aligned} \right\} \text{ at } z = d$$

Using cylindrical coordinates, we can write

$$f_1 = \int_0^\infty (A_1 e^{-\lambda z} + B_1 e^{\lambda z}) J_0(\lambda r) \lambda d\lambda \quad 0 < z < d$$

$$f_2 = \int_0^\infty (A_2 e^{-\lambda z}) J_0(\lambda r) \lambda d\lambda \quad z > d$$

Applying the three boundary conditions we get

$$\begin{bmatrix} 1 & -1 & 0 \\ \sigma_1 e^{-2\lambda d} & -\sigma_1 & -\sigma_2 e^{-2\lambda d} \\ e^{-2\lambda d} & 1 & -e^{-2\lambda d} \end{bmatrix} \begin{bmatrix} A_1 \\ B_1 \\ A_2 \end{bmatrix} = (c_1 - c_2) \bar{Y}_{12}(\lambda) \begin{bmatrix} 0 \\ 0 \\ e^{-\lambda d} \end{bmatrix}$$

Where $\bar{Y}_{12}(\lambda)$ is given by

$$\bar{Y}_{12}(\lambda) = \int_0^\infty Y_{12}(z, d) J_0(\lambda r) r dr$$

Solving the three equations, we get

$$A_1 = B_1 = \frac{1}{2} (1 + R_{21}) (C_1 - C_2) \frac{e^{-\lambda d} \overline{Y}_{12}(\lambda)}{1 + R_{21} e^{-2\lambda d}}$$

$$A_2 = -\frac{1}{2} (1 + R_{21}) (C_1 - C_2) \frac{(e^{\lambda d} - e^{-\lambda d}) \overline{Y}_{12}(\lambda)}{1 + R_{21} e^{-2\lambda d}}$$

and $R_{21} = \frac{\sigma_2 - \sigma_1}{\sigma_2 + \sigma_1}$

II. Two layer over a Half-Space.

we have

$$f_1 = \int_0^\infty A_1 (e^{-\lambda z} + e^{+\lambda z}) \overline{f}_0(\lambda r) \lambda d\lambda \quad 0 < z < d_1$$

$$f_2 = \int_0^\infty (A_2 e^{-\lambda z} + B_2 e^{+\lambda z}) \overline{f}_0(\lambda r) \lambda d\lambda \quad d_1 < z < d_1 + d_2$$

$$f_3 = \int_0^\infty A_3 e^{-\lambda z} \overline{f}_0(\lambda r) \lambda d\lambda \quad z > d_1 + d_2$$

Using the boundary conditions

$$\left. \begin{aligned} f_1 - f_2 &= (C_1 - C_2) Y_{12} \\ \sigma_1 \frac{\partial f_1}{\partial z} &= \sigma_2 \frac{\partial f_2}{\partial z} \end{aligned} \right\} \text{at } z = d_1, \quad \left. \begin{aligned} f_2 - f_3 &= (C_2 - C_3) Y_{23} \\ \sigma_2 \frac{\partial f_2}{\partial z} &= \sigma_3 \frac{\partial f_3}{\partial z} \end{aligned} \right\} \text{at } z = d_1 + d_2$$

we get

$$\begin{bmatrix} 1 + e^{-2\lambda d_1} & -e^{-2\lambda d_1} & -1 & 0 \\ \sigma_1(1 - e^{-2\lambda d_1}) & \sigma_2 e^{-2\lambda d_1} & -\sigma_2 & 0 \\ 0 & e^{-2\lambda(d_1+d_2)} & 1 & -e^{-2\lambda(d_1+d_2)} \\ 0 & \sigma_2 e^{-2\lambda(d_1+d_2)} & -\sigma_2 & -\sigma_1 e^{-2\lambda(d_1+d_2)} \end{bmatrix} \begin{bmatrix} A_1 \\ A_2 \\ B_2 \\ B_3 \end{bmatrix} = \begin{bmatrix} e^{-\lambda d_1} (c_1 - c_2) \overline{Y}_{12}(\lambda) \\ 0 \\ e^{-\lambda(d_1+d_2)} (c_2 - c_3) \overline{Y}_{12}(\lambda) \\ 0 \end{bmatrix}$$

Solving these equations, we get

$$A_1 = \frac{1}{2} (1 + R_{21}) \left[\frac{\Delta_1 e^{-\lambda d_1}}{\Delta} (c_1 - c_2) \overline{Y}_{12}(\lambda) + \frac{\Delta_2 e^{-\lambda(d_1+d_2)}}{\Delta} (c_2 - c_3) \overline{Y}_{23}(\lambda) \right]$$

where

$$\Delta_1 = (1 + R_{32} e^{-2\lambda d_2}) \quad \Delta_2 = (1 + R_{32})$$

$$\Delta = (1 + R_{32} e^{-2\lambda(d_1+d_2)}) + R_{21} e^{-2\lambda d_1} (1 + R_{32} e^{-2\lambda(d_2-d_1)})$$

III. Vertical Contact.

We have

$$f_1 = \int_0^\infty e^{-\lambda x} (A_1 \cos \lambda z + B_1 \sin \lambda z) d\lambda \quad x > 0$$

$$f_2 = \int_0^\infty e^{+\lambda x} (A_2 \cos \lambda z + B_2 \sin \lambda z) d\lambda \quad x < 0$$

where f_1 and f_2 satisfy the boundary conditions

$$\frac{\partial f_1}{\partial z} = \frac{\partial f_2}{\partial z} = 0 \quad \text{at } z=0$$

$$\left. \begin{aligned} \sigma_1 \frac{\partial f_1}{\partial x} &= \sigma_2 \frac{\partial f_2}{\partial x} \\ f_1 - f_2 &= (c_1 - c_2) Y_{12} \end{aligned} \right\} \quad \text{at } x=0$$

Applying the first boundary condition we get

$$\left(\frac{\partial f}{\partial z} \right)_{z=0} = \int_0^\infty e^{-\lambda x} (B_1 \cos \lambda z) \lambda d\lambda$$

and a similar equation for f_2 . Therefore we get

$$B_1 = B_2 = 0$$

Applying the other boundary conditions we get

$$\begin{bmatrix} 1 & -1 \\ \sigma_1 & \sigma_2 \end{bmatrix} \begin{bmatrix} A_1 \\ A_2 \end{bmatrix} = (c_1 - c_2) \overline{Y}_{12}(\lambda) \begin{bmatrix} 1 \\ 0 \end{bmatrix}$$

where $\overline{Y}_{12}(\lambda)$ is given by

$$\overline{Y}_{12}(\lambda) = \frac{1}{2\pi} \int_0^\infty Y_{12}(0, z) \cos \lambda z dz$$

Solving these two equations we get

$$A_1 = \frac{1}{2} (1 + R_{21}) (c_1 - c_2) \overline{Y}_{12}(\lambda)$$

$$A_2 = -\frac{1}{2} (1 - R_{21}) (c_1 - c_2) \overline{Y}_{12}(\lambda)$$

IV. Vertical Dike

We have

$$f_1^+ = \int_0^\infty A_1 e^{-\lambda x} \cos \lambda z d\lambda \quad x > 0$$

$$f_2 = \int_0^{\infty} (A_2 e^{-\lambda x} + B_2 e^{\lambda x}) \cos \lambda z d\lambda \quad -d < x < 0$$

$$f_1^- = \int_0^{\infty} B_3 e^{\lambda x} \cos \lambda z d\lambda \quad x < -d$$

We also have the boundary conditions

$$\left. \begin{aligned} f_1^+ - f_2 &= (c_1 - c_2) Y_{12} \\ \sigma_1 \frac{\partial f_1^+}{\partial x} &= \sigma_2 \frac{\partial f_2}{\partial x} \end{aligned} \right\} \text{ at } x = 0$$

$$f_1^- - f_2 = (c_1 - c_2) Y_{12}$$

$$\sigma_1 \frac{\partial f_1^-}{\partial x} = \sigma_2 \frac{\partial f_2}{\partial x}$$

Applying these boundary conditions, we get

$$\begin{bmatrix} 1 & -1 & -1 & 0 \\ \sigma_1 & -\sigma_2 & \sigma_2 & 0 \\ 0 & -1 & -e^{-2\lambda d} & e^{-2\lambda d} \\ 0 & \sigma_2 & -\sigma_2 e^{-2\lambda d} & \sigma_1 e^{-2\lambda d} \end{bmatrix} \begin{bmatrix} A_1 \\ A_2 \\ B_2 \\ B_3 \end{bmatrix} = (c_1 - c_2) \overline{Y}_{12}(\lambda) \begin{bmatrix} 1 \\ 0 \\ e^{-\lambda d} \\ 0 \end{bmatrix}$$

therefore, we get

$$A_1 = \frac{1}{2} (1 + R_{21}) (c_1 - c_2) \frac{(1 - e^{-\lambda d}) \overline{Y}_{12}(\lambda)}{(1 - R_{21} e^{-\lambda d})}$$

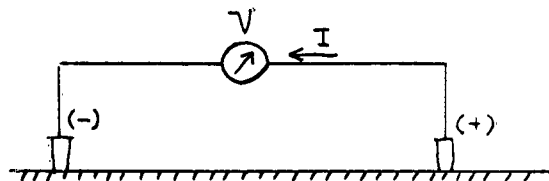
$$A_2 = -\frac{1}{2} (1 - R_{21}) (c_1 - c_2) \frac{e^{-\lambda d} \overline{Y}_{12}(\lambda)}{(1 - R_{21} e^{-\lambda d})}$$

$$B_2 = -\frac{1}{2} (1 - R_{21}) (c_1 - c_2) \frac{\overline{Y}_{12}(\lambda)}{(1 - R_{21} e^{-\lambda d})}$$

Appendix B

Relationship between Δf and $\Delta\phi$

Two potential electrodes are making contact with the ground as shown in the figure. From the relation



$$I = -\sigma \nabla f$$

we concluded immediately that in the wire

$$I \propto (f_e^+ - f_e^-)$$

where subscript e refers to the electrode system.

But we have

$$f_e^+ = \phi_e^+ + c_e^+ \mu_e^+$$

$$f_e^- = \phi_e^- + c_e^- \mu_e^-$$

where $c\mu$ is the electric potential contribution due to chemical activity. We already know that the electric potential ϕ is continuous across the electrode contact ($\phi_e = \phi_g$ where g refers to the ground), therefore

$$(f_e^+ - f_e^-) = (\phi_g^+ - \phi_g^-) + (c_e^+ \mu_e^+ - c_e^- \mu_e^-)$$

It is obvious that Δf and $\Delta\phi$ are equal only when the product $c\mu$ is the same for both pots. This conditions is seldom satisfied in practice for the following two reasons: (a) the lateral variations in the chemical

conditions of the surface soil can produce drastically different chemical reactions at the two electrodes;
(b) differences in concentration of the non-polarizing electrolyte in the two pots as well as different porosities can produce small potential differences of a few millivolts. The second effect is recognized by geophysicists using S. P. method and is compensated for by a "pot correction."

BIBLIOGRAPHY

- Cagniard, L., 1956, Electricite' Tellurique, Handbook der Physik, S. Flugge (editor), Springer-Verlag, Berlin, V. 47, p. 407-469.
- Callen, H. B., 1960, Thermodynamics, John Wiley and Sons, Inc., New York.
- Carslaw, H. S., and Jaeger, J. B., 1947, Conduction of Heat in Solids, Oxford University Press.
- DeGroot, S. R., 1961, Thermodynamics of Irreversible Processes, North-Holland Publishing Co., Amsterdam.
- DeGroot, S. R., and Mazur, P., 1962, Non-Equilibrium Thermodynamics, North-Holland Publishing Co., Amsterdam.
- Denbigh, K. G., 1951, The Thermodynamics of Steady State, Methuen's Nomographs, London.
- Dobrin, M. B., 1952, Introduction to Geophysical Prospecting, McGraw-Hill Book Co., Inc., New York.
- Dwight, H. B., 1958, Mathematical Tables, Dover Publications, Inc., New York.
- Erdelyi, and al., 1953, Higher Transcendental Functions, Bateman Manuscript Project, A. Erdelyi (editor), McGraw-Hill Book Co., New York.
- _____, 1954, Table of Integral Transforms, Bateman Manuscript Project, McGraw-Hill Book Co., New York.
- Fitts, Donald D., 1962, Non-Equilibrium Thermodynamics, McGraw-Hill Book Co., New York.
- Garrels, R. M., 1960, Mineral Equilibria, Harper and Brothers, New York.
- Glaser, A., and Kruszyna, R., 1962a, On-site Self-potential and Resistivity Measurements—Project Gnome, Allied Research Associates report No. ARA-1052.
- _____, 1962b, On-site Self-potential and Resistivity Measurements—Hardhat event of Project Nougat, Allied Research Associates report No. ARA-1054.

- Glasstone, S., 1954, An Introduction to Electrochemistry, D. van Nostrand Co., New York.
- Griggs, D. T., and Press, F., 1960, Probing the Earth with Nuclear Explosions, University of California, Lawrence Radiation Laboratory Report UCRL-6030T.
- Guggenheim, E. A., 1957, Thermodynamics, Interscience Publishers, New York.
- Harned, H. S., and Owen, B. B., 1950, The Physical Chemistry of Electrolytic Solutions, Reinhold Publishing Corp., New York.
- Hawkes, H. E., and Webb, J. S., 1962, Geochemistry in Mineral Exploration, Harper and Row, Publishers, New York.
- Heath, S., M. I. T. Bachelor's Thesis (under preparation)
- Heiland, C. A., 1946, Geophysical Exploration, Prentice-Hall, Inc., New York.
- Hem, J. D., 1959, Study and Interpretation of the Chemical Characteristics of Natural Water, U. S. G. S. Water Supply paper No. 1473.
- Janke and Emde, 1943, Table of Functions, Dover Publications, New York.
- Johnson, G. W., and Violet, C. E., 1959, Underground Nuclear Detonations, University of California, Lawrence Radiation Laboratory, report UCRL-5626.
- Johnson, G. W., 1960, Application of Nuclear Explosions as Seismic Sources, University of California, Lawrence Radiation Laboratory, report UCRL-6030T.
- Kermabon, A. J., 1956, A Study of Some Electro-Kinetic Properties of Rocks, M. S. Thesis, M. I. T., Department of Geology and Geophysics.
- Kruxzyna, R. T., 1962, On-Site Self-potential and Resistivity Measurements, Further Participation in Project Nougat, Allied Research Associates report (unpublished).

- Madden, 1960, Thermoelectric Measurements, M. I. T. DSR Project 9017 (unpublished), personal communications.
- Madden, Marshall, Fahlquist, and Neves, 1957, Background Effects in the Induced Polarization Method of Geophysical Exploration, A. E. C. report RME-3150.
- Madden, T. R., and Marshall, D. J., 1959, Induced Polarization, Final Report, A. E. C. report RME-3160.
- Madden, T. R., and Cantwell, T., 1960, A Proposal for Research into Electrical Methods for Onsite Inspection Procedures, M. I. T., Department of Geology and Geophysics, (unpublished).
- Madden, T. R., and Cantwell, T., 1962, Interim Report to Allied Research Associates, Geophysical Laboratory, M. I. T., Project DSR 9017 (unpublished).
- Marshall, D. J., 1959, Interfacial Polarization in Membranes and Its Significance in the Induced Polarization of Geologic Materials, Ph.D. Thesis, M. I. T., Department of Geology and Geophysics.
- Meents, W. F., Bell, A. H., Rees, O. W., and Tilbury, W. G., 1952, Illinois Oil-field Brines, State of Illinois Geological Survey, Illinois Petroleum No. 66.
- Morse, P. M., and Feshbach, H., 1953, Methods of Theoretical Physics, McGraw-Hill Book Co., New York.
- Mounce, W. D., and Rust, W. M., 1945, "Natural Potential in Well Logging," Transactions AIME (Geophysics), V. 164, p. 288-294.
- Pourbaix, M. J. N., 1949, Thermodynamics of Dilute Aqueous Solutions, E. Arnold and Co., London.
- Prigogine, I., 1955, Thermodynamics of Irreversible Processes, Charles C. Thomas Publisher, Springfield, Illinois.
- Proceedings of the Seventh Meeting of the International Committee of Electrochemical Thermodynamics and Kinetics (Iindaw, 1955), 1957, Butterworths Scientific Publications, London.

- Ramsey, A. S., 1959, An Introduction to the Theory of Newtonian Attraction, Cambridge University Press, Cambridge.
- Sato, M., and Mooney, H. M., 1960, "Electrochemical Mechanism of Sulfide Self-potentials," Geophysics, V. 25, No. 1, p. 226-249.
- Sato, M., 1960a, "Oxidation of Sulfide Ore Bodies, I, Geochemical Environments in Terms of Eh and pH," Economic Geology, V. 55, No. 5, p. 928-961.
- Sato, M., 1960b, "Oxidation of Sulfide Ore Bodies, II, Oxidation Mechanisms of Sulfide Minerals," Economic Geology, V. 55, No. 6, p. 1202-1231.
- Schlumberger, C. and M., and Leonardon, E. G., 1934a, "Electrical Logging, A Method of Determining Bottom-Hole Data by Electrical Measurements," AIME Geophysical Prospecting, p. 237-272.
- _____, 1934b, "A New Contribution to Subsurface Studies by Means of Electrical Measurements in Drill Holes," AIME Geophysical Prospecting, p. 273-288.
- Scott, B. I. H., 1962, "Electricity in Plants," Scientific American, V. 207, No. 4, p. 107-117.
- Wyllie, M. R. J., 1949, "A Quantitative Analysis of the Electrochemical Component of the Self-potential Curve," Transaction AIME, V. 186, p. 17-26.
- _____, 1955, "The Role of Clay in Well-Logging Interpretation, State of California," Division of Mines Bulletin 169, p. 282.

BIOGRAPHY

The author, Bijan Nourbehecht was born in Teheran, Iran on May 9, 1936. After attending grammar school in Iran, he went to Paris, France where he graduated from Lycee Michelet in 1954. After attending briefly Mathematiques Superieures classes at Lycee St. Louis, he transferred successively to Oklahoma State University and Colorado School of Mines where he received the degree of Geophysical Engineer in 1958. In September 1959, he enrolled at M. I. T. and since then he has been a candidate for a Ph.D. degree in the Department of Geology and Geophysics.

The author's experience includes three years of research and field work at the Bear Creek Mining Co., one summer of research at Geophysical Service Inc., and one year as Lecturer in Geology at the Boston College.

The author is a member of Tau Beta Pi, Sigma Xi, Society of Exploration Geophysicists, and European Association of Exploration Geophysicists. During the academic year 1961--1962, he was the recipient of the Gulf Oil Co. Fellowship.

In August 1962, the author accepted the position of Associate Professor of Physics with the National University of Iran.

Errata

p. 34	equation 2.41	change	$\left(\frac{L'_{33}}{L'_{33}}\right)_T$	to	$\left(\frac{L'_{31}}{L'_{33}}\right)_T$
p. 43	line 10	change	"evaluate at"	to	"evaluate at $z = d$ "
p. 46	equation 3.17	change	$f_1(\xi, 0)$	to	$f_1(r, 0)$
p. 48	first equation	change	$J_0\left(\frac{\pi}{d} \xi\right)$	to	$J_0\left(\frac{\pi}{d} r\right)$
p. 48	last line	change	$\Delta_1 = (1 + R_{32})$	to	$\Delta_2 = (1 + R_{32})$
p. 49	line 19	change	"depth of d"	to	"depth of d"
p. 50	equation 3.40	change	$\frac{ R \cdot \vec{n} }{R^2}$	to	$\frac{ \vec{R} \cdot \vec{r} }{R^2}$
p. 51	line 21	change	(x, y)	to	(x, z)
p. 52	equation 3.24	change	$d\lambda$	to	$d z$
p. 54	equation 3.30	add	$d\lambda$		
p. 56	equation 3.34b	change	$\frac{\partial f_i}{\partial z}$	to	$\frac{\partial f_i}{\partial x} - \lambda x$
p. 57	equation 3.36a	change the second	λd	to	λx
p. 93	equation 5.10.1	change to	$Fe^{++} \rightleftharpoons Fe^{+++} + e^-$		
p. 98	last line	cross out	" Δ "		
p. 98	last line	cross out	"of"		
p. 102	equation 5.20	add bracket			

UNCLASSIFIED

UNCLASSIFIED